*Proceedings of the*
*Annual Stability Conference*
*Structural Stability Research Council*
*Charlotte, North Carolina, April 11-14 2023*

# DSM design of CFS lipped channel columns undergoing distortional-global interaction at elevated temperatures

Elisson Bilheiro Ferreira Filho[1], Alexandre Landesmann[1], Dinar Camotim[2]

## Abstract

This work reports the results of an ongoing numerical investigation dealing with the post-buckling behavior, strength and DSM (Direct Strength Method) design of fixed-ended cold-formed steel (CFS) lipped channel (LC) columns experiencing distortional-global (flexural-torsional) (D-FT) interaction at elevated temperatures caused by fire conditions. It extends the scope of the parametric study recently reported by Ferreira Filho *et al.* (2022), by obtaining a fairly extensive additional set of numerical failure loads, covering wider (i) cross-section dimensions and (ii) interaction D-FT types and levels – this is done by means of ABAQUS shell finite element GMNIA, using models previously developed by the authors and adopting an EC3-based (2005) model to describe the temperature-dependence of the CFS material properties. The whole set of assembled failure load data is then used to search for an efficient DSM-based design approach to predict them. The starting point of this search is provided by the combination of the strength curves developed by Landesmann *et al.* (2019) and Bicelli *et al.* (2021), following the idea first put forward by Schafer (2002) and later used by Martins *et al.* (2018) – however, these authors only considered columns at room temperature and used the currently codified DSM column global design curve. On the basis of the findings reported in this work, it is possible to draw a few conclusions that provide (i) clues to reach a more efficient DSM-based design approach and (ii) encouragement to extend the current research effort to columns with other cross-section shapes and/or support conditions, aimed at achieving a safe, economic and reliable general DSM-based design approach for CFS columns failing in D-FT interactive modes at elevated temperatures.

## 1. Introduction

The use of cold-formed steel (CFS) in the construction industry has been growing steadily during the last few decades, mostly due to its several advantages, such as an outstanding fabrication versatility, a very high structural efficiency (strength-to-weight ratio), and quite low production and erection costs. However, the natural search for economic solutions invariably leads to quite slender CFS members, which are prone to various pure instabilities, namely local (L), distortional (D) or global (G) buckling, as well as to coupling (mode interaction) phenomena involving two or more of them (L-D, L-G, D-G or L-D-G). Figs. 1(a)-(d) concern a lipped channel column and show buckled cross-sections corresponding to L, D, major-axis FT and minor-axis flexural modes, respectively.

[1] Programa de Engenharia Civil, COPPE, Universidade Federal do Rio de Janeiro, Brazil. <elisson.filho+alandes@coc.ufrj.br>
[2] CERIS, DECivil, Instituto Superior Técnico (IST), Universidade de Lisboa, Portugal. <dcamotim@civil.ist.utl.pt>

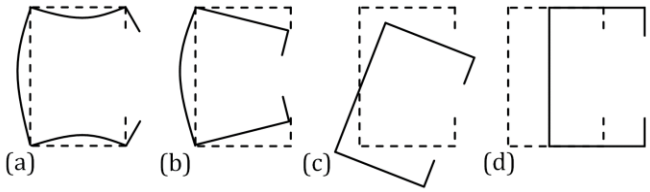


**Figure 1.** Lipped channel column buckled cross-sections corresponding to (a) local, (b) distortional, (c) major-axis flexural-torsional and (d) minor-axis flexural modes.

In order to overcome the above difficulties, the Direct Strength Method (DSM – *e.g.*, Camotim *et al.* 2016, Schafer 2019), prescribed by the current North-American (AISI 2022), Australian/New Zealand (AS/NZS 2018) and Brazilian (ABNT 2010) specifications for CFS structures, is nowadays widely accepted as the most rational approach for the design of such members. The currently codified column design curves deal only with L, D, G and L-G interactive failures at room (or normal) temperature. The currently codified (AISI 2022, AS/NZS 2018, ABNT 2010) nominal axial strengths relevant for this work are the distortional ($P_{nD}$) and global ($P_{nG}$) ones, which are given by the expressions

$$P_{nD} = \begin{cases} P_y & \lambda_D \le 0.561 \\ P_y \left(1 - \dfrac{0.25}{\lambda_D^{1.2}}\right)\dfrac{1}{\lambda_D^{1.2}} & \lambda_D > 0.561 \end{cases} \qquad \lambda_D = \sqrt{\frac{P_y}{P_{crD}}} \quad , \quad (1)$$

$$P_{nG} = \begin{cases} P_y \left(0.658^{\lambda_G^2}\right) & \lambda_G \le 1.5 \\ P_y \left(\dfrac{0.877}{\lambda_G^2}\right) & \lambda_G > 1.5 \end{cases} \qquad \lambda_G = \sqrt{\frac{P_y}{P_{crG}}} \quad , \quad (2)$$

where (i) $P_y = A \cdot f_y$ ($A$ and $f_y$ are the cross-section area and steel yield stress) and (ii) $\lambda_D$, $\lambda_G$, $P_{crD}$ and $P_{crG}$ are the D and G slenderness values and buckling loads, respectively.

According to Dinis & Camotim (2011), D-G interactive failures in CFS columns may occur when $P_{crD}$ and $P_{crG}$ are sufficiently close, provided that $P_y$ is large enough to allow the corresponding deformation modes to influence the column post-buckling behavior. Naturally, the D-G interaction effects are more pronounced when the two buckling loads are very close – indeed, numerical (shell finite element − SFE) studies (Dinis & Camotim 2011, Camotim & Dinis 2013, Martins *et al.* 2018), all involving lipped channel (LC) columns, showed that the strongest interaction invariably occurs in columns with global-to-distortional critical buckling loads ratios $R_{GD}=P_{crG}/P_{crD}$ comprised between 0.80 and 1.20, a range characterizing the so-called "True D-G interaction". In columns outside this $R_{GD}$ range, D-G interaction may still occur if $P_y$ is considerably higher than the largest of $P_{crG}$ and $P_{crD}$ (thus allowing the interaction to emerge and develop) – it is termed "Secondary distortional bifurcation D-G interaction", if $R_{GD}<0.8$, and "Secondary global bifurcation D-G interaction", if $R_{GD}>1.20$ (Martins *et al.* 2018).

Martins *et al*. (2018) reported a numerical investigation on the post-buckling behavior, strength and DSM-based design of fixed-ended CFS columns (including LC ones) affected by different levels of D-G interaction ($R_{GD}$ values) at room temperature. These authors showed that the $P_{nD}$ values (Eq. (1)) overestimated virtually all numerical D-G interactive failure loads gathered by them – the amount of overestimation was particularly severe in the high slenderness range. Conversely, and quite surprisingly, it was also found that the $P_{nG}$ values (Eq. (2)) underestimated almost all numerical D-G interactive failure loads associated with flexural-torsional buckling (including the LC column ones) – moreover, the

underestimations were quite significant for $\lambda_G$>2.0 and grew rapidly with the slenderness (*e.g.*, 250% for $\lambda_G$=3.5). It is worth noting that, as it would be logical to expect, the $P_{nG}$ values overestimated the D-G interactive failure loads associated with flexural buckling (*e.g.*, the zed-section column ones), which prompted the development and proposal of a novel DSM-based design approach.

The surprising $P_{nG}$ underestimation of most numerical D-G interactive failure loads corresponding to flexural-torsional buckling (D-FT failure loads), reported by Martins *et al.* (2018), was subsequently explained by Dinis *et al.* (2019, 2020), who investigated the $P_{nG}$ accuracy in predicting pure CFS column FT failure loads at room temperature. Following an extensive parametric study, involving CFS fixed-ended columns with various cross-section shapes, these authors showed that the $P_{nG}$ design curve only provides accurate FT failure loads predictions in the low-to-moderate slenderness range ($\lambda_G \leq 1.5$) – for $\lambda_G$>1.5, they yield FT failure load underestimations that may be extremely high percentagewise − similar findings had been reported earlier by Peköz & Sümer (1992), and Bandula Heva & Mahendran (2012). In order to improve this undesirable situation, Dinis *et al.* (2020) proposed the DSM-based strength curve set

$$P_{nFT} = \begin{cases} P_y \left( 0.658^{\lambda_{FT}^2} \right) & \lambda_{\mathrm{FT}} \leq 1.5 \\ P_y \left( \dfrac{a}{\lambda_{FT}^b} \right) & \lambda_{\mathrm{FT}} > 1.5 \end{cases} \qquad \lambda_{FT} = \sqrt{\frac{P_y}{P_{crFT}}} \qquad , \quad (3)$$

$$\text{with } a = 0.39 \times 1.5^b \text{ , } b = 0.06\beta_{FT} + 0.71 \leq 2.0 \text{ and } \beta_{FT} = \frac{I_I + I_w/A}{I_{II}} \text{ ,}$$

where (i) the global slenderness $\lambda_G$ is replaced by a flexural-torsional one ($\lambda_{FT}$), (ii) the exponential expression appearing in $P_{nG}$ is kept, and (iii) parameter $\lambda_{FT}$ involves the cross-section major ($I_I$) and minor ($I_{II}$) moments of inertia, warping constant ($I_w$), and area ($A$) – it should be noted that the presence of $\lambda_{FT}$ reflects the design curve dependence on the column cross-section geometry (shape and dimensions). However, it remains to be investigated how the findings reported by Martins *et al.* (2018), concerning the DSM-based prediction of column D-FT interactive failure loads, are affected when the $P_{nFT}$ values replace their $P_{nG}$ counterparts.

Landesmann *et al.* (2019) and Bicelli *et al.* (2021) numerically investigated the post-buckling behavior, ultimate strength and DSM design of CFS columns failing in pure D and FT modes, respectively, at elevated temperatures. Initially, these authors gathered extensive failure load data, concerning CFS columns with (i) several cross-section geometries (shape and dimensions) and lengths, (ii) different room-temperature yield stresses (covering wide D or FT slenderness ranges), (iii) 8 (uniform) elevated temperatures ($T \leq 800$ *ºC*), and (iv) temperature-dependent steel material behaviors following a model based on the EC3-1-2 (2005) one. These failure data were subsequently used to assess the adequacy of the strength curves given by Eqs. (1) and (3), modified to include the temperature effects (see Section 3.1 of this paper) and denoted $P_{nD.T}$ and $P_{nFT.T}$, respectively, in predicting them. It was concluded that the $P_{nD.T}$ and $P_{nFT.T}$ values are not able to predict adequately the column D or FT failure loads in the low-to-moderate slenderness range − a large number of those predictions are substantially unsafe. In order to improve them, the $P_{nD.T}$ and $P_{nFT.T}$ DSM-based strength curves were modified/lowered in the low-to-moderate slenderness, leading to

$$P_{nD.T}=\begin{cases} P_{yT}\cdot\left(k_p/k_y\right) & \lambda_{D.T}\le\dfrac{0.561}{\left(k_p/k_y\right)} \\ P_{yT}\left[1-\dfrac{0.25}{\left(k_p/k_y\right)}\dfrac{1}{\lambda_{D.T}^{1.2}}\right]\dfrac{1}{\lambda_{D.T}^{1.2}} & \lambda_{D.T}>\dfrac{0.561}{\left(k_p/k_y\right)} \end{cases} \qquad \lambda_{D.T}=\sqrt{\frac{P_{yT}}{P_{crD.T}}}\,, \tag{4}$$

$$P_{nFT.T}=\begin{cases} P_{yT}\eta\left(0.658\right)^{\eta^{1.2}\cdot\lambda_{\mathrm{FT.T}}^{2}} & \lambda_{\mathrm{FT.T}}\le 1.5 \\ P_{yT}\left(\dfrac{a}{\lambda_{FT.T}^{b}}\right) & \lambda_{\mathrm{FT.T}}>1.5 \end{cases} \qquad \lambda_{FT.T}=\sqrt{\frac{P_{yT}}{P_{crFT.T}}}\,, \tag{5}$$

with, $\eta=1.3\cdot10^{-6}T^2-1.4\cdot10^{-3}T+1.127\le 1$,

where (i) $\lambda_{D.T}=(P_{yT}/P_{crD.T})^{0.5}$ and $\lambda_{FT.T}=(P_{yT}/P_{crFT.T})^{0.5}$ are the D and FT slenderness values at temperature $T$, respectively, (ii) $P_{yT}$, $P_{crD.T}$ and $P_{crFT.T}$ are the squash and critical D and FT buckling loads at temperature $T$, and (iii) $k_p$ and $k_y$ are the proportionality limit and yield stress reduction factors prescribed in EC3-1-2 (2005). At room/moderate temperature (20/100 °C), Eqs. (1) and (3) are recovered from these expressions. Although Eqs. (4) and (5) were shown to provide fairly accurate and mostly safe failure load predictions for CFS columns collapsing in pure D or FT modes at elevated temperatures, it remains an open question whether they can also be used (with more or less relevant modifications) to estimate adequately failure loads of CFS columns undergoing D-FT interaction at elevated temperatures.

Very recently, the authors (Ferreira Filho *et al.* 2022) reported numerical results dealing with the post-buckling behavior, strength and DSM design of CFS fixed-ended LC columns affected by different levels of "True D-FT interaction" at elevated temperatures (up to 800 ºC). On the basis of the numerical failure load data obtained, it was concluded that an efficient DSM-based design approach to handle such columns is clearly needed. The purpose of this work is to widen the scope of the above investigation, by presenting and discussing numerical results concerning CFS columns (i) under both normal and elevated temperatures, and (ii) undergoing not only "True D-FT interaction" (TI), but also "Secondary-distortional bifurcation" (SDI) and "Secondary-global bifurcation" SGI) D-FT interaction – different levels of D-FT interaction are considered for the three types. Together with the failure load data reported by Ferreira Filho *et al.* (2022), the additional set of column D-FT interactive failure loads, obtained through an extensive parametric study, is used to further assess the merits of the available DSM-based design approaches in handling CFS fixed-ended LC columns affected by virtually any type or level of D-G interaction, both at room and elevated temperatures – in the former case, the DSM-based FT design approach, developed by Dinis et al. (2020) for fixed-ended columns at room temperature, is used.

As done previously (*e.g.*, Bicelli *et al*. 2021), all the numerical D-FT interactive failure loads obtained in this work (i) concern columns containing initial geometrical imperfections with critical-mode FT shapes (shown to be the most detrimental ones by Martins *et al.* 2018) and $L$/1000 amplitude, and (ii) are obtained by means of ABAQUS (2014) SFE GMNIA, adopting a validated model often employed by the authors in the past. The LC columns analyzed (i) display a wide variety of cross-section dimensions, lengths and room-temperature yield stresses (selected to cover wide slenderness ranges), and (ii) are subjected to several uniforms elevated temperatures (up to 800 ºC). It is worth mentioning that the D-FT interactive failure loads reported by Martins *et al.* (2018) and concerning fixed-ended LC columns at room temperature are also included in this study.

## 2. Column Geometry Selection – Buckling Behavior

The first task of this work consists of carefully selecting CFS fixed-ended LC column cross-section dimensions and lengths ensuring a high susceptibility to D-FT interaction both at room and elevated temperatures. As done in previous studies, the column selection procedure involves sequences of "trial-and-error" buckling analyses, performed in the code GBTUL (2018), based on Generalized Beam Theory (GBT) and intended to identify columns buckling in D and/or FT[3] modes and undergoing different levels of TI, SGI or SDI D-FT interaction (*i.e.*, such that their $R_{GD}$ values cover an adequately wide range around 1.0) – moreover, it is also ensured that both the D and FT critical buckling loads are well below their local and minor-axis flexure counterparts (thus making sure that no other coupling phenomenon comes into play).

Table 1 provides the output of this effort, consisting of 21 LC geometries ($b_w$, $b_f$, $b_l$ and $t$ – see Fig. 2(c)) – note that most of these columns were analyzed by Martins *et al.* (2018) at room temperature. This table

**Table 1.** Selected LC column geometries, critical buckling loads and relevant buckling load ratios (mm and kN).

| Column | $b_w$ | $b_f$ | $b_l$ | $t$ | $\beta_{FT}$ | $L$ | $P_{crFT}$ | $P_{crD}$ | $P_{crL}$ | $P_{crFm}$ | $R_{GD}$ | $R_{MAX}$ |
|---|---|---|---|---|---|---|---|---|---|---|---|---|
| LC1 | 120 | 100 | 10 | 4.5 | 3.91 | 3950 | 318 | 648 | 2250 | 1060 | 0.49 | 1.64 |
| LC2 | 110 | 90 | 10 | 3.17 | 4.54 | 3500 | 200 | 310 | 841 | 712 | 0.64 | 2.30 |
| LC3 | 150 | 150 | 15 | 4 | 3.85 | 5550 | 288 | 414 | 1199 | 1514 | 0.70 | 2.90 |
| LC4 | 150 | 130 | 12 | 4.06 | 4.42 | 5000 | 318 | 425 | 1310 | 1275 | 0.75 | 3.00 |
| LC5 | 150 | 130 | 10 | 4.2 | 4.35 | 5000 | 325 | 408 | 1459 | 1279 | 0.80 | 3.13 |
| LC6 | 130 | 115 | 10 | 3.55 | 4.30 | 4000 | 278 | 310 | 994 | 1185 | 0.90 | 3.21 |
| LC7 | 130 | 110 | 10 | 3.5 | 4.55 | 3750 | 299 | 316 | 941 | 1190 | 0.95 | 2.98 |
| LC8 | 100 | 80 | 15 | 5 | 3.59 | 1450 | 1381 | 1427 | 3865 | 5250 | 0.97 | 2.71 |
| LC9 | 90 | 90 | 10 | 3 | 3.39 | 2250 | 270 | 276 | 810 | 1523 | 0.98 | 2.93 |
| LC10 | 140 | 140 | 13 | 3.5 | 4.00 | 4500 | 291 | 297 | 869 | 1616 | 0.98 | 2.93 |
| LC11 | 150 | 130 | 13 | 4 | 4.46 | 4150 | 435 | 441 | 1293 | 1850 | 0.99 | 2.93 |
| LC12 | 100 | 90 | 15 | 5 | 3.13 | 1550 | 1269 | 1277 | 3591 | 6086 | 0.99 | 2.81 |
| LC13 | 90 | 80 | 10 | 3 | 3.85 | 2000 | 315 | 315 | 871 | 1444 | 1.00 | 2.77 |
| LC14 | 120 | 100 | 10 | 4.5 | 3.91 | 2500 | 671 | 652 | 2114 | 2645 | 1.03 | 3.15 |
| LC15 | 120 | 140 | 12 | 3.02 | 3.43 | 4000 | 216 | 198 | 553 | 1653 | 1.09 | 2.56 |
| LC16 | 100 | 120 | 10 | 2.96 | 3.00 | 2900 | 230 | 192 | 603 | 1914 | 1.20 | 2.62 |
| LC17 | 120 | 100 | 10 | 4.5 | 3.91 | 2200 | 814 | 655 | 2114 | 3416 | 1.24 | 2.60 |
| LC18 | 150 | 130 | 10 | 2.9 | 5.40 | 4850 | 216 | 167 | 466 | 939 | 1.29 | 2.16 |
| LC19 | 100 | 120 | 10 | 3.15 | 2.89 | 2600 | 291 | 224 | 736 | 2534 | 1.30 | 2.53 |
| LC20 | 140 | 110 | 10 | 3.25 | 5.35 | 3500 | 350 | 265 | 675 | 1300 | 1.32 | 1.93 |
| LC21 | 140 | 110 | 10 | 3.19 | 5.41 | 3300 | 378 | 256 | 629 | 1436 | 1.47 | 1.66 |

[3] The GBT-based buckling analyses reported by Martins *et al.* (2018) showed that the so-called "global" (flexural-torsional) buckling modes, associated with lengths in the vicinity of $L_{DG}$ (see Fig. 2(a)) combine, in fact, contributions from major-axis flexural, torsional and anti-symmetric distortional deformations (corresponding to the GBT deformations mode **2**, **4** and **6**, respectively). In other words, a more correct designation of these buckling modes should "flexural-torsional-distortional" (FTD) – nevertheless, and for the sake of simplicity, such buckling modes are termed "flexural-torsional" in the remainder of this work. Moreover, the authors are currently investigating how the presence of anti-symmetric distortional deformations in the so-called "flexural-torsional" buckling modes influences the column post-buckling behavior, ultimate strength and DSM-based design – the outcome of this research effort will be reported in the very near future.

also provides the column (i) $\beta_{FT}$ values and lengths, (ii) flexural-torsional ($P_{crFT}$), distortional ($P_{crD}$), local ($P_{crL}$) and minor-axis flexural ($P_{crFm}$) critical buckling loads, (iii) $R_{GD}$ values (ranging from 0.49 to 1.47) and (iv) $R_{MAX}$ values, corresponding to the ratio between $min\{P_{crL}, P_{crFm}\}$ and $max\{P_{crD}, P_{crFT}\}$.

Figure 2(a) depicts the signature curves of LC12 columns at four temperatures, namely 20/100 °C (room/moderate), 400 °C, 600 °C and 800 °C – they provide the variation of the column elastic critical buckling load at temperature $T$ ($P_{crT}$) with its length ($L$ – logarithmic scale). The EC3-based CFS constitutive model, addressed in Section 3.1, is adopted and all buckling loads are calculated for $E_{20}$=210 GPa (steel Young's modulus at room temperature) and $\nu$=0.3 (Poisson's ratio, deemed temperature independent). Moreover, the 3 column lengths indicated considered ($L$=130 cm, $L_{DG}$=155 cm and $L$=180 cm) correspond to columns with $R_{GD}$<1.0 ($P_{crD}$>$P_{crFT}$), $R_{GD}$=1.0 ($P_{crD}$=$P_{crFT}$) and $R_{GD}$>1.0 ($P_{crD}$<$P_{crFT}$), *i.e.*, susceptible to SDI, TI and SGI D-FT interaction, respectively – Fig. 2(b) displays the critical D and FT buckling modes associated with each column length. It is worth noting that a signature curve corresponding to an elevated temperature (400, 600, 800 ºC) can be obtained, from its room-temperature counterpart, through a "vertical translation" whose magnitude depends only on the Young's modulus erosion caused by the temperature rise – therefore, the column buckling load natures and mode shapes corresponding to a given length are independent of the temperature value.

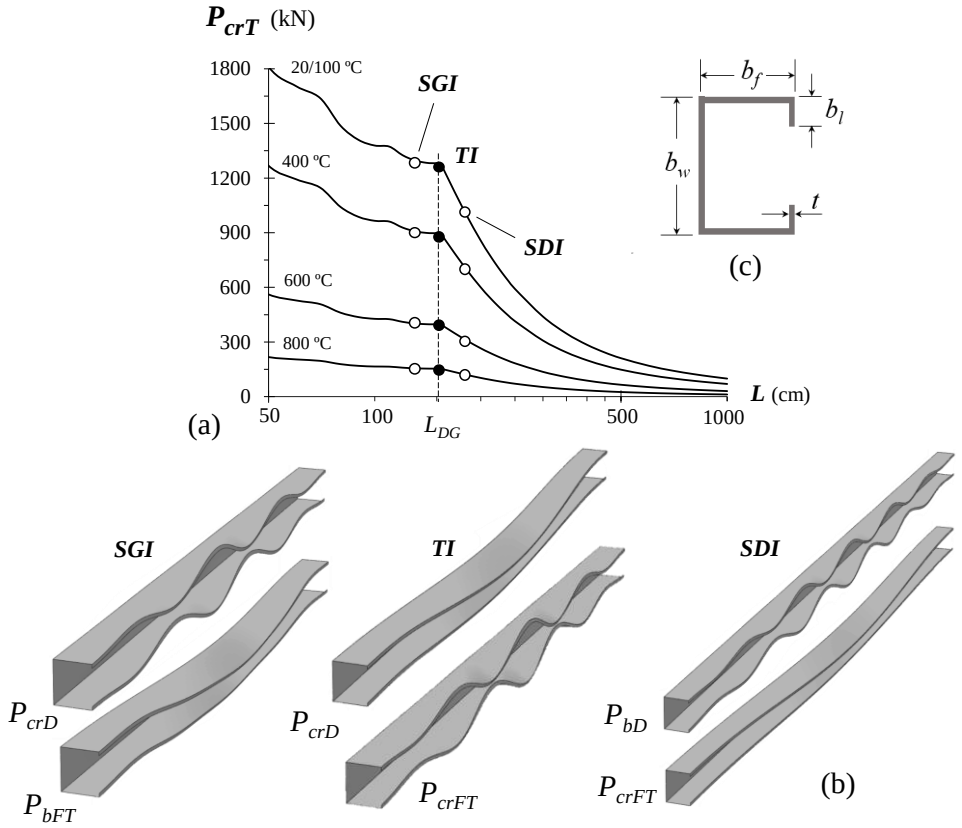


**Figure 2.** LC12 column (a) $P_{crT}$ vs. $L$ signature curves for $T$=20/100-400-600-800 ºC (EC3-based model) with lengths associated with SGI, TI and SDI, (b) critical and non-critical D and FT buckling modes, and (c) LC geometry and dimensions

## 3. Numerical Model

The post-buckling equilibrium paths and failure loads of the columns affected by D-FT interaction are determined by means of ABAQUS (2014) SFE GMNIA, employing models similar to those used by the

authors in past studies involving CFS columns at room and elevated temperatures (*e.g.*, Camotim & Dinis 2013, Martins *et al.* 2018, Bicelli *et al.* 2021). The columns are discretized into fine S4 element meshes (ABAQUS nomenclature – 4-node general-purpose shell finite elements with six degrees of freedom per node and full integration). The analyses are performed by means of an incremental-iterative technique combining Newton-Raphson's method with an arc-length control strategy. They simulate the response of columns subjected to uniform temperature distributions (*i.e.*, the columns are deemed engulfed in flames, thus sharing the surrounding air temperature – see Landesmann *et al.* 2019) and subsequently axially compressed up to failure – steady state analyses providing failure loads at elevated temperatures. Previous studies (*e.g.*, Martins *et al.* 2018) showed that finite element meshes with a length-to-width ratio close to 1 provide accurate results, while involving a reasonable computational effort. The column fixed-ended support conditions are modelled by attaching rigid plates to the column end cross-sections, thus fully restraining warping, all the rotations, the bending translations – the axial translation is free at one end section, thus enabling the imposition of small longitudinal displacements (analyses under displacement control), and prevented at the other. The axial compression is applied through imposed axial displacements of the end plate points corresponding to the cross-section centroids (see Fig. 3). These displacements are imposed in small increments, by means of the ABAQUS automatic loading stepping procedure. As noted earlier, all columns analyzed contain FT initial geometrical imperfections (the most detrimental shape – see Dinis & Camotim 2013, Martins *et al.* 2018) with amplitude $L/1000$. The buckling mode shapes were obtained through preliminary ABAQUS buckling analyses, performed with the same shell finite element mesh subsequently used to carry out the GMNIA – this procedure makes it easy to "transform" the buckling analysis output into a GMNIA input. It is still worth noting that strain-hardening, residual stress and rounded corner strength effects were disregarded in this work, since several authors (*e.g.*, Ellobody & Young 2005) have shown that their combined influence on the column failure load is negligible.

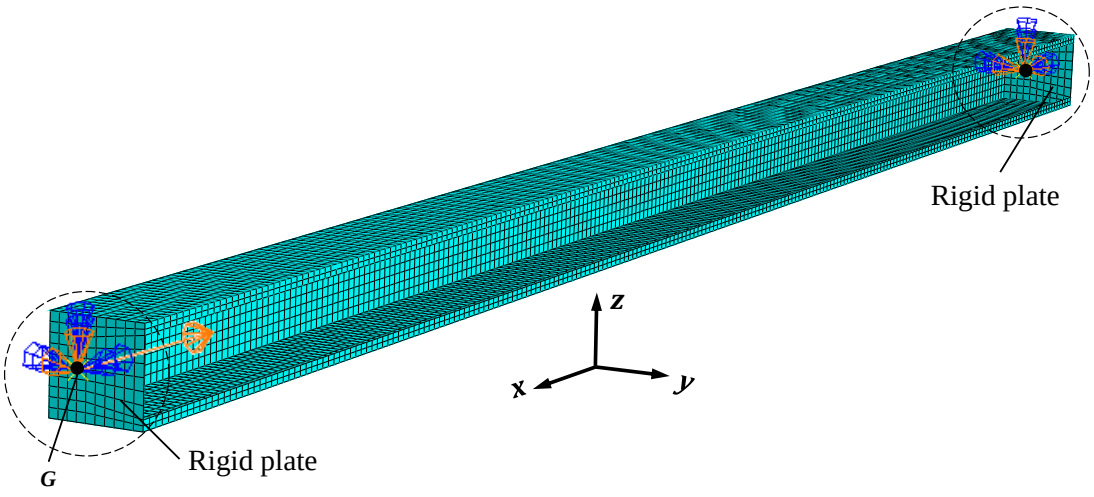


**Figure 3.** SFE discretization of the columns analyzed in this work, including the free and prevented displacements at the rigid plates attached to the two end cross-sections.

### *3.1 Steel Material Behavior*

The multi-linear stress-strain curve available in ABAQUS (2014) is adopted to model the steel material behaviors associated with the various yield stresses considered. The CFS constitutive law at elevated temperature adopted in this work is based on that prescribed in EC3-1.2 (2005), which was previously adopted in the numerical simulations reported by Landesmann *et al.* (2019), Bicelli *et al.* (2021) and

Arrais *et al.* (2021). Figure 4(a) makes it possible to visualize the temperature-dependence of the reduction factors applicable to the CFS Young's modulus ($k_E=E_T/E_{20}$), nominal yield stress ($k_y=f_{yT}/f_{y20}$) and proportionality limit stress ($k_p=f_{pT}/f_{y20}$) – their values are presented, in tabulated form, in EC3-1.2 (2005). As for Fig. 4(b), it illustrates the qualitative differences between the EC3-based stress-strain curves for all the temperatures considered in this work – plots $f_T/f_{y20}$ vs. $\varepsilon$, where the applied stress at a given temperature, $f_T$, is normalized with respect to the room-temperature yield stress $f_{y20}$. The EC3-based stress-strain curve model comprises three regions, corresponding to distinct strain ranges − note that the stress-strain curve proportionality limit strain ($\varepsilon_{pT}=f_{pT}/E_T$) and non-linear shape depend considerably on the temperature (for $T$=20/100 ºC, the constitutive law is bi-linear – elastic-perfectly plastic material).

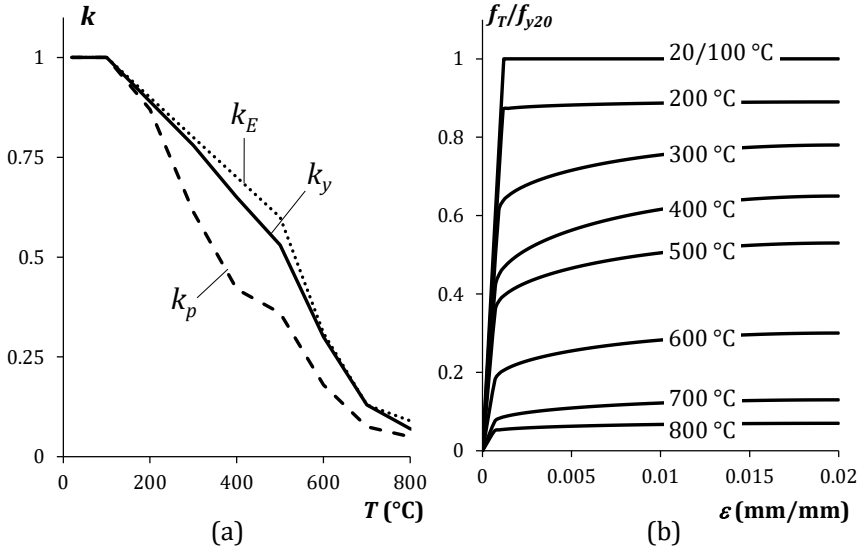


**Figure 4.** EC3-based CFS constitutive model: (a) variation of $k_E$, $k_y$, $k_p$ with $T$ and (b) stress-strain curves $f_T/f_{y20}$ vs. $\varepsilon$ ($\varepsilon\leq0.02$) for the uniform temperatures considered in this work.

At elevated temperatures, the first part of the well-defined yield plateau exhibited by the $T$=20/100 °C curve is replaced by a strain-hardening region that becomes gradually more pronounced as the temperature rises. The stress-strain curve is linear elastic, with slope $E_T$ ($E_{20}=210\,GPa$), up to the proportionality limit stress $f_{pT}$. Then, it becomes elliptic in the transition between the elastic and plastic ranges, up to the effective yield stress $f_{yT}$, occurring at $\varepsilon_{yT}$ =0.02 and accounting for kinematic strain-hardening. Lastly, it ends with a flat yield plateau, up to the limit strain $\varepsilon_{uT}$=0.15 (not shown in Fig. 4(b)). Prandtl-Reuss's plasticity model (von Mises yield criterion and associated flow rule) is adopted in all cases. Finally, since the post-buckling analyses carried out involve large inelastic strains, the nominal/engineering static stress-strain curve is replaced by a relation between the true stress and the logarithmic plastic strain, reading

$$f_T=\begin{cases}\varepsilon\cdot E_T & \varepsilon\leq\varepsilon_{pT}\\ f_{pT}-c+(b/a)\left[a^2-\left(\varepsilon_{yT}-\varepsilon\right)^2\right]^{0.5} & \varepsilon_{pT}<\varepsilon<\varepsilon_{yT}\\ f_{yT} & \varepsilon_{yT}\leq\varepsilon\leq\varepsilon_{uT}\end{cases}, \quad (6)$$

with, $a^2=\left(\varepsilon_{yT}-\varepsilon_{pT}\right)\left(\varepsilon_{yT}-\varepsilon_{pT}+\dfrac{c}{E_T}\right)$, $b^2=c\left(\varepsilon_{yT}-\varepsilon_{pT}\right)E_T+c^2$, $c=\dfrac{\left(f_{yT}-f_{pT}\right)^2}{\left(\varepsilon_{yT}-\varepsilon_{pT}\right)E_T-2\left(f_{yT}-f_{pT}\right)}$.

*3.2 Validation Studies*

Due to the lack of experimental data concerning CFS columns affected by D-G (or D-FT, to be more precise) interaction, the ABAQUS SFE model employed to determine the post-buckling behavior and strength of CFS columns experiencing D-FT interaction at room and elevated temperatures is validated in this section against numerical simulations reported by Gunalan *et al.* (2014) and Rokilan & Mahendran (2021) – they concern LC columns failing in pure D or FT modes at room and elevated (uniform) temperatures that were also experimentally tested by Bandula Heva & Mahendran (2012 and Ranawaka & Mahendran (2010). Figures 5(a)-(b), taken from the above publications works, provide an overall view of the experimental set-up specially designed and built at the Structures Laboratory of the Queensland University of Technology (QUT), in Australia.


**Figure 5.** Overall view of the experimental set-up and LC test specimens tested by Bandula Heva & Mahendran (2012) and Ranawaka & Mahendran (2010), which failed in (a) D and (b) FT modes at elevated temperatures.

Table 2 provides the data concerning the LC columns considered in the validation study, namely (i) their failure mode (D or FT), (ii) the mean values of their cross-section dimensions and lengths, and the amplitudes of the (D or FT) initial geometrical imperfection adopted in the SFE GMNIA simulations, (iii) the temperatures considered, (iv) the steel grade $E_T$ and $f_{yT}$ values, and (v) the column failure loads reported by Gunalan *et al*. (2014) and Rokilan & Mahendran (2021) ($P_{uRep}$), and those obtained in this work ($P_{uTW}$), together with the percentage differences between them.

It is worth noting that, besides the innovative experimental test campaigns, involving large numbers of column specimens, this research group also performed extensive numerical studies at room and elevated temperatures. The column analyses, carried out in the code ABAQUS, (i) accounted for the influence of residual stresses, (ii) included critical-mode (D or FT) initial geometrical imperfections exhibiting the experimentally measured amplitudes, and (iii) adopted the steel grade material properties ($E_T$ and $f_{yT}$) indicated in Table 2, using experimentally-based Ramberg-Osgood type constitutive models. The CFS column specimens were made of sheets with nominal thickness 0.80 mm (G250 steel grade), 0.95 mm (G250 and G550 steel grades) and 1.90-1.95 mm (G450 and G250 steel grades). As for the numerical analyses performed in this work, they replicate those performed by Gunalan *et al.* (2014) and Rokilan & Mahendran (2021), except for the fact that the residual stresses were disregarded and a different steel constitutive model was adopted (EC3-based, instead of Ramberg-Osgood).

**Table 2.** Columns considered in the validation study: geometries and comparison between the numerical failure loads reported by Gunalan *et al.* (2014) and Rokilan & Mahendran (2021), and those obtained in this work.

| Mode | Column (mm) | Imperfection | $T$ (°C) | Steel Grade | $E_T$ (GPa) | $f_{yT}$ (MPa) | $P_{uRep}$ (kN) | $P_{uTW}$ (kN) | $\frac{P_{uRep} - P_{uTW}}{P_{uRep}}$ |
|---|---|---|---|---|---|---|---|---|---|
| Distortional | $b_w$ = 30.97<br>$b_f$ = 31.16<br>$b_l$ = 5.80<br>$t$ = 0.94<br>$L$ = 190 | 0.72·$t$ | 20 | G250-095 | 200 | 320.0 | 29.9 | 29.2 | 2.28% |
| | | | 200 | | 185 | 263.4 | 25.0 | 24.4 | 2.40% |
| | | | 350 | | 125.4 | 163.2 | 14.6 | 14.3 | 2.25% |
| | | | 500 | | 97.6 | 104.6 | 9.4 | 9.4 | 0.15% |
| | | | 650 | | 70 | 52.5 | 4.9 | 4.9 | 0.77% |
| | | | 800 | | 19.2 | 18.9 | 1.6 | 1.7 | -4.25% |
| | $b_w$ = 30.87<br>$b_f$ = 31.35<br>$b_l$ = 5.52<br>$t$ = 0.80<br>$L$ = 190 | 0.74·$t$ | 20 | G550-0.80 | 200 | 610.0 | 31.3 | 33.5 | -7.15% |
| | | | 200 | | 170.8 | 605.1 | 27.3 | 27.7 | -1.58% |
| | | | 350 | | 142 | 534.4 | 22.7 | 24.6 | -8.25% |
| | | | 500 | | 79.6 | 261.7 | 12.8 | 13.5 | -5.12% |
| | | | 650 | | 62 | 56.7 | 4.0 | 4.3 | -7.00% |
| | | | 800 | | 26 | 31.1 | 2.0 | 2.1 | -7.11% |
| | $b_w$ = 31.44<br>$b_f$ = 31.61<br>$b_l$ = 5.80<br>$t$ = 0.95<br>$L$ = 190 | 1.05·$t$ | 20 | G550-0.95 | 205 | 615.0 | 41.6 | 43.7 | -5.01% |
| | | | 200 | | 176.9 | 592.2 | 38.7 | 39.7 | -2.63% |
| | | | 350 | | 141 | 539.4 | 30.6 | 32.8 | -7.11% |
| | | | 500 | | 80.4 | 289.7 | 19.0 | 20.0 | -5.20% |
| | | | 650 | | 66 | 50.4 | 4.5 | 4.7 | -4.71% |
| | | | 800 | | 28.7 | 27.1 | 2.3 | 2.3 | 0.02% |
| Flexural-torsional | $b_w$ = 74.9<br>$b_f$ = 50.0<br>$b_l$ = 15.0<br>$t$ = 1.95<br>$L$ = 1740 | $L$/2559 | 20 | G250-1.95 | 188 | 271 | 90.7 | 88.5 | 2.38% |
| | | $L$/4047 | 200 | | 159.7 | 247 | 84.3 | 81.1 | 3.79% |
| | | $L$/3783 | 300 | | 134.4 | 178 | 62.4 | 59.2 | 5.18% |
| | | $L$/3000 | 400 | | 109.1 | 129 | 41.1 | 42.9 | -4.31% |
| | | $L$/3625 | 500 | | 83.7 | 91.4 | 26.6 | 28.2 | -5.93% |
| | | $L$/5438 | 600 | | 58.3 | 60.2 | 19.0 | 19.9 | -4.87% |
| | | $L$/4579 | 700 | | 32.9 | 33.7 | 10.9 | 11.7 | -7.17% |
| | $b_w$ = 74.9<br>$b_f$ = 49.8<br>$b_l$ = 14.8<br>$t$ = 1.88<br>$L$ = 1740 | $L$/2949 | 20 | G450-1.90 | 206 | 515 | 129.0 | 127.2 | 1.41% |
| | | $L$/1955 | 200 | | 175 | 510 | 110.0 | 111.0 | -0.95% |
| | | $L$/3000 | 300 | | 147.3 | 489 | 96.4 | 92.8 | 3.70% |
| | | $L$/4350 | 400 | | 119.5 | 357 | 78.0 | 79.9 | -2.43% |
| | | $L$/3955 | 500 | | 91.7 | 201 | 53.4 | 54.0 | -1.18% |
| | | $L$/4971 | 600 | | 63.9 | 56.7 | 20.5 | 18.9 | 7.82% |
| | | $L$/3867 | 700 | | 36.1 | 36.1 | 11.3 | 11.86 | -4.92% |
| | $b_w$ = 55.0<br>$b_f$ = 34.8<br>$b_l$ = 7.8<br>$t$ = 0.95<br>$L$ = 1740 | $L$/2486 | 20 | G550-0.95 | 205 | 615 | 25.4 | 26.2 | -3.10% |
| | | $L$/2023 | 200 | | 178.3 | 596 | 22.5 | 23.0 | -2.21% |
| | | $L$/2719 | 300 | | 151.6 | 553 | 19.3 | 19.7 | -2.22% |
| | | $L$/2522 | 400 | | 125 | 443 | 15.8 | 16.3 | -3.05% |
| | | $L$/7550 | 600 | | 71.7 | 58 | 6.2 | 6.5 | -4.27% |
| | | $L$/3625 | 700 | | 45 | 48 | 4.6 | 4.6 | 0.41% |

The observation of Table 2 reveals that the absolute values of the percentage differences between (i) the column failure loads reported by Gunalan *et al*. (2014) and Rokilan & Mahendran (2021) ($P_{uRep}$), and (ii) those obtained in this work ($P_{uTW}$), for columns with three (nominal) yield stresses and subjected to various temperatures, have a mean value equal to 3.79% and never exceed 8.25%. In addition, only for 7 (out of 36) columns do those differences exceed 6%. In view of the quite good correlation expressed by the above indicators, it seems fair to argue that the ABAQUS SFE model employed in this work may be deemed satisfactorily validated.

## 4. Column D-FT Interactive Strength at Elevated Temperatures

### *4.1 Elastic-Plastic Post-Buckling Behavior*

The influence of the elevated temperature on the elastic-plastic post-buckling behavior and failure load of selected CFS LC columns undergoing D-FT interaction is addressed in this section. Since it was found that such influence is qualitatively quite similar for all the columns analyzed undergoing a given D-FT interaction type (TI, SGI or SDI), only the post-buckling results of three columns are presented and discussed here – they constitute a representative sample of the whole set of columns dealt with.

Figure 6(a) shows the equilibrium paths $P/P_{cr.20}$ vs. $(v+v_0)/t$ of the columns LC1 ($R_{GD}$=0.49) LC14 ($R_{GD}$=1.03) and LC17 ($R_{GD}$=1.24) with $\lambda_{cr}\cong$1.5 subject to temperatures $T$=20/100-200-300-400-500-600-700-800 ºC – $P_{cr.20}=min\{P_{crG}; P_{crD}\}$ (elastic critical buckling loads at room temperature – see Section 2), $v$ is the mid-span top flange-lip corner vertical displacement and $v_0$ its initial value. The white circles stand for the failure loads ($P_{uT}=A\cdot f_{uT}$) and the room temperature elastic equilibrium paths are also shown, for comparison purposes. As for Fig. 6(b), it displays the failure modes and plastic strain contours at collapse ($P=P_{uT}$) of the above columns at temperatures $T$=20/100-300-500-700 *ºC*. The observation of these post-buckling results prompts the following remarks:

(i) Due to its quite low $R_{GD}$ value and moderate slenderness ($\lambda_{cr}\cong$1.5), it is not surprising that the behaviors of the LC1 columns are virtually pure flexural-torsional, as attested by the observation of their collapse mode shapes in Fig. 6(b), where no distortional deformations are visible.

(ii) Conversely, the behaviors of the LC14 and LC17 columns are visibly affected by D-FT interaction, as attested by the observation of their collapse mode shapes in Fig. 6(b), which clearly combine distortional and flexural-torsional deformations. No qualitative differences are observed between the two sets of equilibrium paths (note that the horizontal axis scales are different).

(iii) As expected and regardless of the $R_{GD}$ value, the column strengths and failure loads decrease as the temperature rises, which means that the corresponding equilibrium paths "move downwards" (see Fig. 6(a)). The drop is most severe between 500 ºC and 600 ºC, which reflects the sudden increase in the rate of the CFS material behavior degradation, mostly felt through the proportionality limit strain and smoothness of the elliptic transition between the elastic and plastic ranges (see Figs. 4(a)-(b)) – note that, for $T\geq$600 °C, the CFS stress-strain curve exhibits again a well-defined yield plateau.

(iv) Out of the various equilibrium path trios (columns LC1, LC14 and LC17) corresponding to a given temperature, those associated with the LC1 columns are the smoothest – this is just a logical consequence of the fact that these columns exhibit a clearly pure flexural-torsional post-buckling behavior, not affected by D-FT interaction. The LC14 and LC17 column equilibrium paths, which are qualitatively similar, exhibit inflexion points prior to failure (less perceptible for the most elevated temperatures) – note that the former fall slightly below the latter, thus reflecting the higher strength and failure load erosion caused by the TI D-FT interaction (with respect to its SGI counterpart).

(v) Because the thermal action effects are negligible (uniform temperature and free-to-deform columns), the failure modes of a given column at different temperatures are practically identical – see Fig. 6(b).

(vi) The LC1 column plastic strain contours (including the yielded region locations) differ visibly for their (very similar) LC14 and LC17 column counterparts. In the latter, yielding starts at the bottom and top lip regions located at mid-height and in the vicinity of the fixed ends, respectively, then develops slowly at the mid-span top web-flange corner region (mostly) and end bottom web-flange corner regions, which explains the very pronounced elastic-plastic strength reserve prior to failure (note the closeness between the elastic and elastic-plastic equilibrium paths of the columns at 20/100 ºC) –

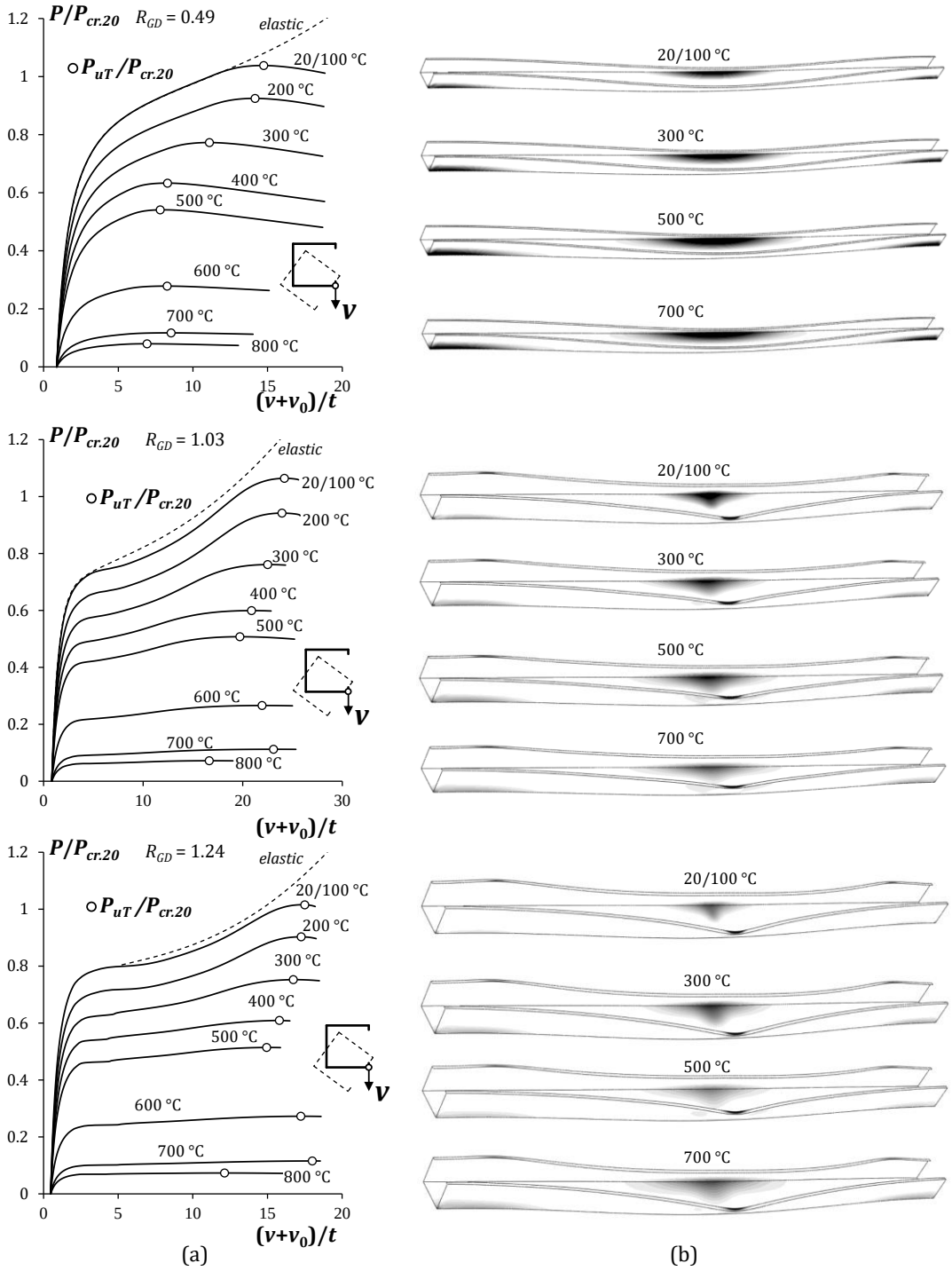


**Figure 6.** (a) Equilibrium paths $P/P_{cr.20}$ vs. $(v+v_0)/t$ and (b) (b) collapse modes with plastic strain contours of columns LC1, LC14 and LC17 columns, undergoing SDI, TI and SGI D-FT interaction, respectively, at elevated temperatures.

failure occurs after extensive yielding of the mid-height top web-flange corner region. In the LC1 columns, failure occurs soon after the first yielding (small elastic-plastic strength reserve) and is preceded by extensive yielding of the mid-height top web-flange corner region and end bottom web-flange corner regions.

(vii) No clear trend is observed regarding the influence, on the amount of elastic-plastic strength reserve and ductility prior to failure, of the column geometry, yield stress or temperature.

*4.2 Failure load data*

This section reports the output of the parametric study carried out to gather failure load data that will be used to assess the merits of the available DSM-based design approaches to predict the failure loads of fixed-ended LC columns undergoing TI, SGI and SDI D-FT interaction at elevated temperatures. A total of 2016 columns are analyzed, corresponding to all possible combinations of the (i) 21 geometries (cross-section dimensions and lengths) given in Table 1, (ii) 8 uniform temperatures ($T$=20/100-200-300-400-500-600-700-800 *ºC*), intended to simulate fire conditions, and (iii) 12 room-temperature yield stresses, selected to enable covering wide D-FT slenderness ranges for all columns sets (comprised between 0.20 and 3.72 – recall that $\lambda_{cr}=[P_y/P_{cr}]^{0.5}$). The numerical failure loads obtained in this parametric study are given in *21* tables included in Annex I: Tables I.1 to I.21 – each one regarding a given LC column geometry (see Table 1). Fig. 7 shows $P_{uT}/P_{yT}$ *vs.* $\lambda_{FT.T}$ plots for the various temperatures considered in this work – the elastic buckling curve $(\lambda_{FT.T})^{-2}$ is also included, for comparative purposes. In all plots, the white, black and grey circles stand for the failure loads of columns affected by TI, SGI and SDI D-FT interaction, respectively. The joint observation of these plots and tables prompts the following remarks:

(i) Regardless of the temperature, the $P_{uT}/P_{yT}$ vs. $\lambda_{FT.T}$ "clouds" follow the trend of "Winter-type" strength curves and the "vertical dispersion" is quite small along the slenderness ranges considered.

(ii) The failure loads of the column affected by SDI ($R_{GD}$<0.8), TI (0.8≤$R_{GD}$≤1.20) and SGI ($R_{GD}$>1.20) D-FT interaction are fairly well mingled (white, black and grey circles "on top of each other), particularly in the moderate slenderness range. Nevertheless, it is possible to observe that ($ii_1$) the TI failure loads are a bit higher in the stocky columns ($\lambda_{FT.T}$≤1.5) at $T$≥400 ºC and ($ii_2$) the SDI failure loads are marginally smaller in the slender columns ($\lambda_{FT.T}$≥2.0) at all temperatures.

(iii) In the low-to-moderate slenderness range ($\lambda_{FT.T}$≤1.5), all $P_{uT}/P_{yT}$ values concerning elevated temperatures (T>100 ºC) are below their room/moderate-temperature counterparts (the elastic

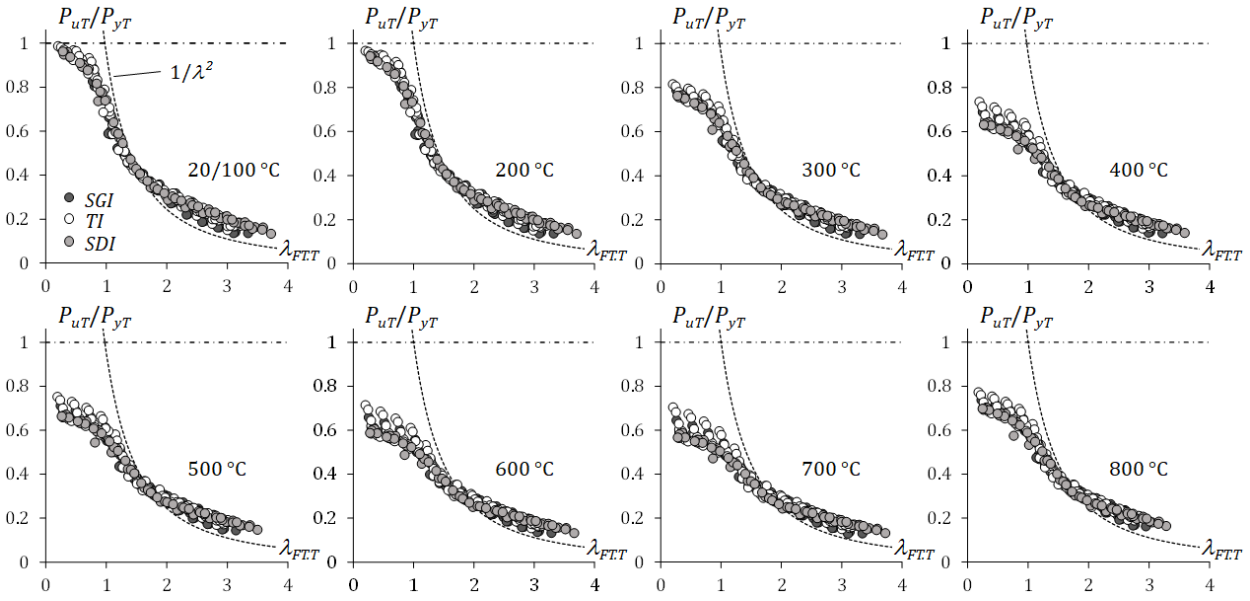


**Figure 7.** $P_{uT}/P_{yT}$ vs. $\lambda_{FT.T}$ plots concerning all the LC columns analyzed in this work ($T$=20/100-800 ºC) – the elastic buckling curves are also displayed.

buckling curves provide a useful reference to quantify these differences) – this does not happen in the moderate and high slenderness ranges ($\lambda_{FT.T}$>1.5).

(iv) The $P_{uT}/P_{yT}$ drop caused by the temperature increase does not follow the "logical" temperature sequence, *i.e.*, the decrease with the temperature is not monotonic. Indeed, the $P_{uT}/P_{yT}$ reduction is ordered in the sequence $T$ =20/100-200-300-800-500-400-600-700ºC (the "out of sequence" values are underlined). This unexpected finding, which has no obvious mechanical explanation based on the EC3-based temperature-dependent CFS constitutive model, must be investigated in the future – it may be related to the influence of the ratio $k_y/k_p$.

The above results are promising concerning the possibility of reaching an efficient (safe, accurate and reliable) DSM-based design approach for columns undergoing D-FT interaction at elevated temperatures.

## 5. DSM-Based Design at Elevated Temperatures

### *5.1 Available DSM-based design approach against column D and FT failures*

The DSM-based prediction of the failure loads gathered in the previous section, concerning CFS fixed-ended LC columns experiencing TI, SGI and SDI D-FT interaction at elevated temperatures, is addressed in this section. The first step consists of assessing the merits/adequacy of the available DSM-based design approaches against column pure D ($P_{nD.T}$) and FT ($P_{nFT.T}$) failures at elevated temperatures, proposed by Landesmann *et al.* (2019) and Bicelli *et al.* (2021), respectively – see Eqs. (4) and (5).

Figures 8 and 9 show the $P_{uT}/P_{nD.T}$ vs. $\lambda_{D.T}$ and $P_{uT}/P_{nFT.T}$ vs. $\lambda_{FT.T}$ plots for all the columns analyzed in this work, thus enabling a quick and visual assessment of the quality (accuracy and safety) of the failure load predictions provided by the strength curves defined in Eqs. (4) and (5) – note that all the $P_{uT}/P_{nD.T}$ and $P_{uT}/P_{nFT.T}$ values are given in Tables I.1 to I.21, included in Annex I. A more quantitative assessment can be found in Table 3, which provides the $P_{uT}/P_{nD.T}$ and $P_{uT}/P_{nFT.T}$ statistical indicators (averages, standard deviations and maximum/minimum values), as well as the numbers of "clearly unsafe" failure load estimates (in the sense that $P_{uT}/P_{nD.T}$ <0.95 or $P_{uT}/P_{nFT.T}$ <0.95). The observation of the results presented in these figures and tables prompts the following comments:

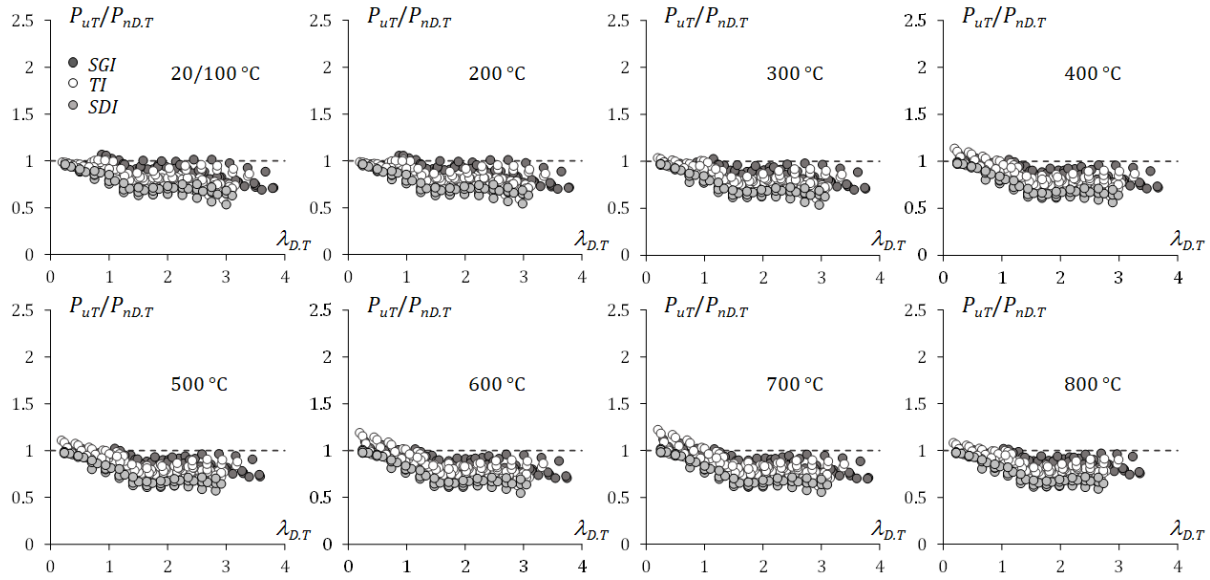


**Figure 8.** $P_{uT}/P_{nD.T}$ *vs.* $\lambda_{D.T}$ plots for all the LC columns analyzed in this work ($T$=20/100-800 ºC).

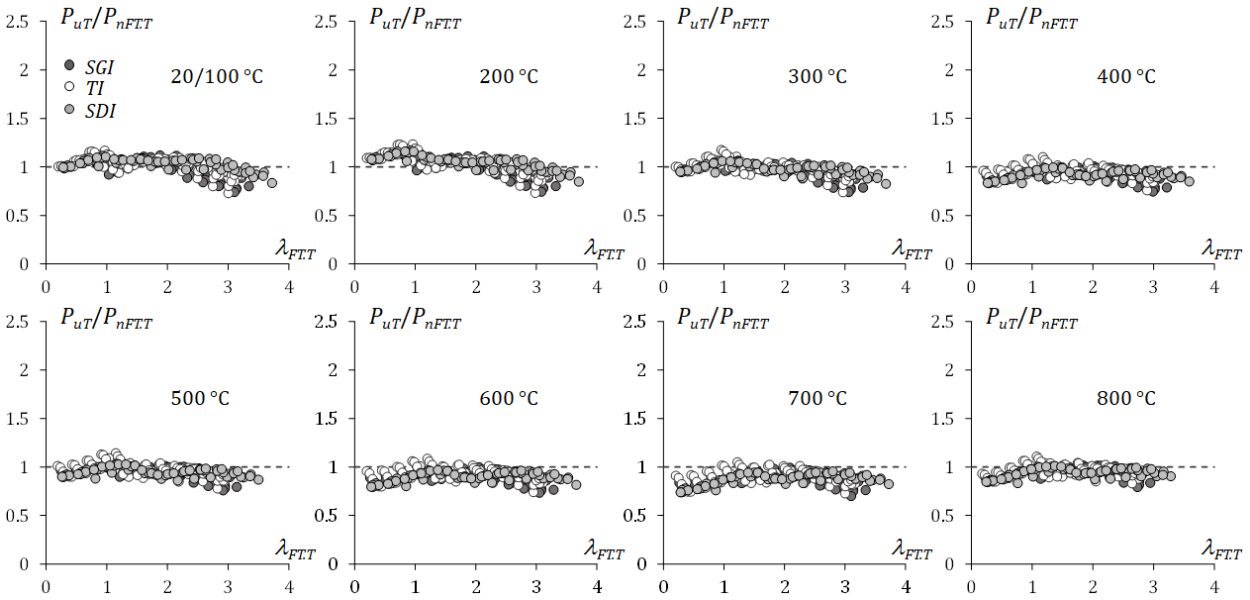


**Figure 9.** $P_{uT}/P_{nFT.T}$ *vs.* $\lambda_{FT.T}$ plots for all the LC columns analyzed in this work ($T$=20/100-800 ºC).

**Table 3.** $P_{uT}/P_{nD.T}$ and $P_{uT}/P_{nFT.T}$ statistical indicators for the LC columns analyzed in this work ($T$=20/100-800 ºC).

| $T$ (°C) | | 100 | | 200 | | 300 | | 400 | | 500 | | 600 | | 700 | | 800 | |
|---|---|---|---|---|---|---|---|---|---|---|---|---|---|---|---|---|---|
| $P_{uT}/P_{nD.T}$ | $\lambda_{D.T}$ | ≤1.0 | >1.0 | ≤1.0 | >1.0 | ≤1.0 | >1.0 | ≤1.0 | >1.0 | ≤1.0 | >1.0 | ≤1.0 | >1.0 | ≤1.0 | >1.0 | ≤1.0 | >1.0 |
| | *n* | 67 | 185 | 68 | 184 | 68 | 184 | 68 | 184 | 73 | 179 | 68 | 184 | 67 | 185 | 76 | 176 |
| | *Ave.* | 0.915 | 0.800 | 0.939 | 0.799 | 0.938 | 0.789 | 0.958 | 0.790 | 0.950 | 0.792 | 0.970 | 0.788 | 0.979 | 0.786 | 0.947 | 0.800 |
| | *S.D.* | 0.060 | 0.104 | 0.057 | 0.104 | 0.058 | 0.100 | 0.070 | 0.098 | 0.063 | 0.098 | 0.081 | 0.098 | 0.086 | 0.098 | 0.057 | 0.098 |
| | *Max.* | 1.067 | 1.023 | 1.056 | 1.029 | 1.037 | 1.027 | 1.138 | 1.017 | 1.108 | 1.022 | 1.190 | 1.015 | 1.221 | 1.015 | 1.082 | 1.017 |
| | *Min.* | 0.755 | 0.533 | 0.758 | 0.543 | 0.771 | 0.537 | 0.765 | 0.563 | 0.768 | 0.572 | 0.763 | 0.547 | 0.762 | 0.556 | 0.772 | 0.590 |
| | *<0.95* | 32 | 170 | 34 | 170 | 34 | 171 | 30 | 175 | 36 | 169 | 26 | 176 | 21 | 178 | 37 | 163 |
| $P_{uT}/P_{nFT.T}$ | $\lambda_{FT.T}$ | ≤2.0 | >2.0 | ≤2.0 | >2.0 | ≤2.0 | >2.0 | ≤2.0 | >2.0 | ≤2.0 | >2.0 | ≤2.0 | >2.0 | ≤2.0 | >2.0 | ≤2.0 | >2.0 |
| | *n* | 144 | 108 | 145 | 107 | 146 | 106 | 150 | 102 | 156 | 96 | 146 | 106 | 144 | 108 | 166 | 86 |
| | *Ave.* | 1.057 | 0.971 | 1.089 | 0.969 | 1.008 | 0.938 | 0.934 | 0.916 | 0.974 | 0.927 | 0.910 | 0.902 | 0.875 | 0.893 | 0.948 | 0.946 |
| | *S.D.* | 0.039 | 0.091 | 0.055 | 0.088 | 0.048 | 0.071 | 0.057 | 0.057 | 0.053 | 0.056 | 0.062 | 0.058 | 0.071 | 0.060 | 0.055 | 0.049 |
| | *Max.* | 1.167 | 1.114 | 1.233 | 1.107 | 1.173 | 1.041 | 1.101 | 1.011 | 1.143 | 1.013 | 1.085 | 1.010 | 1.050 | 1.011 | 1.108 | 1.022 |
| | *Min.* | 0.921 | 0.728 | 0.964 | 0.733 | 0.903 | 0.738 | 0.831 | 0.745 | 0.877 | 0.758 | 0.795 | 0.734 | 0.740 | 0.701 | 0.834 | 0.794 |
| | *<0.95* | 4 | 40 | 0 | 41 | 8 | 50 | 94 | 70 | 64 | 54 | 108 | 88 | 126 | 92 | 83 | 32 |

(i) Concerning the LC columns at room-moderate temperatures ($T$≤100 ºC), most of their failure loads are clearly overestimated by the $P_{nD.T}$ values – the exceptions are some stocky column failure loads, which are either slightly underestimated or overestimated. In order to back this assertion, note that the $P_{uT}/P_{nD.T}$ averages, standard deviations, maximum and minimum values read 0.915-0.060-1.067-0.755, for $\lambda_{D.T}$≤1.0, and 0.800-0.104-1.023-0.533, for $\lambda_{D.T}$>1.0 (see Table 3). Moreover, the numbers of "clearly unsafe" failure load estimates are 32 (out of 67), for $\lambda_{D.T}$≤1.0, and 170 (out of 185), for $\lambda_{D.T}$>1.0. It is worth noting that, the above overestimation is slightly larger for the

column affected by SDI D-FT interaction than for those undergoing TI and SGI D-FT interaction. Therefore, it can be concluded that the occurrence of D-FT interaction generally entails a failure load erosion (with respect to the pure D ultimate strength), which is relatively small for the stocky columns and becomes quite visible in most of the remaining ones – it tends to grow with $\lambda_{D.T}$.

(ii) Again, for the LC columns at room-moderate temperatures ($T \leq 100$ ºC), a large number of their failure loads are fairly accurately estimated by the $P_{nFT.T}$ values – the exceptions are most of the slender columns ($\lambda_{FT.T} > 2.0$), particularly those undergoing TI and SGI D-FT interaction, whose failure loads are reasonably overestimated. To back this assertion, note that the averages, standard deviations, maximum and minimum $P_{uT}/P_{nFT.T}$ values read 1.057-0.039-1.167-0.921, for $\lambda_{FT.T} \leq 2.0$, and 0.971-0.091-1.114-0.728, for $\lambda_{FT.T} > 2.0$ (see Table 3). Therefore, it can be concluded that the occurrence of D-FT interaction entails very little or no failure load erosion (with respect to the pure FT ultimate strength) for the less slender columns ($\lambda_{FT.T} \leq 2.0$) – conversely, the failure load erosion is clearly visible for the most slender columns affected by TI and SGI D-FT interaction (less so for those experiencing SDI D-FT interaction).

(iii) Concerning the quality of the $P_{nD.T}$ failure load predictions, the findings included in item (i) above remain essentially valid for the columns at elevated temperatures ($T > 100$ ºC). The only (small) difference is the fact that, for $T \geq 400$ ºC, the failure loads of a few stocky ($\lambda_{D.T} \leq 1.0$) columns affected by TI D-FT interaction are slightly underestimated by the $P_{nD.T}$ values – see Fig. 8.

(iv) Concerning the quality of the $P_{nFT.T}$ failure load predictions, the findings included in item (ii) above remain essentially valid for the columns at elevated temperatures not exceeding 300 C. For higher temperatures, the vast majority of the column failure loads are moderately overestimated – the only exception are the columns at $T$=800 ºC, for which the number of failure load overestimations is visibly smaller. Moreover, it is also interesting to notice that the largest failure load overestimations occur for the stocky ($\lambda_{FT.T} \leq 1.0$) columns affected by SDI D-FT interaction and the very slender ($\lambda_{FT.T} > 2.5$) columns undergoing TI and SGI D-FT interaction − see Fig. 9. Therefore, it can be concluded that the occurrence of D-FT interaction only entails moderate failure load erosion (with respect to the pure FT ultimate strength) for most columns at 400 ºC$\leq T <$800 ºC – for columns at $T$=200 ºC and $T$=300 ºC, visible failure load overestimations only occur for the most slender ($\lambda_{FT.T} > 2.0$) columns, particularly for those affected by TI and SGI D-FT interaction.

The findings reported above show that the $P_{nD.T}$ (see Eq. (4) – Landesmann *et al.* 2019) and $P_{nFT.T}$ (see Eq. (5) – Bicelli *et al.* 2021) DSM-based design approaches are unable to predict adequately the failure loads of CFS fixed-ended LC columns affected by D-FT interaction at both room and elevated temperatures. Nevertheless, it should be noted that the failure load prediction qualities provided by the $P_{nD.T}$ and $P_{nFT.T}$ values differ visibly: while the former yield clear overestimations (except for some columns with $\lambda_{D.T} \leq 1.0$), the latter provide (i) fairly accurate estimates for columns with $\lambda_{FT.T} \leq 2.0$ at temperatures $T \leq 300$ ºC, and (ii) moderate overestimations for the remaining columns.

### *5.2 DSM-based design approach against column D-FT interactive failures*

Next, the methodology first put forward by Schafer (2002) to handle interactive failures in CFS members, which was subsequently used by several authors in the context of various coupling phenomena, is adopted here to establish DSM-based design approaches intended to predict the failure loads of columns experiencing TI, SGI and SDI D-FT interaction. The application of this methodology to Eqs. (4) and (5) leads to two DSM-based design approaches, denoted here as $P_{nD\text{-}FT.T}$ and $P_{nFT\text{-}D.T}$, respectively. While the former involves replacing $P_{yT}$ with $P_{nFT.T}$ in Eq. (4), the latter consists of replacing $P_{yT}$ with $P_{nD.T}$ in Eq. (5) – the expressions providing the $P_{nD\text{-}FT.T}$ and $P_{nFT\text{-}D.T}$, values then read

$$P_{nD-FT.T}=\begin{cases} P_{nFT.T}\cdot\left(k_p/k_y\right) & \lambda_{DFT.T}\le\dfrac{0.561}{\left(k_p/k_y\right)} \\ P_{nFT.T}\left[1-\dfrac{0.25}{\left(k_p/k_y\right)}\dfrac{1}{\lambda_{DFT.T}^{1.2}}\right]\dfrac{1}{\lambda_{DFT.T}^{1.2}} & \lambda_{DFT.T}>\dfrac{0.561}{\left(k_p/k_y\right)} \end{cases} \qquad \lambda_{DFT.T}=\sqrt{\frac{P_{nFT.T}}{P_{crD.T}}}\ , \qquad (7)$$

$$P_{nFT-D.T}=\begin{cases} P_{nD.T}\,\eta\left(0.658\right)^{\eta^{1.2}\cdot\lambda_{FTD.T}^{2}} & \lambda_{FTD.T}\le 1.5 \\ P_{nD.T}\left(\dfrac{a}{\lambda_{FTD.T}^{b}}\right) & \lambda_{FTD.T}>1.5 \end{cases} \qquad \lambda_{FTD.T}=\sqrt{\frac{P_{nD.T}}{P_{crFT.T}}}\ , \qquad (8)$$

where (i) $\lambda_{DFT.T}$ and $\lambda_{FTD.T}$ are the interactive slenderness values, and (ii) $P_{crD.T}$ and $P_{crFT.T}$ are the D and FT critical buckling loads at a given temperature $T$. The influence of the temperature on $\lambda_{DFT.T}$ and $\lambda_{FTD.T}$ is felt through (i) $P_{crD.T}$ and $P_{crFT.T}$, and (ii) $P_{nD.T}$ and $P_{nFT.T}$, all dependent on the Young's modulus, whose value decreases with $T$. At this stage, it is worth mentioning that Martins *et al.* (2018) followed this same methodology for CFS fixed-ended columns affected by D-FT at room temperature. However, they used the currently codified DSM global design curve ($P_{nG}$), instead of $P_{nFT}$ (not yet available at the time – it only appeared two years later) – naturally, this fact must be taken into account when interpreting the findings reported by Martins *et al.* (2018).

Figures 10 and 11 show the $P_{uT}/P_{nD\text{-}FT.T}$ vs. $\lambda_{FT.T}$ and $P_{uT}/P_{nFT\text{-}D.T}$ vs. $\lambda_{FT.T}$ plots for all the columns analyzed in this work. Note that, for the sake of clarity, the slenderness $\lambda_{FT.T}$ replaces its interactive counterparts $\lambda_{DFT.T}$ and $\lambda_{FTD.T}$ in these plots – the $P_{uT}/P_{nD\text{-}FT.T}$ vs. $\lambda_{DFT.T}$ and $P_{uT}/P_{nFT\text{-}D.T}$ vs. $\lambda_{FTD.T}$ plots are more difficult to interpret. As done before, the $P_{uT}/P_{nD\text{-}FT.T}$ and $P_{uT}/P_{nFT\text{-}D.T}$ statistical indicators and numbers of "clearly unsafe" failure load estimates are given in Table 4 – the $P_{uT}/P_{nD\text{-}FT.T}$ and $P_{uT}/P_{nFT\text{-}D.T}$ values of all the columns analyzed in this work are provided in Tables I.1 to I.21, included in Annex I. The observation of the results presented in these two figures and table prompts the following remarks:

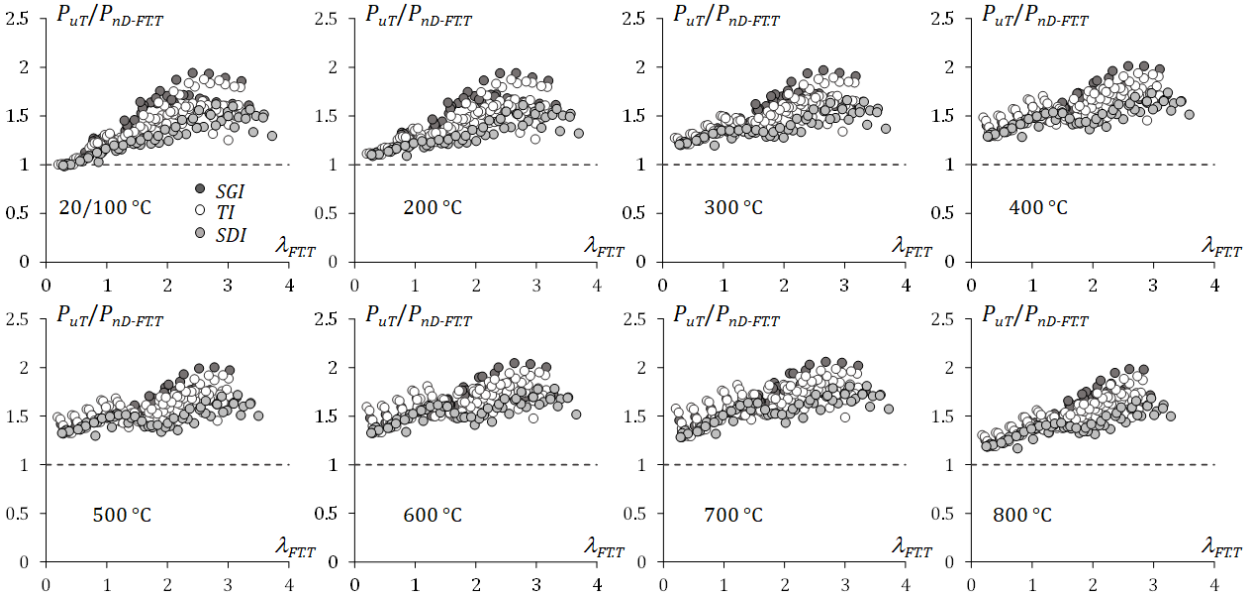


**Figure 10.** $P_{uT}/P_{nD\text{-}FT.T}$ vs. $\lambda_{FT.T}$ plots for all the columns analyzed in this work ($T$=20/100-800 ºC).

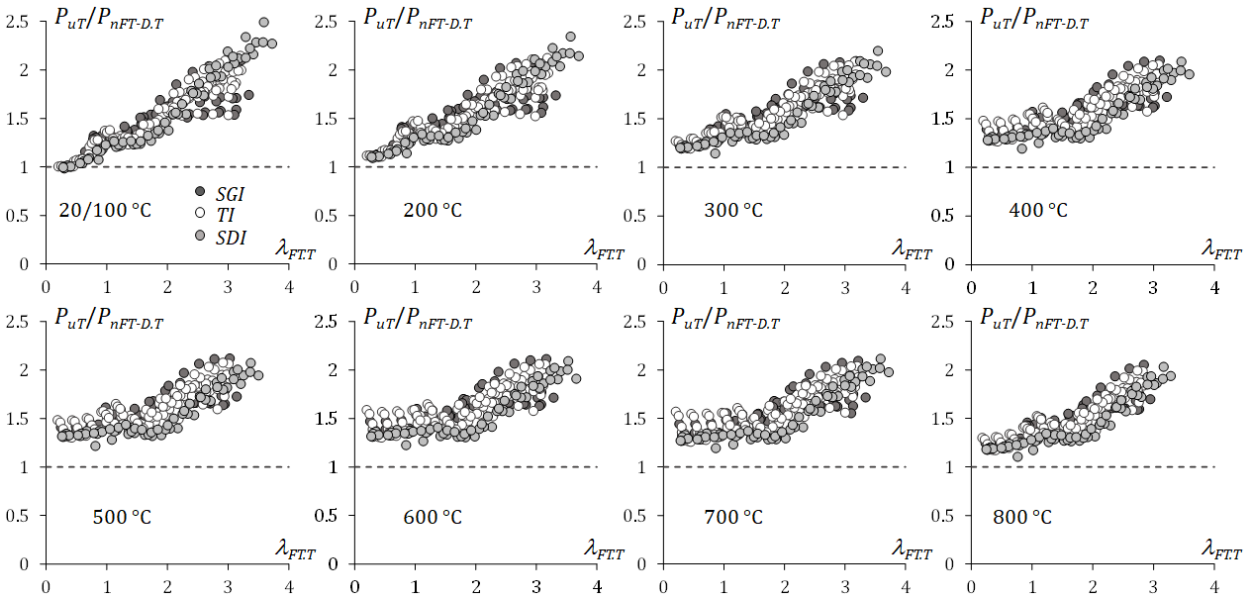


**Figure 11.** $P_{uT}/P_{nFT\text{-}D.T}$ vs. $\lambda_{FT.T}$ plots for all the columns analyzed in this work ($T$=20/100-800 ºC).

**Table 4**. $P_{uT}/P_{nD\text{-}FT.T}$ and $P_{uT}/P_{nFT\text{-}D.T}$ statistical indicators for the LC columns analyzed in this work ($T$=20/100-800 ºC).

| $T$ (°C) | | 20/100 | 200 | 300 | 400 | 500 | 600 | 700 | 800 |
|---|---|---|---|---|---|---|---|---|---|
| $P_{uT}/P_{nD\text{-}FT.T}$ | *n* | 252 | 252 | 252 | 252 | 252 | 252 | 252 | 252 |
| | *Ave.* | 1.384 | 1.412 | 1.477 | 1.569 | 1.556 | 1.623 | 1.632 | 1.479 |
| | *S.D.* | 0.237 | 0.206 | 0.177 | 0.160 | 0.148 | 0.156 | 0.173 | 0.183 |
| | *Max.* | 1.943 | 1.940 | 1.969 | 2.012 | 2.001 | 2.046 | 2.058 | 1.984 |
| | *Min.* | 0.984 | 1.091 | 1.197 | 1.286 | 1.297 | 1.326 | 1.283 | 1.167 |
| | *<0.95* | 0 | 0 | 0 | 0 | 0 | 0 | 0 | 0 |
| $P_{uT}/P_{nFT\text{-}D.T}$ | *n* | 252 | 252 | 252 | 252 | 252 | 252 | 252 | 252 |
| | *Ave.* | 1.492 | 1.532 | 1.540 | 1.554 | 1.575 | 1.580 | 1.552 | 1.467 |
| | *S.D.* | 0.340 | 0.294 | 0.250 | 0.217 | 0.208 | 0.210 | 0.220 | 0.222 |
| | *Max.* | 2.491 | 2.343 | 2.198 | 2.099 | 2.120 | 2.113 | 2.114 | 2.052 |
| | *Min.* | 0.984 | 1.091 | 1.143 | 1.192 | 1.218 | 1.226 | 1.193 | 1.103 |
| | *<0.95* | 0 | 0 | 0 | 0 | 0 | 0 | 0 | 0 |

(i) The D-FT failure load predictions yielded by the $P_{nD\text{-}FT.T}$ and $P_{nFT\text{-}D.T}$ values are qualitatively similar for all the columns analyzed in this work. Indeed, both estimations provide exclusively safe failure load estimates and, regardless of the temperature, the amount of underestimation grows visibly with the column slenderness $\lambda_{FT.T}$ – this growth is slightly more pronounced in the $P_{uT}/P_{nFT\text{-}D.T}$ vs. $\lambda_{FT.T}$ plots. Moreover, the observation of the Table 4 also shows that, in average, the amount of underestimation also grows slightly with the temperature, with three exceptions: minute average decrease between 400 ºC and 500 ºC ($P_{uT}/P_{nD\text{-}FT.T}$) and at visible average decrease between 700 ºC and 800 ºC ($P_{uT}/P_{nD\text{-}FT.T}$ and $P_{uT}/P_{nFT\text{-}D.T}$).

(ii) The $P_{uT}/P_{nD\text{-}FT.T}$ vs. $\lambda_{FT.T}$ and $P_{uT}/P_{nFT\text{-}D.T}$ vs. $\lambda_{FT.T}$ plots displayed in Figs. 10 and 11 are very similar, both qualitatively and quantitatively, which is attested by the statistical indicators given in Table 4. Indeed, the $P_{uT}/P_{nD\text{-}FT.T}$ and $P_{uT}/P_{nFT\text{-}D.T}$ averages, standard deviations and maximum/minimum values, concerning the eight temperatures considered in this work, fall inside the following interval

sets: 1.384-1.632 vs. 1.467-1.580, 0.148-0.237 vs. 0.208-0.340, 1.940-2.058 vs. 2.052-2.491 and 0.984-1.326 vs. 0.984-1.226, respectively for the $P_{uT}/P_{nD\text{-}FT.T}$ and $P_{uT}/P_{nFT\text{-}D.T}$ values.

(iii) For $T$=20/100+200+300+500 ºC, the $P_{nD\text{-}FT.T}$ failure load predictions marginally outperform their $P_{nFT\text{-}D.T}$ counterparts, as attested by the slightly lower $P_{uT}/P_{nD\text{-}FT.T}$ averages, standard deviations and maximum values (even if two minimum values are a bit higher).

(iv) Conversely, for $T$=400+600+700+800 ºC the $P_{nFT\text{-}D.T}$ failure load predictions are marginally superior to their $P_{nD\text{-}FT.T}$ counterparts, as attested by the slightly better $P_{nD\text{-}FT.T}$ averages, maximum and minimum values (even if the standard deviations are a bit higher).

(v) In general, and as it would be logical to anticipate, the $P_{nD\text{-}FT.T}$ and $P_{nFT\text{-}D.T}$ lower failure load overestimations occur for the columns affected by SDI D-FT interaction, whose post-buckling behavior is predominantly FT.

In summary, the joint observation of the results presented in Figs. 8 to 11 and Tables 3, 4 and I.1 to I.21 (included in Annex I) makes it possible to draw the following conclusions, concerning the DSM-based design of CFS fixed-ended LC columns undergoing TI, SGI or SDI D-FT interaction:

(i) The $P_{nD.T}$ strength curves, developed for CFS fixed-ended columns failing in pure D modes at elevated temperatures, are clearly unable to handle adequately columns experiencing TI, SGI or SDI D-FT interaction at either room or elevated temperatures – practically all failure loads estimates are unsafe and the overestimation is considerable for a very large number of columns.

(ii) The $P_{nFT.T}$ strength curves, developed for CFS fixed-ended columns failing in pure FT modes at elevated temperatures, are only able to handle reasonably well columns experiencing SDI D-FT interaction at temperatures up to 300 ºC[4]. Most of the remaining column failure load estimates are unsafe (although less so than their $P_{nD.T}$ counterparts).

(iii) Since the contents of the previous two items show that the occurrence of failure load erosion due to D-FT interaction, it was necessary to search for a DSM-based design approach capable of handling adequately columns affected by (TI, SGI or SDI) D-FT interaction. Two such design approaches were considered, namely the $P_{nD\text{-}FT.T}$ and $P_{nFT\text{-}D.T}$ ones, both based on an idea first put forward by Schafer (2002) and both providing qualitatively and quantitatively similar failure load predictions. However, those failure load predictions were shown to be inadequate: although all of them are safe, a large number of them are excessively conservative and, therefore, lead to uneconomic designs.

(iv) The contents of the above items clearly show the need to search for an efficient (safe, accurate and reliable) DSM-based design approach to handle LC columns undergoing D-FT interaction at room and elevated temperatures failures. It seems that a good starting point is the $P_{nFT.T}$ design approach – the corresponding strength curves need to be modified/"lowered" and the modifications should involve the buckling load ratio $R_{GD}$ (and maybe also the temperature $T$).

[4] Since the post-buckling behavior of the columns affected by SDI D-FT is predominantly FT, it is surprising to observe that the failure load prediction quality provided by the $P_{nFT.T}$ values at room temperature falls below that achieved by Bicelli *et al.* (2021). Although further investigation (already under way) is necessary to clarify this issue, it seems plausible that this unexpected discrepancy stems from the fact that the all the columns considered in this work exhibit a flexural-torsional-distortional post-buckling behavior (see footnote 3, in page 5), while those analyzed by Bicelli *et al.* (2021) exhibited a pure flexural-torsional post-buckling behavior. It is possible that the presence of anti-symmetric distortional deformations (GBT deformation mode **6**) in the so-called "global" buckling mode causes the column post-buckling strength and failure load to drop.

## 6. Concluding Remarks

This work reported the available results of an ongoing numerical investigation dealing with the post-buckling behavior, strength and DSM design of cold-formed steel fixed-ended columns experiencing interaction between distortional and flexural/torsional and distortional buckling at room and elevated temperatures – the results presented and discussed concern lipped channel columns under temperatures up to 800 ºC, typically caused by fire conditions.

After providing the motivation for this research effort, which included an overview of the available DSM-based design approaches against pure distortional and pure flexural-torsional failures at room and elevated temperatures (Landesmann *et al.* 2019, Bicelli *et al.* 2021), the paper addressed the selection of column geometries prone to three types of D-FT interaction, depending on the $R_{GD}=P_{crG}/P_{crD}$ value: "True D-G interaction" (TI – $0.9 \leq R_{GD} \leq 1.10$), "Secondary distortional bifurcation D-G interaction" (SDI – $R_{GD}<0.9$) and "Secondary global bifurcation D-G interaction" (SGI – $R_{GD}>1.10$) – note that the last two occur when the squash load $P_y$ is sufficiently higher than the largest of $P_{crG}$ and $P_{crD}$. Then, the influence of the (elevated) temperature on the post-buckling behavior and failure of columns affected by these three types of D-FT interaction is briefly investigated.

Then, numerical failure load data were gathered, concerning a total of 2016 columns affected by various types and levels of D-FT interaction and (i) exhibiting 21 geometries (cross-section dimensions and lengths), (ii) having 12 room-temperature yield stresses, chosen to cover wide D-FT slenderness ranges (0.20 to 3.72), and (iii) subjected to 8 uniform temperatures (up to 800 *ºC*). Finally, the above numerical D-FT interactive failure loads were used to assess the merits of their prediction by (i) the available DSM-based design approaches against pure D ($P_{nD.T}$) and pure FT ($P_{nFT.T}$) failures and (ii) the DSM-based design approaches that combine the previous ones ($P_{nD\text{-}FT.T}$ and $P_{nFT\text{-}D.T}$). The main findings of this merit assessment are the following:

(i) The $P_{nD.T}$ values provide unsafe estimates of all the D-FT interactive failure loads obtained in this work – moreover, the vast majority of them are substantially overestimated (the very few exceptions concern very stocky columns).

(ii) The $P_{nFT.T}$ values only provide safe and accurate estimates of the failure loads of columns affected by SDI D-FT interaction at temperatures up to 300 ºC. The overwhelming majority of the remaining column failure loads are visibly overestimated (but much less than by the $P_{nD.T}$ values).

(iii) The $P_{nD\text{-}FT.T}$ and $P_{nFT\text{-}D.T}$ values provide very similar, quantitatively and qualitatively, failure load estimates for the failure load data gathered in this work. Although all these estimates are safe, the vast majority of them are uneconomic (excessively conservative) − the amount of failure load overestimation grows with the column slenderness.

(iv) It was shown that there is a clear need for an efficient DSM-based design approach to handle fixed-ended lipped channel columns undergoing D-FT interaction. It seems that a good starting point consists of modifying/"lowering" the strength curves prescribed by the $P_{nFT.T}$ design approach, by incorporating numerically-determined parameters dependent on the buckling load ratio $R_{GD}$ (and maybe also the temperature $T$).

Finally, it is worth noting that the findings reported in this work provide encouragement to search for a DSM-based design approach for CFS lipped channel columns affected by D-FT interaction at room and elevated temperatures. Once this immediate goal is achieved, the scope of the ongoing research effort will be extended to columns with other cross-section shapes and/or support conditions, in order to attain the

final goal of an efficient DSM-based design approach for CFS singly-symmetric (with respect to the major axis) columns failing in D-FT interactive modes at room and elevated temperatures.


## Acknowledgments

The first two authors gratefully acknowledge the financial support of the Brazilian institutions (i) CAPES (Coordenação de Aperfeiçoamento de Pessoal de Nível Superior) – Finance Code 001, (ii) CNPq (Conselho Nacional de Desenvolvimento Científico e Tecnológico) – Finance Codes 141042/2020-6 and 13197/2020-2, and (iii) FAPERJ (Fundação Carlos Chagas Filho de Amparo à Pesquisa do Estado do Rio de Janeiro) – Finance Code E-26/200.959/2021 (second author). The third author gratefully acknowledges the financial support of FCT (Fundação para a Ciência e a Tecnologia – Portugal), through project UIDB/04625/2020 (funding the research unit CERIS).


## References


ABNT (Brazilian Standards Association) (2010). *Brazilian Standard on Design of Cold-Formed Steel Structures* (ABNT NBR 14762:2010), Rio de Janeiro. (Portuguese).

AISI (American Iron and Steel Institute) (2022). *North American Specification (NAS) for the Design of Cold-Formed Steel Structural Members* (2016 edition reaffirmed in 2020 with Supplement 3), AISI-S100-16 w/S3-22, Washington DC.

Arrais F, Lopes N, Real PV (2021). Fire design of slender cold-formed lipped channel and sigma section members with uniform temperature under compression, *Fire Safety Journal*, **122**(June), paper 103340.

AS/NZS (Standards of Australia and Standards of New Zealand) (2018). *Cold-Formed Steel Structures* (AS/NZS 4600:2018 – 3rd edition), Sydney-Wellington.

Bandula Heva Y, Mahendran M (2012). Flexural-torsional buckling tests of cold-formed steel compression members at elevated temperatures, *Steel and Composite Structures*, **14**(3), 205-227.

Bebiano R, Camotim D, Gonçalves R (2018). GBTUL 2.0 – a second-generation code for the GBT-based buckling and vibration analysis of thin-walled members, *Thin-Walled Structures*, **124**(March), 235-257.

Bicelli AA, Landesmann A, Camotim D, Dinis PB (2021). Flexural–torsional failure and DSM design of fixed-ended cold-formed steel columns at elevated temperatures. *Thin-Walled Structures*, **169**(December), paper 108362.

Camotim D, Dinis PB (2013). Distortional-global interaction in lipped channel columns. *Proceedings of the Institution of Civil Engineers - Structures and Building*, **166**(September), 381-391.

Camotim D, Dinis PB, Martins AD (2016). Direct Strength Method (DSM) – a general approach for the design of cold-formed steel structures, *Recent Trends in Cold-Formed Steel Construction*, C. Yu (ed.), Woodhead Publishing (Series in Civil and Structural Engineering), Amsterdam, 69-105.

Comité Européen de Normalisation (CEN) (2005). *Eurocode 3: Design of Steel Structures – Part 1.2: General Rules – Structural Fire Design*, Brussels.

Dinis PB, Camotim D (2011). Post-buckling behaviour and strength of cold-formed steel lipped channel columns experiencing distortional-global interaction. *Computers & Structures*, **89**(February),422-434.

Dinis PB, Camotim D, Landesmann A, Martins AD (2019). On the Direct Strength Method design of columns against global failures, *Thin-Walled Structures*, **139**(June), 242-270.

Dinis PB, Camotim D, Landesmann A, Martins AD (2020). Improving the Direct Strength Method prediction of column flexural-torsional failure loads, *Thin-Walled Structures*, **148**(March), paper 106461.

Ellobody E, Young B (2005). Behavior of cold-formed steel plain angle columns, *Journal of Structural Engineering* (ASCE), **131**(3), 469-478.

Ferreira Filho EB, Landesmann A, Camotim D (2022). Distortional-global interactive failure and DSM design of CFS lipped channel columns at elevated temperatures, *The Online Collection for Conference Papers in Civil*

*Engineering* (International Colloquium on Stability and Ductility of Steel Structures – SDSS 2022, Aveiro, September 14-16), P. Vila Real, N. Lopes (Eds.), **5**(4), 448-457, Ernst & Sohn.

Gunalan S, Bandula Heva Y, Mahendran M (2014). Flexural-torsional buckling behaviour and design of cold-formed steel compression members at elevated temperatures. *Engineering Structures*, **79**(November), 149-168.

Landesmann A, Camotim D, Silva FCM (2019). DSM design of cold-formed steel columns failing in distortional modes at elevated temperatures, *International Journal of Steel Structures*, **19**(3), 1023-1041.

Martins AD, Camotim D, Dinis PB (2018). On the distortional-global interaction in cold-formed steel columns: relevance, post-buckling behaviour, strength and DSM design. *Journal of Constructional Steel Research*, **145**(June), 449-470.

Peköz T, Sümer O (1992), Design provisions for cold-formed steel columns and beam-columns, *Research Report* RP92-1, American Iron and Steel Institute (AISI), Washington DC.

Ranawaka T, Mahendran M (2010). Numerical modelling of light gauge cold-formed steel compression members subjected to distortional buckling at elevated temperatures. *Thin-Walled Structures*, **48**(April-May), 334-44.

Rokilan M, Mahendran M (2021). DSM design of CFS columns subject to distortional buckling at elevated temperatures. *Fire Safety Journal*, **125**(October), paper 103395.

Schafer BW (2002). Local, distortional and Euler buckling in thin-walled columns, *Journal of Structural Engineering* (ASCE), **128**(3), 288-299.

Schafer BW (2019). Advances in the Direct Strength Method of cold-formed steel design, *Thin-Walled Structures*, **140**(July), 533-541.

Simulia Inc. (2014). ABAQUS Standard (version 6.14-1).

## Annex I: Data Concerning the CFS Fixed-Ended LC Columns Analyzed in this Work

This annex consists of 21 tables (I.1 to I.21), dealing individually with each lipped channel (LC) cross-section geometry considered in this work (see Table 1 of the paper). Each table concerns 12 room temperature yield stresses ($f_{y20}$), associated with equally spaced slenderness values $\lambda_{cr.20}$, and 8 temperatures ($T$=20/100-200-300-400-500-600-700-800 ºC), and provides the values of (i) the critical (D or FT) slenderness at room temperature ($\lambda_{cr.20}$), (ii) the FT and D slenderness values at temperature $T$ ($\lambda_{FT.T}$ and $\lambda_{D.T}$), (iii) the failure-to-squash load ratios at temperature $T$ ($P_{uT}/P_{yT}$), and (iv) the numerical failure-to-predicted load ratios at temperature $T$ ($P_{uT}/P_{nFT.T}$, $P_{uT}/P_{nD.T}$, $P_{uT}/P_{nDFT.T}$ and $P_{uT}/P_{nFTD.T}$).

**Table I.1**: Numerical failure loads and their DSM estimates concerning the **LC1** column geometry with 12 room temperature yielding stresses (corresponding to equally spaced slenderness values) and 8 temperatures varying from $T$=20/100 to $T$=800 ºC.

| $T$ (ºC) | $\lambda_{cr,20}$ | 0.25 | 0.50 | 0.75 | 1.00 | 1.25 | 1.50 | 1.75 | 2.00 | 2.25 | 2.50 | 2.75 | 3.00 |
|---|---|---|---|---|---|---|---|---|---|---|---|---|---|
| 20/100 | $\lambda_{FT,T}$ | 0.355 | 0.711 | 0.865 | 1.153 | 1.442 | 1.730 | 2.018 | 2.307 | 2.595 | 2.883 | 3.172 | 3.460 |
| | $\lambda_{D,T}$ | 0.250 | 0.500 | 0.750 | 1.000 | 1.250 | 1.500 | 1.750 | 2.000 | 2.250 | 2.500 | 2.750 | 3.000 |
| | $P_{uT}/P_{yT}$ | 0.960 | 0.883 | 0.736 | 0.596 | 0.444 | 0.344 | 0.287 | 0.252 | 0.227 | 0.204 | 0.183 | 0.163 |
| | $P_{uT}/P_{nFT,T}$ | 1.012 | 1.091 | 1.007 | 1.040 | 1.061 | 1.009 | 0.973 | 0.972 | 0.975 | 0.969 | 0.951 | 0.921 |
| | $P_{uT}/P_{nD,T}$ | 0.960 | 0.883 | 0.806 | 0.795 | 0.718 | 0.661 | 0.643 | 0.651 | 0.662 | 0.668 | 0.665 | 0.653 |
| | $P_{uT}/P_{nDFT,T}$ | 1.012 | 1.091 | 1.029 | 1.144 | 1.214 | 1.217 | 1.246 | 1.316 | 1.390 | 1.450 | 1.488 | 1.502 |
| | $P_{uT}/P_{nFTD,T}$ | 1.012 | 1.091 | 1.073 | 1.207 | 1.230 | 1.268 | 1.375 | 1.543 | 1.737 | 1.932 | 2.117 | 2.283 |
| 200 | $\lambda_{FT,T}$ | 0.354 | 0.707 | 0.860 | 1.147 | 1.434 | 1.720 | 2.007 | 2.294 | 2.581 | 2.867 | 3.154 | 3.441 |
| | $\lambda_{D,T}$ | 0.249 | 0.497 | 0.746 | 0.994 | 1.243 | 1.492 | 1.740 | 1.989 | 2.237 | 2.486 | 2.735 | 2.983 |
| | $P_{uT}/P_{yT}$ | 0.941 | 0.867 | 0.725 | 0.594 | 0.445 | 0.344 | 0.286 | 0.252 | 0.226 | 0.204 | 0.183 | 0.164 |
| | $P_{uT}/P_{nFT,T}$ | 1.096 | 1.160 | 1.059 | 1.072 | 1.056 | 1.004 | 0.966 | 0.964 | 0.969 | 0.965 | 0.949 | 0.921 |
| | $P_{uT}/P_{nD,T}$ | 0.962 | 0.887 | 0.801 | 0.794 | 0.720 | 0.661 | 0.641 | 0.647 | 0.659 | 0.666 | 0.664 | 0.654 |
| | $P_{uT}/P_{nDFT,T}$ | 1.121 | 1.187 | 1.092 | 1.180 | 1.220 | 1.221 | 1.245 | 1.313 | 1.387 | 1.448 | 1.489 | 1.506 |
| | $P_{uT}/P_{nFTD,T}$ | 1.120 | 1.182 | 1.140 | 1.269 | 1.279 | 1.297 | 1.383 | 1.530 | 1.702 | 1.873 | 2.032 | 2.171 |
| 300 | $\lambda_{FT,T}$ | 0.351 | 0.702 | 0.854 | 1.139 | 1.424 | 1.708 | 1.993 | 2.278 | 2.562 | 2.847 | 3.132 | 3.416 |
| | $\lambda_{D,T}$ | 0.247 | 0.494 | 0.741 | 0.987 | 1.234 | 1.481 | 1.728 | 1.975 | 2.222 | 2.469 | 2.715 | 2.962 |
| | $P_{uT}/P_{yT}$ | 0.766 | 0.719 | 0.608 | 0.533 | 0.422 | 0.328 | 0.269 | 0.237 | 0.215 | 0.196 | 0.178 | 0.161 |
| | $P_{uT}/P_{nFT,T}$ | 0.969 | 1.028 | 0.941 | 0.995 | 1.003 | 0.951 | 0.903 | 0.903 | 0.916 | 0.922 | 0.916 | 0.898 |
| | $P_{uT}/P_{nD,T}$ | 0.975 | 0.915 | 0.780 | 0.776 | 0.722 | 0.656 | 0.622 | 0.625 | 0.640 | 0.651 | 0.654 | 0.649 |
| | $P_{uT}/P_{nDFT,T}$ | 1.232 | 1.308 | 1.197 | 1.271 | 1.314 | 1.289 | 1.278 | 1.335 | 1.413 | 1.481 | 1.530 | 1.556 |
| | $P_{uT}/P_{nFTD,T}$ | 1.222 | 1.263 | 1.143 | 1.266 | 1.298 | 1.291 | 1.335 | 1.459 | 1.617 | 1.778 | 1.927 | 2.059 |
| 400 | $\lambda_{FT,T}$ | 0.343 | 0.685 | 0.834 | 1.111 | 1.389 | 1.667 | 1.945 | 2.223 | 2.501 | 2.778 | 3.056 | 3.334 |
| | $\lambda_{D,T}$ | 0.241 | 0.482 | 0.723 | 0.964 | 1.205 | 1.445 | 1.686 | 1.927 | 2.168 | 2.409 | 2.650 | 2.891 |
| | $P_{uT}/P_{yT}$ | 0.643 | 0.612 | 0.520 | 0.476 | 0.403 | 0.322 | 0.262 | 0.229 | 0.210 | 0.193 | 0.178 | 0.162 |
| | $P_{uT}/P_{nFT,T}$ | 0.860 | 0.913 | 0.831 | 0.899 | 0.944 | 0.913 | 0.859 | 0.852 | 0.873 | 0.888 | 0.892 | 0.884 |
| | $P_{uT}/P_{nD,T}$ | 0.995 | 0.947 | 0.804 | 0.765 | 0.730 | 0.668 | 0.619 | 0.611 | 0.628 | 0.642 | 0.650 | 0.650 |
| | $P_{uT}/P_{nDFT,T}$ | 1.331 | 1.412 | 1.286 | 1.391 | 1.460 | 1.413 | 1.363 | 1.390 | 1.467 | 1.540 | 1.595 | 1.630 |
| | $P_{uT}/P_{nFTD,T}$ | 1.314 | 1.342 | 1.192 | 1.251 | 1.309 | 1.303 | 1.308 | 1.396 | 1.544 | 1.697 | 1.841 | 1.971 |
| 500 | $\lambda_{FT,T}$ | 0.334 | 0.668 | 0.813 | 1.084 | 1.355 | 1.626 | 1.897 | 2.168 | 2.439 | 2.710 | 2.981 | 3.252 |
| | $\lambda_{D,T}$ | 0.235 | 0.470 | 0.705 | 0.940 | 1.175 | 1.410 | 1.645 | 1.880 | 2.115 | 2.350 | 2.585 | 2.820 |
| | $P_{uT}/P_{yT}$ | 0.671 | 0.640 | 0.544 | 0.499 | 0.423 | 0.338 | 0.274 | 0.237 | 0.216 | 0.199 | 0.183 | 0.168 |
| | $P_{uT}/P_{nFT,T}$ | 0.923 | 0.972 | 0.881 | 0.941 | 0.971 | 0.935 | 0.877 | 0.862 | 0.878 | 0.894 | 0.899 | 0.893 |
| | $P_{uT}/P_{nD,T}$ | 0.988 | 0.943 | 0.801 | 0.768 | 0.737 | 0.675 | 0.625 | 0.612 | 0.625 | 0.640 | 0.649 | 0.650 |
| | $P_{uT}/P_{nDFT,T}$ | 1.358 | 1.432 | 1.297 | 1.386 | 1.430 | 1.392 | 1.338 | 1.354 | 1.426 | 1.500 | 1.558 | 1.597 |
| | $P_{uT}/P_{nFTD,T}$ | 1.344 | 1.372 | 1.218 | 1.281 | 1.341 | 1.331 | 1.328 | 1.399 | 1.534 | 1.680 | 1.819 | 1.945 |
| 600 | $\lambda_{FT,T}$ | 0.350 | 0.699 | 0.851 | 1.135 | 1.418 | 1.702 | 1.986 | 2.269 | 2.553 | 2.836 | 3.120 | 3.404 |
| | $\lambda_{D,T}$ | 0.246 | 0.492 | 0.738 | 0.984 | 1.230 | 1.476 | 1.722 | 1.967 | 2.213 | 2.459 | 2.705 | 2.951 |
| | $P_{uT}/P_{yT}$ | 0.605 | 0.574 | 0.488 | 0.447 | 0.382 | 0.307 | 0.251 | 0.221 | 0.204 | 0.188 | 0.172 | 0.157 |
| | $P_{uT}/P_{nFT,T}$ | 0.832 | 0.880 | 0.802 | 0.871 | 0.923 | 0.887 | 0.837 | 0.839 | 0.863 | 0.879 | 0.882 | 0.873 |
| | $P_{uT}/P_{nD,T}$ | 1.009 | 0.957 | 0.813 | 0.763 | 0.726 | 0.663 | 0.614 | 0.612 | 0.630 | 0.644 | 0.651 | 0.649 |
| | $P_{uT}/P_{nDFT,T}$ | 1.386 | 1.467 | 1.337 | 1.451 | 1.538 | 1.479 | 1.411 | 1.444 | 1.524 | 1.595 | 1.647 | 1.677 |
| | $P_{uT}/P_{nFTD,T}$ | 1.366 | 1.384 | 1.226 | 1.266 | 1.319 | 1.312 | 1.315 | 1.414 | 1.566 | 1.719 | 1.861 | 1.987 |
| 700 | $\lambda_{FT,T}$ | 0.355 | 0.711 | 0.865 | 1.153 | 1.442 | 1.730 | 2.018 | 2.307 | 2.595 | 2.883 | 3.172 | 3.460 |
| | $\lambda_{D,T}$ | 0.250 | 0.500 | 0.750 | 1.000 | 1.250 | 1.500 | 1.750 | 2.000 | 2.250 | 2.500 | 2.750 | 3.000 |
| | $P_{uT}/P_{yT}$ | 0.587 | 0.555 | 0.472 | 0.432 | 0.369 | 0.297 | 0.243 | 0.217 | 0.200 | 0.184 | 0.169 | 0.154 |
| | $P_{uT}/P_{nFT,T}$ | 0.779 | 0.829 | 0.760 | 0.835 | 0.902 | 0.872 | 0.825 | 0.834 | 0.860 | 0.875 | 0.877 | 0.867 |
| | $P_{uT}/P_{nD,T}$ | 1.018 | 0.962 | 0.817 | 0.762 | 0.722 | 0.659 | 0.611 | 0.614 | 0.633 | 0.646 | 0.652 | 0.649 |
| | $P_{uT}/P_{nDFT,T}$ | 1.350 | 1.437 | 1.317 | 1.447 | 1.563 | 1.512 | 1.430 | 1.481 | 1.562 | 1.631 | 1.680 | 1.706 |
| | $P_{uT}/P_{nFTD,T}$ | 1.328 | 1.344 | 1.193 | 1.231 | 1.284 | 1.282 | 1.294 | 1.408 | 1.569 | 1.728 | 1.876 | 2.007 |
| 800 | $\lambda_{FT,T}$ | 0.314 | 0.627 | 0.763 | 1.017 | 1.271 | 1.526 | 1.780 | 2.034 | 2.289 | 2.543 | 2.797 | 3.051 |
| | $\lambda_{D,T}$ | 0.220 | 0.441 | 0.661 | 0.882 | 1.102 | 1.323 | 1.543 | 1.764 | 1.984 | 2.205 | 2.425 | 2.646 |
| | $P_{uT}/P_{yT}$ | 0.703 | 0.674 | 0.574 | 0.533 | 0.461 | 0.374 | 0.302 | 0.256 | 0.230 | 0.212 | 0.196 | 0.180 |
| | $P_{uT}/P_{nFT,T}$ | 0.866 | 0.918 | 0.834 | 0.902 | 0.951 | 0.974 | 0.911 | 0.875 | 0.880 | 0.895 | 0.905 | 0.905 |
| | $P_{uT}/P_{nD,T}$ | 0.984 | 0.944 | 0.804 | 0.772 | 0.753 | 0.698 | 0.642 | 0.614 | 0.619 | 0.633 | 0.645 | 0.651 |
| | $P_{uT}/P_{nDFT,T}$ | 1.213 | 1.286 | 1.167 | 1.262 | 1.332 | 1.381 | 1.325 | 1.313 | 1.365 | 1.436 | 1.500 | 1.549 |
| | $P_{uT}/P_{nFTD,T}$ | 1.201 | 1.238 | 1.103 | 1.173 | 1.256 | 1.269 | 1.269 | 1.314 | 1.428 | 1.573 | 1.720 | 1.861 |

**Table I.2**: Numerical failure loads and their DSM estimates concerning the **LC2** column geometry with 12 room temperature stresses (corresponding to equally spaced slenderness values) and 8 temperatures varying from $T$=20/100 to $T$=800 ºC.

| $T$ (ºC) | $\lambda_{cr.20}$ | 0.25 | 0.50 | 0.75 | 1.00 | 1.25 | 1.50 | 1.75 | 2.00 | 2.25 | 2.50 | 2.75 | 3.00 |
|---|---|---|---|---|---|---|---|---|---|---|---|---|---|
| 20/100 | $\lambda_{FT.T}$ | 0.310 | 0.620 | 0.931 | 1.241 | 1.551 | 1.861 | 2.172 | 2.482 | 2.792 | 3.102 | 3.413 | 3.723 |
| | $\lambda_{D.T}$ | 0.250 | 0.500 | 0.750 | 1.000 | 1.250 | 1.500 | 1.750 | 2.000 | 2.250 | 2.500 | 2.750 | 3.000 |
| | $P_{uT}/P_{yT}$ | 0.957 | 0.901 | 0.775 | 0.566 | 0.410 | 0.329 | 0.285 | 0.251 | 0.217 | 0.184 | 0.155 | 0.133 |
| | $P_{uT}/P_{nFT.T}$ | 0.996 | 1.058 | 1.114 | 1.078 | 1.088 | 1.044 | 1.052 | 1.054 | 1.024 | 0.966 | 0.894 | 0.834 |
| | $P_{uT}/P_{nD.T}$ | 0.957 | 0.901 | 0.848 | 0.755 | 0.663 | 0.633 | 0.640 | 0.646 | 0.634 | 0.604 | 0.565 | 0.533 |
| | $P_{uT}/P_{nDFT.T}$ | 0.996 | 1.058 | 1.131 | 1.159 | 1.206 | 1.227 | 1.306 | 1.378 | 1.405 | 1.385 | 1.337 | 1.297 |
| | $P_{uT}/P_{nFTD.T}$ | 0.996 | 1.058 | 1.181 | 1.224 | 1.237 | 1.347 | 1.543 | 1.757 | 1.936 | 2.066 | 2.159 | 2.269 |
| 200 | $\lambda_{FT.T}$ | 0.309 | 0.617 | 0.926 | 1.234 | 1.543 | 1.851 | 2.160 | 2.468 | 2.777 | 3.085 | 3.394 | 3.702 |
| | $\lambda_{D.T}$ | 0.249 | 0.497 | 0.746 | 0.994 | 1.243 | 1.492 | 1.740 | 1.989 | 2.237 | 2.486 | 2.735 | 2.983 |
| | $P_{uT}/P_{yT}$ | 0.937 | 0.883 | 0.767 | 0.567 | 0.411 | 0.329 | 0.285 | 0.250 | 0.217 | 0.184 | 0.157 | 0.136 |
| | $P_{uT}/P_{nFT.T}$ | 1.080 | 1.130 | 1.170 | 1.104 | 1.084 | 1.037 | 1.044 | 1.048 | 1.018 | 0.958 | 0.896 | 0.848 |
| | $P_{uT}/P_{nD.T}$ | 0.959 | 0.903 | 0.848 | 0.758 | 0.665 | 0.631 | 0.637 | 0.644 | 0.631 | 0.600 | 0.567 | 0.543 |
| | $P_{uT}/P_{nDFT.T}$ | 1.104 | 1.156 | 1.202 | 1.194 | 1.214 | 1.228 | 1.305 | 1.377 | 1.404 | 1.380 | 1.345 | 1.324 |
| | $P_{uT}/P_{nFTD.T}$ | 1.104 | 1.153 | 1.255 | 1.282 | 1.272 | 1.355 | 1.527 | 1.714 | 1.862 | 1.955 | 2.036 | 2.141 |
| 300 | $\lambda_{FT.T}$ | 0.306 | 0.613 | 0.919 | 1.225 | 1.532 | 1.838 | 2.144 | 2.451 | 2.757 | 3.063 | 3.370 | 3.676 |
| | $\lambda_{D.T}$ | 0.247 | 0.494 | 0.741 | 0.987 | 1.234 | 1.481 | 1.728 | 1.975 | 2.222 | 2.469 | 2.715 | 2.962 |
| | $P_{uT}/P_{yT}$ | 0.763 | 0.726 | 0.661 | 0.530 | 0.393 | 0.309 | 0.268 | 0.239 | 0.211 | 0.182 | 0.154 | 0.133 |
| | $P_{uT}/P_{nFT.T}$ | 0.956 | 0.998 | 1.062 | 1.059 | 1.030 | 0.967 | 0.977 | 0.995 | 0.983 | 0.943 | 0.877 | 0.824 |
| | $P_{uT}/P_{nD.T}$ | 0.971 | 0.924 | 0.848 | 0.771 | 0.673 | 0.617 | 0.619 | 0.630 | 0.626 | 0.604 | 0.567 | 0.537 |
| | $P_{uT}/P_{nDFT.T}$ | 1.216 | 1.270 | 1.351 | 1.347 | 1.329 | 1.289 | 1.351 | 1.430 | 1.469 | 1.462 | 1.410 | 1.370 |
| | $P_{uT}/P_{nFTD.T}$ | 1.208 | 1.237 | 1.280 | 1.318 | 1.287 | 1.313 | 1.454 | 1.631 | 1.776 | 1.876 | 1.921 | 1.983 |
| 400 | $\lambda_{FT.T}$ | 0.299 | 0.598 | 0.897 | 1.196 | 1.495 | 1.794 | 2.093 | 2.392 | 2.691 | 2.990 | 3.289 | 3.587 |
| | $\lambda_{D.T}$ | 0.241 | 0.482 | 0.723 | 0.964 | 1.205 | 1.445 | 1.686 | 1.927 | 2.168 | 2.409 | 2.650 | 2.891 |
| | $P_{uT}/P_{yT}$ | 0.637 | 0.613 | 0.572 | 0.495 | 0.387 | 0.301 | 0.259 | 0.234 | 0.209 | 0.184 | 0.162 | 0.141 |
| | $P_{uT}/P_{nFT.T}$ | 0.845 | 0.883 | 0.946 | 0.992 | 0.993 | 0.920 | 0.920 | 0.948 | 0.954 | 0.929 | 0.897 | 0.849 |
| | $P_{uT}/P_{nD.T}$ | 0.986 | 0.949 | 0.885 | 0.795 | 0.700 | 0.623 | 0.610 | 0.624 | 0.626 | 0.611 | 0.592 | 0.563 |
| | $P_{uT}/P_{nDFT.T}$ | 1.307 | 1.367 | 1.464 | 1.536 | 1.537 | 1.423 | 1.442 | 1.519 | 1.567 | 1.569 | 1.555 | 1.514 |
| | $P_{uT}/P_{nFTD.T}$ | 1.294 | 1.315 | 1.341 | 1.350 | 1.321 | 1.298 | 1.395 | 1.558 | 1.704 | 1.808 | 1.898 | 1.956 |
| 500 | $\lambda_{FT.T}$ | 0.292 | 0.583 | 0.875 | 1.166 | 1.458 | 1.749 | 2.041 | 2.333 | 2.624 | 2.916 | 3.207 | 3.499 |
| | $\lambda_{D.T}$ | 0.235 | 0.470 | 0.705 | 0.940 | 1.175 | 1.410 | 1.645 | 1.880 | 2.115 | 2.350 | 2.585 | 2.820 |
| | $P_{uT}/P_{yT}$ | 0.666 | 0.642 | 0.600 | 0.519 | 0.406 | 0.315 | 0.267 | 0.241 | 0.217 | 0.192 | 0.166 | 0.147 |
| | $P_{uT}/P_{nFT.T}$ | 0.909 | 0.944 | 1.001 | 1.034 | 1.015 | 0.939 | 0.928 | 0.955 | 0.964 | 0.944 | 0.899 | 0.869 |
| | $P_{uT}/P_{nD.T}$ | 0.981 | 0.945 | 0.883 | 0.798 | 0.706 | 0.629 | 0.609 | 0.622 | 0.627 | 0.615 | 0.588 | 0.572 |
| | $P_{uT}/P_{nDFT.T}$ | 1.338 | 1.390 | 1.474 | 1.523 | 1.494 | 1.383 | 1.396 | 1.472 | 1.528 | 1.540 | 1.510 | 1.502 |
| | $P_{uT}/P_{nFTD.T}$ | 1.327 | 1.346 | 1.370 | 1.381 | 1.350 | 1.319 | 1.396 | 1.549 | 1.694 | 1.797 | 1.855 | 1.944 |
| 600 | $\lambda_{FT.T}$ | 0.305 | 0.610 | 0.916 | 1.221 | 1.526 | 1.831 | 2.136 | 2.442 | 2.747 | 3.052 | 3.357 | 3.662 |
| | $\lambda_{D.T}$ | 0.246 | 0.492 | 0.738 | 0.984 | 1.230 | 1.476 | 1.722 | 1.967 | 2.213 | 2.459 | 2.705 | 2.951 |
| | $P_{uT}/P_{yT}$ | 0.599 | 0.575 | 0.536 | 0.467 | 0.368 | 0.287 | 0.250 | 0.226 | 0.202 | 0.178 | 0.156 | 0.132 |
| | $P_{uT}/P_{nFT.T}$ | 0.816 | 0.851 | 0.912 | 0.966 | 0.960 | 0.897 | 0.906 | 0.936 | 0.940 | 0.915 | 0.883 | 0.816 |
| | $P_{uT}/P_{nD.T}$ | 0.998 | 0.958 | 0.893 | 0.797 | 0.699 | 0.621 | 0.612 | 0.625 | 0.625 | 0.609 | 0.589 | 0.547 |
| | $P_{uT}/P_{nDFT.T}$ | 1.360 | 1.419 | 1.520 | 1.610 | 1.599 | 1.495 | 1.511 | 1.587 | 1.627 | 1.621 | 1.602 | 1.517 |
| | $P_{uT}/P_{nFTD.T}$ | 1.345 | 1.357 | 1.375 | 1.370 | 1.335 | 1.307 | 1.414 | 1.576 | 1.717 | 1.816 | 1.903 | 1.910 |
| 700 | $\lambda_{FT.T}$ | 0.310 | 0.620 | 0.931 | 1.241 | 1.551 | 1.861 | 2.172 | 2.482 | 2.792 | 3.102 | 3.413 | 3.723 |
| | $\lambda_{D.T}$ | 0.250 | 0.500 | 0.750 | 1.000 | 1.250 | 1.500 | 1.750 | 2.000 | 2.250 | 2.500 | 2.750 | 3.000 |
| | $P_{uT}/P_{yT}$ | 0.581 | 0.556 | 0.517 | 0.451 | 0.356 | 0.279 | 0.244 | 0.221 | 0.197 | 0.173 | 0.149 | 0.131 |
| | $P_{uT}/P_{nFT.T}$ | 0.763 | 0.800 | 0.865 | 0.931 | 0.943 | 0.884 | 0.902 | 0.931 | 0.931 | 0.906 | 0.857 | 0.824 |
| | $P_{uT}/P_{nD.T}$ | 1.007 | 0.964 | 0.896 | 0.796 | 0.696 | 0.618 | 0.615 | 0.627 | 0.624 | 0.607 | 0.576 | 0.556 |
| | $P_{uT}/P_{nDFT.T}$ | 1.323 | 1.386 | 1.499 | 1.613 | 1.635 | 1.532 | 1.563 | 1.632 | 1.661 | 1.650 | 1.597 | 1.571 |
| | $P_{uT}/P_{nFTD.T}$ | 1.306 | 1.317 | 1.337 | 1.333 | 1.304 | 1.285 | 1.409 | 1.578 | 1.719 | 1.825 | 1.884 | 1.975 |
| 800 | $\lambda_{FT.T}$ | 0.274 | 0.547 | 0.821 | 1.094 | 1.368 | 1.642 | 1.915 | 2.189 | 2.462 | 2.736 | 3.010 | 3.283 |
| | $\lambda_{D.T}$ | 0.220 | 0.441 | 0.661 | 0.882 | 1.102 | 1.323 | 1.543 | 1.764 | 1.984 | 2.205 | 2.425 | 2.646 |
| | $P_{uT}/P_{yT}$ | 0.699 | 0.675 | 0.636 | 0.561 | 0.448 | 0.348 | 0.287 | 0.257 | 0.233 | 0.209 | 0.185 | 0.164 |
| | $P_{uT}/P_{nFT.T}$ | 0.855 | 0.891 | 0.952 | 1.003 | 1.006 | 0.975 | 0.937 | 0.954 | 0.972 | 0.967 | 0.940 | 0.906 |
| | $P_{uT}/P_{nD.T}$ | 0.979 | 0.945 | 0.890 | 0.813 | 0.731 | 0.650 | 0.611 | 0.616 | 0.627 | 0.624 | 0.609 | 0.590 |
| | $P_{uT}/P_{nDFT.T}$ | 1.196 | 1.247 | 1.333 | 1.404 | 1.409 | 1.373 | 1.344 | 1.405 | 1.473 | 1.508 | 1.510 | 1.498 |
| | $P_{uT}/P_{nFTD.T}$ | 1.188 | 1.211 | 1.248 | 1.282 | 1.285 | 1.263 | 1.307 | 1.445 | 1.604 | 1.740 | 1.844 | 1.937 |

**Table I.3**: Numerical failure loads and their DSM estimates concerning the **LC3** column geometry with 12 room temperature stresses (corresponding to equally spaced slenderness values) and 8 temperatures varying from $T$=20/100 to $T$=800 ºC.

| $T$ (ºC) | $\lambda_{cr.20}$ | 0.25 | 0.50 | 0.75 | 1.00 | 1.25 | 1.50 | 1.75 | 2.00 | 2.25 | 2.50 | 2.75 | 3.00 |
|---|---|---|---|---|---|---|---|---|---|---|---|---|---|
| 20/100 | $\lambda_{FT.T}$ | 0.299 | 0.598 | 0.897 | 1.196 | 1.495 | 1.794 | 2.093 | 2.392 | 2.691 | 2.990 | 3.289 | 3.588 |
| | $\lambda_{D.T}$ | 0.250 | 0.500 | 0.750 | 1.000 | 1.250 | 1.500 | 1.750 | 2.000 | 2.250 | 2.500 | 2.750 | 3.000 |
| | $P_{uT}/P_{yT}$ | 0.948 | 0.893 | 0.780 | 0.588 | 0.428 | 0.347 | 0.303 | 0.273 | 0.244 | 0.213 | 0.185 | 0.162 |
| | $P_{uT}/P_{nFT.T}$ | 0.984 | 1.037 | 1.092 | 1.070 | 1.092 | 1.054 | 1.064 | 1.087 | 1.084 | 1.046 | 0.994 | 0.944 |
| | $P_{uT}/P_{nD.T}$ | 0.948 | 0.893 | 0.854 | 0.784 | 0.692 | 0.667 | 0.681 | 0.704 | 0.713 | 0.698 | 0.673 | 0.649 |
| | $P_{uT}/P_{nDFT.T}$ | 0.984 | 1.037 | 1.113 | 1.164 | 1.225 | 1.256 | 1.346 | 1.452 | 1.524 | 1.543 | 1.533 | 1.517 |
| | $P_{uT}/P_{nFTD.T}$ | 0.984 | 1.037 | 1.161 | 1.228 | 1.235 | 1.345 | 1.541 | 1.783 | 2.011 | 2.188 | 2.339 | 2.491 |
| 200 | $\lambda_{FT.T}$ | 0.297 | 0.595 | 0.892 | 1.189 | 1.487 | 1.784 | 2.081 | 2.379 | 2.676 | 2.973 | 3.271 | 3.568 |
| | $\lambda_{D.T}$ | 0.249 | 0.497 | 0.746 | 0.994 | 1.243 | 1.492 | 1.740 | 1.989 | 2.237 | 2.486 | 2.735 | 2.983 |
| | $P_{uT}/P_{yT}$ | 0.928 | 0.876 | 0.771 | 0.588 | 0.429 | 0.346 | 0.302 | 0.272 | 0.244 | 0.214 | 0.186 | 0.163 |
| | $P_{uT}/P_{nFT.T}$ | 1.067 | 1.110 | 1.150 | 1.101 | 1.078 | 1.044 | 1.054 | 1.078 | 1.078 | 1.044 | 0.994 | 0.944 |
| | $P_{uT}/P_{nD.T}$ | 0.950 | 0.896 | 0.852 | 0.786 | 0.694 | 0.664 | 0.676 | 0.700 | 0.710 | 0.698 | 0.674 | 0.650 |
| | $P_{uT}/P_{nDFT.T}$ | 1.091 | 1.135 | 1.183 | 1.201 | 1.225 | 1.255 | 1.341 | 1.448 | 1.523 | 1.546 | 1.537 | 1.523 |
| | $P_{uT}/P_{nFTD.T}$ | 1.091 | 1.132 | 1.235 | 1.291 | 1.278 | 1.361 | 1.534 | 1.752 | 1.954 | 2.106 | 2.225 | 2.343 |
| 300 | $\lambda_{FT.T}$ | 0.295 | 0.591 | 0.886 | 1.181 | 1.476 | 1.772 | 2.067 | 2.362 | 2.657 | 2.953 | 3.248 | 3.543 |
| | $\lambda_{D.T}$ | 0.247 | 0.494 | 0.741 | 0.987 | 1.234 | 1.481 | 1.728 | 1.975 | 2.222 | 2.469 | 2.715 | 2.962 |
| | $P_{uT}/P_{yT}$ | 0.756 | 0.719 | 0.659 | 0.543 | 0.412 | 0.321 | 0.280 | 0.255 | 0.231 | 0.206 | 0.181 | 0.160 |
| | $P_{uT}/P_{nFT.T}$ | 0.944 | 0.979 | 1.037 | 1.047 | 1.029 | 0.964 | 0.971 | 1.003 | 1.016 | 0.999 | 0.960 | 0.921 |
| | $P_{uT}/P_{nD.T}$ | 0.962 | 0.914 | 0.845 | 0.790 | 0.704 | 0.643 | 0.647 | 0.672 | 0.687 | 0.683 | 0.664 | 0.644 |
| | $P_{uT}/P_{nDFT.T}$ | 1.202 | 1.246 | 1.320 | 1.333 | 1.337 | 1.297 | 1.362 | 1.467 | 1.549 | 1.585 | 1.583 | 1.574 |
| | $P_{uT}/P_{nFTD.T}$ | 1.194 | 1.215 | 1.256 | 1.319 | 1.304 | 1.313 | 1.450 | 1.647 | 1.834 | 1.983 | 2.091 | 2.198 |
| 400 | $\lambda_{FT.T}$ | 0.288 | 0.576 | 0.864 | 1.153 | 1.441 | 1.729 | 2.017 | 2.305 | 2.593 | 2.881 | 3.170 | 3.458 |
| | $\lambda_{D.T}$ | 0.241 | 0.482 | 0.723 | 0.964 | 1.205 | 1.445 | 1.686 | 1.927 | 2.168 | 2.409 | 2.650 | 2.891 |
| | $P_{uT}/P_{yT}$ | 0.628 | 0.604 | 0.566 | 0.499 | 0.401 | 0.314 | 0.266 | 0.245 | 0.225 | 0.202 | 0.181 | 0.161 |
| | $P_{uT}/P_{nFT.T}$ | 0.831 | 0.863 | 0.920 | 0.969 | 0.980 | 0.920 | 0.902 | 0.940 | 0.965 | 0.958 | 0.939 | 0.906 |
| | $P_{uT}/P_{nD.T}$ | 0.972 | 0.934 | 0.877 | 0.801 | 0.725 | 0.650 | 0.628 | 0.653 | 0.672 | 0.671 | 0.663 | 0.645 |
| | $P_{uT}/P_{nDFT.T}$ | 1.286 | 1.335 | 1.424 | 1.500 | 1.517 | 1.423 | 1.424 | 1.523 | 1.608 | 1.646 | 1.663 | 1.652 |
| | $P_{uT}/P_{nFTD.T}$ | 1.275 | 1.288 | 1.313 | 1.334 | 1.333 | 1.308 | 1.379 | 1.557 | 1.735 | 1.872 | 1.994 | 2.087 |
| 500 | $\lambda_{FT.T}$ | 0.281 | 0.562 | 0.843 | 1.124 | 1.405 | 1.686 | 1.967 | 2.248 | 2.529 | 2.810 | 3.091 | 3.372 |
| | $\lambda_{D.T}$ | 0.235 | 0.470 | 0.705 | 0.940 | 1.175 | 1.410 | 1.645 | 1.880 | 2.115 | 2.350 | 2.585 | 2.820 |
| | $P_{uT}/P_{yT}$ | 0.659 | 0.633 | 0.594 | 0.524 | 0.421 | 0.329 | 0.276 | 0.252 | 0.233 | 0.211 | 0.189 | 0.168 |
| | $P_{uT}/P_{nFT.T}$ | 0.897 | 0.924 | 0.976 | 1.014 | 1.006 | 0.942 | 0.914 | 0.946 | 0.975 | 0.976 | 0.955 | 0.923 |
| | $P_{uT}/P_{nD.T}$ | 0.970 | 0.932 | 0.875 | 0.805 | 0.733 | 0.657 | 0.629 | 0.650 | 0.672 | 0.677 | 0.668 | 0.652 |
| | $P_{uT}/P_{nDFT.T}$ | 1.320 | 1.361 | 1.437 | 1.492 | 1.481 | 1.397 | 1.385 | 1.476 | 1.569 | 1.622 | 1.638 | 1.634 |
| | $P_{uT}/P_{nFTD.T}$ | 1.310 | 1.320 | 1.343 | 1.367 | 1.365 | 1.334 | 1.386 | 1.548 | 1.725 | 1.871 | 1.980 | 2.072 |
| 600 | $\lambda_{FT.T}$ | 0.294 | 0.588 | 0.882 | 1.177 | 1.471 | 1.765 | 2.059 | 2.353 | 2.647 | 2.942 | 3.236 | 3.530 |
| | $\lambda_{D.T}$ | 0.246 | 0.492 | 0.738 | 0.984 | 1.230 | 1.476 | 1.722 | 1.967 | 2.213 | 2.459 | 2.705 | 2.951 |
| | $P_{uT}/P_{yT}$ | 0.585 | 0.564 | 0.530 | 0.470 | 0.381 | 0.299 | 0.256 | 0.237 | 0.217 | 0.195 | 0.174 | 0.155 |
| | $P_{uT}/P_{nFT.T}$ | 0.795 | 0.829 | 0.885 | 0.941 | 0.962 | 0.894 | 0.885 | 0.928 | 0.951 | 0.944 | 0.920 | 0.891 |
| | $P_{uT}/P_{nD.T}$ | 0.975 | 0.940 | 0.883 | 0.801 | 0.723 | 0.646 | 0.628 | 0.654 | 0.672 | 0.670 | 0.657 | 0.642 |
| | $P_{uT}/P_{nDFT.T}$ | 1.326 | 1.381 | 1.476 | 1.568 | 1.603 | 1.490 | 1.474 | 1.587 | 1.667 | 1.698 | 1.701 | 1.694 |
| | $P_{uT}/P_{nFTD.T}$ | 1.312 | 1.325 | 1.344 | 1.352 | 1.345 | 1.317 | 1.394 | 1.577 | 1.751 | 1.885 | 1.992 | 2.092 |
| 700 | $\lambda_{FT.T}$ | 0.299 | 0.598 | 0.897 | 1.196 | 1.495 | 1.794 | 2.093 | 2.392 | 2.691 | 2.990 | 3.289 | 3.588 |
| | $\lambda_{D.T}$ | 0.250 | 0.500 | 0.750 | 1.000 | 1.250 | 1.500 | 1.750 | 2.000 | 2.250 | 2.500 | 2.750 | 3.000 |
| | $P_{uT}/P_{yT}$ | 0.564 | 0.544 | 0.511 | 0.453 | 0.368 | 0.290 | 0.250 | 0.232 | 0.212 | 0.191 | 0.170 | 0.151 |
| | $P_{uT}/P_{nFT.T}$ | 0.740 | 0.776 | 0.838 | 0.904 | 0.943 | 0.879 | 0.879 | 0.924 | 0.943 | 0.937 | 0.911 | 0.882 |
| | $P_{uT}/P_{nD.T}$ | 0.978 | 0.943 | 0.885 | 0.800 | 0.719 | 0.642 | 0.630 | 0.657 | 0.672 | 0.670 | 0.656 | 0.640 |
| | $P_{uT}/P_{nDFT.T}$ | 1.283 | 1.345 | 1.452 | 1.567 | 1.634 | 1.524 | 1.523 | 1.631 | 1.702 | 1.733 | 1.729 | 1.718 |
| | $P_{uT}/P_{nFTD.T}$ | 1.268 | 1.283 | 1.305 | 1.314 | 1.311 | 1.290 | 1.385 | 1.577 | 1.752 | 1.895 | 2.007 | 2.114 |
| 800 | $\lambda_{FT.T}$ | 0.264 | 0.527 | 0.791 | 1.055 | 1.319 | 1.582 | 1.846 | 2.110 | 2.373 | 2.637 | 2.901 | 3.164 |
| | $\lambda_{D.T}$ | 0.220 | 0.441 | 0.661 | 0.882 | 1.102 | 1.323 | 1.543 | 1.764 | 1.984 | 2.205 | 2.425 | 2.646 |
| | $P_{uT}/P_{yT}$ | 0.693 | 0.666 | 0.630 | 0.564 | 0.462 | 0.365 | 0.298 | 0.267 | 0.247 | 0.227 | 0.206 | 0.184 |
| | $P_{uT}/P_{nFT.T}$ | 0.845 | 0.873 | 0.928 | 0.980 | 0.993 | 0.985 | 0.929 | 0.944 | 0.976 | 0.991 | 0.983 | 0.954 |
| | $P_{uT}/P_{nD.T}$ | 0.970 | 0.933 | 0.882 | 0.818 | 0.754 | 0.681 | 0.633 | 0.641 | 0.665 | 0.679 | 0.679 | 0.664 |
| | $P_{uT}/P_{nDFT.T}$ | 1.183 | 1.222 | 1.299 | 1.372 | 1.390 | 1.391 | 1.342 | 1.405 | 1.500 | 1.573 | 1.612 | 1.614 |
| | $P_{uT}/P_{nFTD.T}$ | 1.176 | 1.189 | 1.223 | 1.264 | 1.290 | 1.280 | 1.299 | 1.433 | 1.611 | 1.781 | 1.923 | 2.030 |

**Table I.4**: Numerical failure loads and their DSM estimates concerning the **LC4** column geometry with 12 room temperature stresses (corresponding to equally spaced slenderness values) and 8 temperatures varying from $T$=20/100 to $T$=800 ºC.

| $T$ (ºC) | $\lambda_{cr.20}$ | 0.35 | 0.60 | 0.85 | 1.10 | 1.35 | 1.60 | 1.85 | 2.10 | 2.35 | 2.60 | 2.85 | 3.10 |
|---|---|---|---|---|---|---|---|---|---|---|---|---|---|
| 20/100 | $\lambda_{FT.T}$ | 0.404 | 0.692 | 0.980 | 1.269 | 1.557 | 1.845 | 2.134 | 2.422 | 2.710 | 2.999 | 3.287 | 3.575 |
| | $\lambda_{D.T}$ | 0.350 | 0.600 | 0.850 | 1.100 | 1.350 | 1.600 | 1.850 | 2.100 | 2.350 | 2.600 | 2.850 | 3.100 |
| | $P_{uT}/P_{yT}$ | 0.937 | 0.876 | 0.739 | 0.545 | 0.406 | 0.335 | 0.294 | 0.262 | 0.230 | 0.197 | 0.170 | 0.152 |
| | $P_{uT}/P_{nFT.T}$ | 1.003 | 1.071 | 1.105 | 1.069 | 1.079 | 1.051 | 1.064 | 1.073 | 1.049 | 0.994 | 0.936 | 0.907 |
| | $P_{uT}/P_{nD.T}$ | 0.937 | 0.882 | 0.873 | 0.787 | 0.704 | 0.687 | 0.699 | 0.712 | 0.703 | 0.675 | 0.643 | 0.630 |
| | $P_{uT}/P_{nDFT.T}$ | 1.003 | 1.071 | 1.165 | 1.202 | 1.253 | 1.297 | 1.388 | 1.475 | 1.513 | 1.501 | 1.474 | 1.485 |
| | $P_{uT}/P_{nFTD.T}$ | 1.003 | 1.076 | 1.228 | 1.255 | 1.264 | 1.376 | 1.560 | 1.760 | 1.920 | 2.029 | 2.124 | 2.284 |
| 200 | $\lambda_{FT.T}$ | 0.401 | 0.688 | 0.975 | 1.262 | 1.548 | 1.835 | 2.122 | 2.409 | 2.695 | 2.982 | 3.269 | 3.555 |
| | $\lambda_{D.T}$ | 0.348 | 0.597 | 0.845 | 1.094 | 1.342 | 1.591 | 1.840 | 2.088 | 2.337 | 2.586 | 2.834 | 3.083 |
| | $P_{uT}/P_{yT}$ | 0.918 | 0.860 | 0.733 | 0.546 | 0.406 | 0.335 | 0.293 | 0.262 | 0.231 | 0.200 | 0.175 | 0.153 |
| | $P_{uT}/P_{nFT.T}$ | 1.083 | 1.139 | 1.157 | 1.092 | 1.075 | 1.045 | 1.055 | 1.067 | 1.049 | 1.004 | 0.958 | 0.910 |
| | $P_{uT}/P_{nD.T}$ | 0.939 | 0.882 | 0.872 | 0.790 | 0.705 | 0.685 | 0.695 | 0.709 | 0.705 | 0.682 | 0.658 | 0.633 |
| | $P_{uT}/P_{nDFT.T}$ | 1.108 | 1.166 | 1.222 | 1.231 | 1.259 | 1.298 | 1.385 | 1.473 | 1.520 | 1.521 | 1.513 | 1.494 |
| | $P_{uT}/P_{nFTD.T}$ | 1.107 | 1.163 | 1.302 | 1.318 | 1.305 | 1.398 | 1.557 | 1.738 | 1.884 | 1.986 | 2.082 | 2.170 |
| 300 | $\lambda_{FT.T}$ | 0.399 | 0.683 | 0.968 | 1.253 | 1.537 | 1.822 | 2.107 | 2.392 | 2.676 | 2.961 | 3.246 | 3.530 |
| | $\lambda_{D.T}$ | 0.346 | 0.592 | 0.839 | 1.086 | 1.333 | 1.580 | 1.827 | 2.074 | 2.320 | 2.567 | 2.814 | 3.061 |
| | $P_{uT}/P_{yT}$ | 0.751 | 0.711 | 0.640 | 0.514 | 0.391 | 0.313 | 0.274 | 0.248 | 0.222 | 0.195 | 0.168 | 0.150 |
| | $P_{uT}/P_{nFT.T}$ | 0.960 | 1.008 | 1.060 | 1.049 | 1.026 | 0.969 | 0.980 | 1.004 | 1.000 | 0.970 | 0.916 | 0.885 |
| | $P_{uT}/P_{nD.T}$ | 0.955 | 0.905 | 0.854 | 0.797 | 0.712 | 0.663 | 0.669 | 0.687 | 0.689 | 0.673 | 0.642 | 0.626 |
| | $P_{uT}/P_{nDFT.T}$ | 1.222 | 1.282 | 1.349 | 1.353 | 1.357 | 1.335 | 1.407 | 1.503 | 1.558 | 1.570 | 1.539 | 1.538 |
| | $P_{uT}/P_{nFTD.T}$ | 1.208 | 1.240 | 1.309 | 1.352 | 1.328 | 1.353 | 1.486 | 1.656 | 1.797 | 1.897 | 1.949 | 2.044 |
| 400 | $\lambda_{FT.T}$ | 0.389 | 0.667 | 0.945 | 1.223 | 1.500 | 1.778 | 2.056 | 2.334 | 2.612 | 2.890 | 3.167 | 3.445 |
| | $\lambda_{D.T}$ | 0.337 | 0.578 | 0.819 | 1.060 | 1.301 | 1.542 | 1.783 | 2.024 | 2.265 | 2.505 | 2.746 | 2.987 |
| | $P_{uT}/P_{yT}$ | 0.627 | 0.600 | 0.559 | 0.482 | 0.385 | 0.302 | 0.263 | 0.241 | 0.218 | 0.194 | 0.173 | 0.154 |
| | $P_{uT}/P_{nFT.T}$ | 0.848 | 0.888 | 0.949 | 0.986 | 0.988 | 0.915 | 0.918 | 0.950 | 0.961 | 0.945 | 0.919 | 0.890 |
| | $P_{uT}/P_{nD.T}$ | 0.971 | 0.929 | 0.865 | 0.809 | 0.736 | 0.660 | 0.653 | 0.672 | 0.681 | 0.672 | 0.657 | 0.640 |
| | $P_{uT}/P_{nDFT.T}$ | 1.313 | 1.374 | 1.469 | 1.526 | 1.528 | 1.433 | 1.469 | 1.562 | 1.628 | 1.649 | 1.653 | 1.647 |
| | $P_{uT}/P_{nFTD.T}$ | 1.291 | 1.309 | 1.333 | 1.373 | 1.365 | 1.332 | 1.424 | 1.582 | 1.724 | 1.826 | 1.914 | 1.996 |
| 500 | $\lambda_{FT.T}$ | 0.379 | 0.650 | 0.921 | 1.192 | 1.463 | 1.734 | 2.005 | 2.276 | 2.547 | 2.818 | 3.089 | 3.360 |
| | $\lambda_{D.T}$ | 0.329 | 0.564 | 0.799 | 1.034 | 1.269 | 1.504 | 1.739 | 1.974 | 2.209 | 2.444 | 2.679 | 2.914 |
| | $P_{uT}/P_{yT}$ | 0.658 | 0.629 | 0.586 | 0.506 | 0.404 | 0.317 | 0.272 | 0.248 | 0.226 | 0.202 | 0.180 | 0.161 |
| | $P_{uT}/P_{nFT.T}$ | 0.913 | 0.949 | 1.003 | 1.027 | 1.016 | 0.936 | 0.927 | 0.956 | 0.972 | 0.960 | 0.934 | 0.904 |
| | $P_{uT}/P_{nD.T}$ | 0.968 | 0.926 | 0.863 | 0.815 | 0.743 | 0.667 | 0.653 | 0.671 | 0.682 | 0.676 | 0.662 | 0.646 |
| | $P_{uT}/P_{nDFT.T}$ | 1.344 | 1.396 | 1.477 | 1.511 | 1.496 | 1.403 | 1.428 | 1.517 | 1.592 | 1.622 | 1.627 | 1.624 |
| | $P_{uT}/P_{nFTD.T}$ | 1.326 | 1.341 | 1.362 | 1.408 | 1.397 | 1.357 | 1.430 | 1.577 | 1.720 | 1.823 | 1.904 | 1.979 |
| 600 | $\lambda_{FT.T}$ | 0.397 | 0.681 | 0.964 | 1.248 | 1.532 | 1.815 | 2.099 | 2.383 | 2.666 | 2.950 | 3.234 | 3.517 |
| | $\lambda_{D.T}$ | 0.344 | 0.590 | 0.836 | 1.082 | 1.328 | 1.574 | 1.820 | 2.066 | 2.312 | 2.558 | 2.804 | 3.050 |
| | $P_{uT}/P_{yT}$ | 0.586 | 0.562 | 0.523 | 0.455 | 0.367 | 0.289 | 0.254 | 0.233 | 0.211 | 0.188 | 0.165 | 0.149 |
| | $P_{uT}/P_{nFT.T}$ | 0.814 | 0.854 | 0.915 | 0.960 | 0.959 | 0.892 | 0.903 | 0.937 | 0.946 | 0.930 | 0.894 | 0.877 |
| | $P_{uT}/P_{nD.T}$ | 0.977 | 0.936 | 0.872 | 0.806 | 0.732 | 0.657 | 0.653 | 0.674 | 0.679 | 0.669 | 0.646 | 0.637 |
| | $P_{uT}/P_{nDFT.T}$ | 1.357 | 1.424 | 1.525 | 1.601 | 1.599 | 1.487 | 1.530 | 1.624 | 1.681 | 1.698 | 1.676 | 1.688 |
| | $P_{uT}/P_{nFTD.T}$ | 1.331 | 1.347 | 1.365 | 1.388 | 1.377 | 1.341 | 1.442 | 1.603 | 1.737 | 1.837 | 1.899 | 2.002 |
| 700 | $\lambda_{FT.T}$ | 0.404 | 0.692 | 0.980 | 1.269 | 1.557 | 1.845 | 2.134 | 2.422 | 2.710 | 2.999 | 3.287 | 3.575 |
| | $\lambda_{D.T}$ | 0.350 | 0.600 | 0.850 | 1.100 | 1.350 | 1.600 | 1.850 | 2.100 | 2.350 | 2.600 | 2.850 | 3.100 |
| | $P_{uT}/P_{yT}$ | 0.567 | 0.542 | 0.505 | 0.440 | 0.355 | 0.280 | 0.248 | 0.228 | 0.205 | 0.183 | 0.163 | 0.145 |
| | $P_{uT}/P_{nFT.T}$ | 0.761 | 0.803 | 0.869 | 0.927 | 0.943 | 0.879 | 0.898 | 0.932 | 0.936 | 0.921 | 0.896 | 0.868 |
| | $P_{uT}/P_{nD.T}$ | 0.982 | 0.940 | 0.875 | 0.803 | 0.728 | 0.654 | 0.655 | 0.675 | 0.676 | 0.667 | 0.652 | 0.635 |
| | $P_{uT}/P_{nDFT.T}$ | 1.319 | 1.393 | 1.507 | 1.607 | 1.634 | 1.524 | 1.573 | 1.665 | 1.710 | 1.725 | 1.723 | 1.711 |
| | $P_{uT}/P_{nFTD.T}$ | 1.291 | 1.307 | 1.327 | 1.349 | 1.343 | 1.316 | 1.433 | 1.599 | 1.730 | 1.838 | 1.931 | 2.018 |
| 800 | $\lambda_{FT.T}$ | 0.356 | 0.610 | 0.865 | 1.119 | 1.373 | 1.627 | 1.882 | 2.136 | 2.390 | 2.645 | 2.899 | 3.153 |
| | $\lambda_{D.T}$ | 0.309 | 0.529 | 0.750 | 0.970 | 1.191 | 1.411 | 1.632 | 1.852 | 2.073 | 2.293 | 2.513 | 2.734 |
| | $P_{uT}/P_{yT}$ | 0.691 | 0.663 | 0.623 | 0.547 | 0.447 | 0.351 | 0.293 | 0.264 | 0.242 | 0.220 | 0.197 | 0.174 |
| | $P_{uT}/P_{nFT.T}$ | 0.860 | 0.896 | 0.956 | 0.998 | 1.010 | 0.975 | 0.938 | 0.955 | 0.978 | 0.981 | 0.961 | 0.919 |
| | $P_{uT}/P_{nD.T}$ | 0.967 | 0.928 | 0.872 | 0.829 | 0.770 | 0.691 | 0.655 | 0.663 | 0.680 | 0.684 | 0.674 | 0.649 |
| | $P_{uT}/P_{nDFT.T}$ | 1.203 | 1.255 | 1.338 | 1.397 | 1.422 | 1.395 | 1.379 | 1.448 | 1.532 | 1.586 | 1.603 | 1.581 |
| | $P_{uT}/P_{nFTD.T}$ | 1.189 | 1.210 | 1.245 | 1.307 | 1.331 | 1.300 | 1.336 | 1.462 | 1.616 | 1.749 | 1.848 | 1.907 |

**Table I.5**: Numerical failure loads and their DSM estimates concerning the **LC5** column geometry with 12 room temperature stresses (corresponding to equally spaced slenderness values) and 8 temperatures varying from $T$=20/100 to $T$=800 ºC.

| $T$ (ºC) | $\lambda_{cr.20}$ | 0.25 | 0.50 | 0.75 | 1.00 | 1.25 | 1.50 | 1.75 | 2.00 | 2.25 | 2.50 | 2.75 | 3.00 |
|---|---|---|---|---|---|---|---|---|---|---|---|---|---|
| 20/100 | $\lambda_{FT.T}$ | 0.280 | 0.561 | 0.839 | 1.119 | 1.399 | 1.678 | 1.957 | 2.238 | 2.517 | 2.797 | 3.077 | 3.357 |
| | $\lambda_{D.T}$ | 0.250 | 0.501 | 0.750 | 1.000 | 1.250 | 1.500 | 1.749 | 2.000 | 2.249 | 2.500 | 2.750 | 3.000 |
| | $P_{uT}/P_{yT}$ | 0.962 | 0.910 | 0.816 | 0.640 | 0.472 | 0.372 | 0.318 | 0.283 | 0.257 | 0.230 | 0.198 | 0.171 |
| | $P_{uT}/P_{nFT.T}$ | 0.995 | 1.038 | 1.097 | 1.080 | 1.070 | 1.065 | 1.055 | 1.072 | 1.088 | 1.078 | 1.018 | 0.957 |
| | $P_{uT}/P_{nD.T}$ | 0.962 | 0.910 | 0.894 | 0.853 | 0.762 | 0.716 | 0.713 | 0.730 | 0.750 | 0.752 | 0.719 | 0.684 |
| | $P_{uT}/P_{nDFT.T}$ | 0.995 | 1.038 | 1.124 | 1.200 | 1.244 | 1.297 | 1.363 | 1.461 | 1.560 | 1.621 | 1.599 | 1.566 |
| | $P_{uT}/P_{nFTD.T}$ | 0.995 | 1.038 | 1.170 | 1.264 | 1.265 | 1.322 | 1.457 | 1.647 | 1.858 | 2.044 | 2.137 | 2.221 |
| 200 | $\lambda_{FT.T}$ | 0.279 | 0.557 | 0.835 | 1.113 | 1.391 | 1.669 | 1.946 | 2.225 | 2.503 | 2.782 | 3.060 | 3.338 |
| | $\lambda_{D.T}$ | 0.249 | 0.498 | 0.746 | 0.994 | 1.243 | 1.492 | 1.739 | 1.989 | 2.237 | 2.486 | 2.734 | 2.983 |
| | $P_{uT}/P_{yT}$ | 0.942 | 0.892 | 0.806 | 0.639 | 0.473 | 0.372 | 0.317 | 0.283 | 0.255 | 0.229 | 0.198 | 0.172 |
| | $P_{uT}/P_{nFT.T}$ | 1.078 | 1.113 | 1.159 | 1.121 | 1.072 | 1.057 | 1.046 | 1.063 | 1.074 | 1.068 | 1.012 | 0.959 |
| | $P_{uT}/P_{nD.T}$ | 0.964 | 0.912 | 0.891 | 0.854 | 0.764 | 0.713 | 0.709 | 0.726 | 0.742 | 0.746 | 0.715 | 0.686 |
| | $P_{uT}/P_{nDFT.T}$ | 1.103 | 1.138 | 1.197 | 1.243 | 1.256 | 1.296 | 1.359 | 1.457 | 1.548 | 1.612 | 1.595 | 1.574 |
| | $P_{uT}/P_{nFTD.T}$ | 1.102 | 1.135 | 1.250 | 1.336 | 1.321 | 1.354 | 1.471 | 1.643 | 1.824 | 1.988 | 2.063 | 2.136 |
| 300 | $\lambda_{FT.T}$ | 0.277 | 0.554 | 0.829 | 1.105 | 1.381 | 1.657 | 1.933 | 2.210 | 2.485 | 2.762 | 3.038 | 3.315 |
| | $\lambda_{D.T}$ | 0.247 | 0.495 | 0.741 | 0.987 | 1.234 | 1.481 | 1.727 | 1.975 | 2.221 | 2.468 | 2.715 | 2.962 |
| | $P_{uT}/P_{yT}$ | 0.763 | 0.729 | 0.680 | 0.581 | 0.454 | 0.347 | 0.295 | 0.265 | 0.242 | 0.218 | 0.195 | 0.171 |
| | $P_{uT}/P_{nFT.T}$ | 0.950 | 0.980 | 1.036 | 1.057 | 1.037 | 0.980 | 0.967 | 0.990 | 1.011 | 1.013 | 0.991 | 0.947 |
| | $P_{uT}/P_{nD.T}$ | 0.971 | 0.928 | 0.872 | 0.845 | 0.776 | 0.694 | 0.680 | 0.698 | 0.717 | 0.724 | 0.715 | 0.689 |
| | $P_{uT}/P_{nDFT.T}$ | 1.209 | 1.247 | 1.319 | 1.352 | 1.369 | 1.337 | 1.377 | 1.472 | 1.568 | 1.635 | 1.662 | 1.645 |
| | $P_{uT}/P_{nFTD.T}$ | 1.202 | 1.220 | 1.264 | 1.354 | 1.364 | 1.328 | 1.413 | 1.567 | 1.736 | 1.886 | 1.999 | 2.067 |
| 400 | $\lambda_{FT.T}$ | 0.270 | 0.540 | 0.809 | 1.078 | 1.348 | 1.617 | 1.886 | 2.157 | 2.425 | 2.696 | 2.965 | 3.235 |
| | $\lambda_{D.T}$ | 0.241 | 0.483 | 0.723 | 0.964 | 1.205 | 1.445 | 1.685 | 1.927 | 2.167 | 2.409 | 2.650 | 2.891 |
| | $P_{uT}/P_{yT}$ | 0.632 | 0.611 | 0.579 | 0.524 | 0.440 | 0.343 | 0.282 | 0.255 | 0.235 | 0.215 | 0.194 | 0.174 |
| | $P_{uT}/P_{nFT.T}$ | 0.834 | 0.862 | 0.914 | 0.967 | 0.993 | 0.945 | 0.904 | 0.929 | 0.959 | 0.975 | 0.966 | 0.941 |
| | $P_{uT}/P_{nD.T}$ | 0.978 | 0.945 | 0.896 | 0.841 | 0.796 | 0.709 | 0.666 | 0.679 | 0.701 | 0.714 | 0.711 | 0.698 |
| | $P_{uT}/P_{nDFT.T}$ | 1.290 | 1.334 | 1.414 | 1.496 | 1.537 | 1.473 | 1.440 | 1.521 | 1.619 | 1.696 | 1.733 | 1.741 |
| | $P_{uT}/P_{nFTD.T}$ | 1.280 | 1.293 | 1.317 | 1.357 | 1.400 | 1.351 | 1.367 | 1.500 | 1.660 | 1.810 | 1.925 | 2.013 |
| 500 | $\lambda_{FT.T}$ | 0.263 | 0.527 | 0.789 | 1.052 | 1.315 | 1.578 | 1.840 | 2.103 | 2.366 | 2.629 | 2.892 | 3.155 |
| | $\lambda_{D.T}$ | 0.235 | 0.471 | 0.705 | 0.940 | 1.175 | 1.410 | 1.644 | 1.880 | 2.114 | 2.349 | 2.584 | 2.820 |
| | $P_{uT}/P_{yT}$ | 0.663 | 0.641 | 0.608 | 0.549 | 0.462 | 0.360 | 0.294 | 0.263 | 0.242 | 0.222 | 0.202 | 0.181 |
| | $P_{uT}/P_{nFT.T}$ | 0.900 | 0.926 | 0.972 | 1.015 | 1.027 | 0.969 | 0.919 | 0.936 | 0.965 | 0.983 | 0.978 | 0.956 |
| | $P_{uT}/P_{nD.T}$ | 0.976 | 0.944 | 0.895 | 0.845 | 0.804 | 0.719 | 0.670 | 0.678 | 0.699 | 0.714 | 0.714 | 0.703 |
| | $P_{uT}/P_{nDFT.T}$ | 1.325 | 1.363 | 1.432 | 1.495 | 1.511 | 1.446 | 1.408 | 1.478 | 1.575 | 1.657 | 1.702 | 1.717 |
| | $P_{uT}/P_{nFTD.T}$ | 1.317 | 1.327 | 1.349 | 1.392 | 1.437 | 1.384 | 1.386 | 1.501 | 1.653 | 1.801 | 1.917 | 2.005 |
| 600 | $\lambda_{FT.T}$ | 0.276 | 0.551 | 0.826 | 1.101 | 1.376 | 1.651 | 1.925 | 2.202 | 2.476 | 2.752 | 3.027 | 3.303 |
| | $\lambda_{D.T}$ | 0.246 | 0.493 | 0.738 | 0.984 | 1.230 | 1.476 | 1.721 | 1.967 | 2.213 | 2.459 | 2.705 | 2.951 |
| | $P_{uT}/P_{yT}$ | 0.588 | 0.570 | 0.540 | 0.492 | 0.416 | 0.327 | 0.270 | 0.246 | 0.227 | 0.208 | 0.187 | 0.168 |
| | $P_{uT}/P_{nFT.T}$ | 0.797 | 0.827 | 0.877 | 0.935 | 0.969 | 0.919 | 0.883 | 0.916 | 0.948 | 0.962 | 0.950 | 0.926 |
| | $P_{uT}/P_{nD.T}$ | 0.980 | 0.950 | 0.901 | 0.838 | 0.789 | 0.705 | 0.662 | 0.680 | 0.702 | 0.714 | 0.708 | 0.694 |
| | $P_{uT}/P_{nDFT.T}$ | 1.328 | 1.378 | 1.462 | 1.559 | 1.616 | 1.532 | 1.492 | 1.581 | 1.680 | 1.751 | 1.779 | 1.783 |
| | $P_{uT}/P_{nFTD.T}$ | 1.316 | 1.329 | 1.348 | 1.373 | 1.408 | 1.362 | 1.378 | 1.521 | 1.683 | 1.828 | 1.935 | 2.021 |
| 700 | $\lambda_{FT.T}$ | 0.280 | 0.561 | 0.839 | 1.119 | 1.399 | 1.678 | 1.957 | 2.238 | 2.517 | 2.797 | 3.077 | 3.357 |
| | $\lambda_{D.T}$ | 0.250 | 0.501 | 0.750 | 1.000 | 1.250 | 1.500 | 1.749 | 2.000 | 2.249 | 2.500 | 2.750 | 3.000 |
| | $P_{uT}/P_{yT}$ | 0.566 | 0.549 | 0.521 | 0.474 | 0.401 | 0.316 | 0.263 | 0.241 | 0.223 | 0.204 | 0.183 | 0.164 |
| | $P_{uT}/P_{nFT.T}$ | 0.740 | 0.773 | 0.828 | 0.894 | 0.944 | 0.904 | 0.874 | 0.912 | 0.944 | 0.956 | 0.941 | 0.918 |
| | $P_{uT}/P_{nD.T}$ | 0.982 | 0.952 | 0.902 | 0.836 | 0.785 | 0.701 | 0.662 | 0.683 | 0.705 | 0.714 | 0.706 | 0.692 |
| | $P_{uT}/P_{nDFT.T}$ | 1.283 | 1.340 | 1.435 | 1.549 | 1.635 | 1.566 | 1.515 | 1.623 | 1.721 | 1.787 | 1.807 | 1.810 |
| | $P_{uT}/P_{nFTD.T}$ | 1.270 | 1.285 | 1.307 | 1.331 | 1.368 | 1.329 | 1.359 | 1.514 | 1.681 | 1.829 | 1.937 | 2.032 |
| 800 | $\lambda_{FT.T}$ | 0.247 | 0.494 | 0.740 | 0.987 | 1.234 | 1.480 | 1.726 | 1.974 | 2.220 | 2.467 | 2.714 | 2.961 |
| | $\lambda_{D.T}$ | 0.221 | 0.442 | 0.662 | 0.882 | 1.102 | 1.323 | 1.543 | 1.764 | 1.984 | 2.205 | 2.425 | 2.646 |
| | $P_{uT}/P_{yT}$ | 0.697 | 0.675 | 0.643 | 0.589 | 0.503 | 0.401 | 0.320 | 0.280 | 0.257 | 0.237 | 0.218 | 0.197 |
| | $P_{uT}/P_{nFT.T}$ | 0.849 | 0.874 | 0.923 | 0.977 | 1.005 | 1.004 | 0.942 | 0.939 | 0.963 | 0.986 | 0.993 | 0.979 |
| | $P_{uT}/P_{nD.T}$ | 0.976 | 0.945 | 0.901 | 0.854 | 0.821 | 0.748 | 0.681 | 0.673 | 0.690 | 0.709 | 0.718 | 0.711 |
| | $P_{uT}/P_{nDFT.T}$ | 1.188 | 1.224 | 1.293 | 1.367 | 1.407 | 1.431 | 1.376 | 1.416 | 1.502 | 1.590 | 1.654 | 1.682 |
| | $P_{uT}/P_{nFTD.T}$ | 1.181 | 1.195 | 1.226 | 1.278 | 1.343 | 1.327 | 1.305 | 1.391 | 1.532 | 1.686 | 1.825 | 1.933 |

**Table I.6**: Numerical failure loads and their DSM estimates concerning the **LC6** column geometry with 12 room temperature stresses (corresponding to equally spaced slenderness values) and 8 temperatures varying from $T$=20/100 to $T$=800 ºC.

| $T$ (ºC) | $\lambda_{cr.20}$ | 0.30 | 0.55 | 0.80 | 1.05 | 1.30 | 1.55 | 1.80 | 2.05 | 2.30 | 2.55 | 2.80 | 3.05 |
|---|---|---|---|---|---|---|---|---|---|---|---|---|---|
| 20/100 | $\lambda_{FT.T}$ | 0.316 | 0.579 | 0.843 | 1.106 | 1.371 | 1.634 | 1.898 | 2.161 | 2.425 | 2.688 | 2.952 | 3.216 |
| | $\lambda_{D.T}$ | 0.300 | 0.550 | 0.799 | 1.049 | 1.300 | 1.550 | 1.800 | 2.050 | 2.300 | 2.549 | 2.800 | 3.050 |
| | $P_{uT}/P_{yT}$ | 0.953 | 0.910 | 0.824 | 0.650 | 0.476 | 0.383 | 0.330 | 0.293 | 0.261 | 0.228 | 0.200 | 0.169 |
| | $P_{uT}/P_{nFT.T}$ | 0.993 | 1.047 | 1.109 | 1.085 | 1.046 | 1.067 | 1.063 | 1.069 | 1.066 | 1.027 | 0.987 | 0.909 |
| | $P_{uT}/P_{nD.T}$ | 0.953 | 0.910 | 0.936 | 0.902 | 0.798 | 0.760 | 0.763 | 0.775 | 0.782 | 0.762 | 0.741 | 0.691 |
| | $P_{uT}/P_{nDFT.T}$ | 0.993 | 1.047 | 1.164 | 1.245 | 1.263 | 1.343 | 1.421 | 1.510 | 1.585 | 1.601 | 1.606 | 1.542 |
| | $P_{uT}/P_{nFTD.T}$ | 0.993 | 1.047 | 1.216 | 1.304 | 1.276 | 1.335 | 1.465 | 1.622 | 1.779 | 1.882 | 1.981 | 1.997 |
| 200 | $\lambda_{FT.T}$ | 0.314 | 0.576 | 0.838 | 1.100 | 1.363 | 1.625 | 1.887 | 2.149 | 2.411 | 2.673 | 2.935 | 3.198 |
| | $\lambda_{D.T}$ | 0.298 | 0.546 | 0.795 | 1.043 | 1.293 | 1.541 | 1.790 | 2.039 | 2.287 | 2.535 | 2.784 | 3.033 |
| | $P_{uT}/P_{yT}$ | 0.933 | 0.892 | 0.812 | 0.650 | 0.479 | 0.382 | 0.329 | 0.292 | 0.261 | 0.229 | 0.197 | 0.172 |
| | $P_{uT}/P_{nFT.T}$ | 1.076 | 1.121 | 1.170 | 1.129 | 1.056 | 1.058 | 1.055 | 1.061 | 1.060 | 1.029 | 0.970 | 0.919 |
| | $P_{uT}/P_{nD.T}$ | 0.954 | 0.912 | 0.930 | 0.903 | 0.803 | 0.757 | 0.759 | 0.771 | 0.778 | 0.765 | 0.729 | 0.700 |
| | $P_{uT}/P_{nDFT.T}$ | 1.101 | 1.147 | 1.229 | 1.289 | 1.282 | 1.341 | 1.417 | 1.506 | 1.581 | 1.609 | 1.583 | 1.563 |
| | $P_{uT}/P_{nFTD.T}$ | 1.100 | 1.144 | 1.297 | 1.384 | 1.343 | 1.375 | 1.491 | 1.634 | 1.775 | 1.873 | 1.916 | 1.967 |
| 300 | $\lambda_{FT.T}$ | 0.312 | 0.572 | 0.832 | 1.092 | 1.353 | 1.614 | 1.874 | 2.134 | 2.394 | 2.654 | 2.915 | 3.175 |
| | $\lambda_{D.T}$ | 0.296 | 0.543 | 0.789 | 1.036 | 1.284 | 1.530 | 1.777 | 2.024 | 2.271 | 2.517 | 2.765 | 3.012 |
| | $P_{uT}/P_{yT}$ | 0.759 | 0.729 | 0.684 | 0.591 | 0.463 | 0.356 | 0.307 | 0.275 | 0.248 | 0.222 | 0.196 | 0.174 |
| | $P_{uT}/P_{nFT.T}$ | 0.951 | 0.986 | 1.045 | 1.065 | 1.032 | 0.979 | 0.975 | 0.992 | 1.001 | 0.987 | 0.955 | 0.921 |
| | $P_{uT}/P_{nD.T}$ | 0.965 | 0.927 | 0.892 | 0.887 | 0.818 | 0.732 | 0.728 | 0.742 | 0.754 | 0.750 | 0.732 | 0.713 |
| | $P_{uT}/P_{nDFT.T}$ | 1.210 | 1.255 | 1.330 | 1.379 | 1.392 | 1.368 | 1.427 | 1.518 | 1.599 | 1.643 | 1.651 | 1.652 |
| | $P_{uT}/P_{nFTD.T}$ | 1.202 | 1.226 | 1.292 | 1.401 | 1.400 | 1.352 | 1.443 | 1.576 | 1.711 | 1.815 | 1.887 | 1.955 |
| 400 | $\lambda_{FT.T}$ | 0.305 | 0.558 | 0.812 | 1.066 | 1.321 | 1.575 | 1.829 | 2.083 | 2.336 | 2.590 | 2.844 | 3.099 |
| | $\lambda_{D.T}$ | 0.289 | 0.530 | 0.770 | 1.011 | 1.253 | 1.494 | 1.735 | 1.975 | 2.216 | 2.457 | 2.698 | 2.939 |
| | $P_{uT}/P_{yT}$ | 0.630 | 0.609 | 0.582 | 0.531 | 0.449 | 0.354 | 0.293 | 0.265 | 0.243 | 0.219 | 0.195 | 0.174 |
| | $P_{uT}/P_{nFT.T}$ | 0.836 | 0.866 | 0.920 | 0.973 | 0.991 | 0.952 | 0.911 | 0.932 | 0.955 | 0.954 | 0.931 | 0.900 |
| | $P_{uT}/P_{nD.T}$ | 0.975 | 0.943 | 0.901 | 0.871 | 0.834 | 0.753 | 0.709 | 0.722 | 0.741 | 0.742 | 0.729 | 0.710 |
| | $P_{uT}/P_{nDFT.T}$ | 1.294 | 1.340 | 1.424 | 1.506 | 1.534 | 1.501 | 1.475 | 1.558 | 1.650 | 1.701 | 1.716 | 1.711 |
| | $P_{uT}/P_{nFTD.T}$ | 1.281 | 1.295 | 1.325 | 1.391 | 1.438 | 1.393 | 1.402 | 1.521 | 1.659 | 1.763 | 1.836 | 1.891 |
| 500 | $\lambda_{FT.T}$ | 0.297 | 0.545 | 0.792 | 1.040 | 1.288 | 1.536 | 1.784 | 2.031 | 2.279 | 2.526 | 2.774 | 3.022 |
| | $\lambda_{D.T}$ | 0.282 | 0.516 | 0.751 | 0.986 | 1.222 | 1.457 | 1.692 | 1.927 | 2.161 | 2.396 | 2.631 | 2.867 |
| | $P_{uT}/P_{yT}$ | 0.661 | 0.639 | 0.611 | 0.559 | 0.470 | 0.372 | 0.305 | 0.273 | 0.251 | 0.227 | 0.203 | 0.183 |
| | $P_{uT}/P_{nFT.T}$ | 0.902 | 0.928 | 0.979 | 1.024 | 1.024 | 0.975 | 0.925 | 0.940 | 0.963 | 0.966 | 0.946 | 0.923 |
| | $P_{uT}/P_{nD.T}$ | 0.973 | 0.941 | 0.899 | 0.878 | 0.841 | 0.762 | 0.713 | 0.721 | 0.740 | 0.745 | 0.734 | 0.721 |
| | $P_{uT}/P_{nDFT.T}$ | 1.328 | 1.367 | 1.441 | 1.508 | 1.516 | 1.475 | 1.443 | 1.518 | 1.610 | 1.670 | 1.692 | 1.704 |
| | $P_{uT}/P_{nFTD.T}$ | 1.317 | 1.329 | 1.357 | 1.432 | 1.474 | 1.427 | 1.421 | 1.527 | 1.660 | 1.767 | 1.841 | 1.907 |
| 600 | $\lambda_{FT.T}$ | 0.311 | 0.570 | 0.829 | 1.088 | 1.348 | 1.608 | 1.867 | 2.126 | 2.385 | 2.644 | 2.904 | 3.163 |
| | $\lambda_{D.T}$ | 0.295 | 0.541 | 0.786 | 1.032 | 1.279 | 1.525 | 1.771 | 2.017 | 2.262 | 2.508 | 2.754 | 3.000 |
| | $P_{uT}/P_{yT}$ | 0.586 | 0.569 | 0.543 | 0.499 | 0.428 | 0.337 | 0.281 | 0.256 | 0.235 | 0.212 | 0.188 | 0.170 |
| | $P_{uT}/P_{nFT.T}$ | 0.799 | 0.830 | 0.884 | 0.941 | 0.976 | 0.925 | 0.891 | 0.919 | 0.942 | 0.939 | 0.914 | 0.896 |
| | $P_{uT}/P_{nD.T}$ | 0.977 | 0.948 | 0.905 | 0.865 | 0.834 | 0.748 | 0.706 | 0.723 | 0.741 | 0.740 | 0.723 | 0.713 |
| | $P_{uT}/P_{nDFT.T}$ | 1.332 | 1.383 | 1.473 | 1.569 | 1.627 | 1.542 | 1.524 | 1.614 | 1.704 | 1.749 | 1.753 | 1.768 |
| | $P_{uT}/P_{nFTD.T}$ | 1.317 | 1.330 | 1.356 | 1.406 | 1.459 | 1.403 | 1.416 | 1.543 | 1.680 | 1.781 | 1.844 | 1.923 |
| 700 | $\lambda_{FT.T}$ | 0.316 | 0.579 | 0.843 | 1.106 | 1.371 | 1.634 | 1.898 | 2.161 | 2.425 | 2.688 | 2.952 | 3.216 |
| | $\lambda_{D.T}$ | 0.300 | 0.550 | 0.799 | 1.049 | 1.300 | 1.550 | 1.800 | 2.050 | 2.300 | 2.549 | 2.800 | 3.050 |
| | $P_{uT}/P_{yT}$ | 0.565 | 0.548 | 0.523 | 0.482 | 0.413 | 0.328 | 0.274 | 0.250 | 0.229 | 0.206 | 0.183 | 0.165 |
| | $P_{uT}/P_{nFT.T}$ | 0.743 | 0.777 | 0.834 | 0.900 | 0.947 | 0.913 | 0.882 | 0.914 | 0.936 | 0.929 | 0.902 | 0.887 |
| | $P_{uT}/P_{nD.T}$ | 0.979 | 0.950 | 0.907 | 0.863 | 0.827 | 0.746 | 0.706 | 0.725 | 0.741 | 0.737 | 0.719 | 0.711 |
| | $P_{uT}/P_{nDFT.T}$ | 1.288 | 1.346 | 1.445 | 1.561 | 1.641 | 1.583 | 1.558 | 1.653 | 1.738 | 1.774 | 1.772 | 1.793 |
| | $P_{uT}/P_{nFTD.T}$ | 1.272 | 1.288 | 1.315 | 1.363 | 1.414 | 1.373 | 1.393 | 1.531 | 1.669 | 1.767 | 1.832 | 1.924 |
| 800 | $\lambda_{FT.T}$ | 0.279 | 0.511 | 0.743 | 0.975 | 1.209 | 1.441 | 1.674 | 1.906 | 2.138 | 2.370 | 2.603 | 2.836 |
| | $\lambda_{D.T}$ | 0.264 | 0.485 | 0.705 | 0.925 | 1.146 | 1.367 | 1.587 | 1.808 | 2.028 | 2.248 | 2.469 | 2.690 |
| | $P_{uT}/P_{yT}$ | 0.695 | 0.673 | 0.646 | 0.598 | 0.533 | 0.413 | 0.331 | 0.293 | 0.267 | 0.245 | 0.222 | 0.200 |
| | $P_{uT}/P_{nFT.T}$ | 0.850 | 0.877 | 0.929 | 0.983 | 1.042 | 0.994 | 0.943 | 0.946 | 0.965 | 0.979 | 0.972 | 0.949 |
| | $P_{uT}/P_{nD.T}$ | 0.973 | 0.943 | 0.905 | 0.884 | 0.893 | 0.790 | 0.721 | 0.719 | 0.734 | 0.747 | 0.746 | 0.733 |
| | $P_{uT}/P_{nDFT.T}$ | 1.190 | 1.228 | 1.300 | 1.377 | 1.478 | 1.441 | 1.405 | 1.460 | 1.542 | 1.619 | 1.663 | 1.678 |
| | $P_{uT}/P_{nFTD.T}$ | 1.182 | 1.197 | 1.232 | 1.310 | 1.431 | 1.361 | 1.328 | 1.415 | 1.537 | 1.663 | 1.762 | 1.837 |

**Table I.7**: Numerical failure loads and their DSM estimates concerning the **LC7** column geometry with 12 room temperature stresses (corresponding to equally spaced slenderness values) and 8 temperatures varying from $T$=20/100 to $T$=800 ºC.

| $T$ (ºC) | $\lambda_{cr.20}$ | 0.30 | 0.55 | 0.80 | 1.05 | 1.30 | 1.55 | 1.80 | 2.05 | 2.30 | 2.55 | 2.80 | 3.05 |
|---|---|---|---|---|---|---|---|---|---|---|---|---|---|
| 20/100 | $\lambda_{FT.T}$ | 0.307 | 0.564 | 0.820 | 1.076 | 1.332 | 1.588 | 1.845 | 2.101 | 2.357 | 2.613 | 2.869 | 3.126 |
| | $\lambda_{D.T}$ | 0.300 | 0.550 | 0.800 | 1.050 | 1.300 | 1.550 | 1.800 | 2.050 | 2.300 | 2.550 | 2.800 | 3.050 |
| | $P_{uT}/P_{yT}$ | 0.956 | 0.917 | 0.840 | 0.671 | 0.490 | 0.394 | 0.339 | 0.298 | 0.262 | 0.227 | 0.199 | 0.168 |
| | $P_{uT}/P_{nFT.T}$ | 0.994 | 1.047 | 1.113 | 1.089 | 1.029 | 1.068 | 1.064 | 1.063 | 1.048 | 1.003 | 0.966 | 0.885 |
| | $P_{uT}/P_{nD.T}$ | 0.956 | 0.917 | 0.955 | 0.931 | 0.821 | 0.782 | 0.782 | 0.788 | 0.785 | 0.759 | 0.738 | 0.684 |
| | $P_{uT}/P_{nDFT.T}$ | 0.994 | 1.047 | 1.173 | 1.261 | 1.263 | 1.358 | 1.436 | 1.516 | 1.573 | 1.577 | 1.585 | 1.513 |
| | $P_{uT}/P_{nFTD.T}$ | 0.994 | 1.047 | 1.223 | 1.320 | 1.278 | 1.331 | 1.449 | 1.583 | 1.707 | 1.782 | 1.870 | 1.865 |
| 200 | $\lambda_{FT.T}$ | 0.306 | 0.560 | 0.815 | 1.070 | 1.325 | 1.580 | 1.834 | 2.089 | 2.344 | 2.599 | 2.853 | 3.108 |
| | $\lambda_{D.T}$ | 0.298 | 0.547 | 0.796 | 1.044 | 1.293 | 1.541 | 1.790 | 2.039 | 2.287 | 2.536 | 2.784 | 3.033 |
| | $P_{uT}/P_{yT}$ | 0.936 | 0.899 | 0.828 | 0.671 | 0.492 | 0.393 | 0.338 | 0.297 | 0.263 | 0.229 | 0.196 | 0.165 |
| | $P_{uT}/P_{nFT.T}$ | 1.077 | 1.122 | 1.176 | 1.138 | 1.045 | 1.060 | 1.056 | 1.056 | 1.044 | 1.008 | 0.944 | 0.865 |
| | $P_{uT}/P_{nD.T}$ | 0.957 | 0.919 | 0.948 | 0.933 | 0.825 | 0.779 | 0.778 | 0.784 | 0.783 | 0.763 | 0.722 | 0.669 |
| | $P_{uT}/P_{nDFT.T}$ | 1.102 | 1.148 | 1.238 | 1.309 | 1.284 | 1.356 | 1.433 | 1.512 | 1.572 | 1.589 | 1.553 | 1.482 |
| | $P_{uT}/P_{nFTD.T}$ | 1.101 | 1.145 | 1.306 | 1.406 | 1.349 | 1.377 | 1.483 | 1.605 | 1.717 | 1.790 | 1.810 | 1.788 |
| 300 | $\lambda_{FT.T}$ | 0.304 | 0.557 | 0.810 | 1.062 | 1.315 | 1.568 | 1.821 | 2.074 | 2.327 | 2.580 | 2.833 | 3.086 |
| | $\lambda_{D.T}$ | 0.296 | 0.543 | 0.790 | 1.037 | 1.284 | 1.531 | 1.777 | 2.024 | 2.271 | 2.518 | 2.765 | 3.012 |
| | $P_{uT}/P_{yT}$ | 0.763 | 0.736 | 0.695 | 0.611 | 0.480 | 0.368 | 0.316 | 0.281 | 0.252 | 0.222 | 0.196 | 0.165 |
| | $P_{uT}/P_{nFT.T}$ | 0.955 | 0.989 | 1.048 | 1.078 | 1.034 | 0.985 | 0.981 | 0.991 | 0.994 | 0.971 | 0.937 | 0.859 |
| | $P_{uT}/P_{nD.T}$ | 0.971 | 0.936 | 0.906 | 0.917 | 0.847 | 0.757 | 0.750 | 0.759 | 0.765 | 0.752 | 0.731 | 0.676 |
| | $P_{uT}/P_{nDFT.T}$ | 1.216 | 1.259 | 1.334 | 1.400 | 1.405 | 1.387 | 1.447 | 1.529 | 1.601 | 1.628 | 1.632 | 1.551 |
| | $P_{uT}/P_{nFTD.T}$ | 1.208 | 1.232 | 1.299 | 1.428 | 1.423 | 1.366 | 1.448 | 1.563 | 1.677 | 1.752 | 1.809 | 1.772 |
| 400 | $\lambda_{FT.T}$ | 0.296 | 0.543 | 0.790 | 1.037 | 1.284 | 1.531 | 1.777 | 2.024 | 2.271 | 2.518 | 2.765 | 3.012 |
| | $\lambda_{D.T}$ | 0.289 | 0.530 | 0.771 | 1.012 | 1.253 | 1.494 | 1.735 | 1.975 | 2.216 | 2.457 | 2.698 | 2.939 |
| | $P_{uT}/P_{yT}$ | 0.640 | 0.621 | 0.592 | 0.547 | 0.466 | 0.367 | 0.304 | 0.272 | 0.247 | 0.221 | 0.196 | 0.165 |
| | $P_{uT}/P_{nFT.T}$ | 0.848 | 0.877 | 0.926 | 0.983 | 0.999 | 0.960 | 0.920 | 0.936 | 0.953 | 0.943 | 0.918 | 0.841 |
| | $P_{uT}/P_{nD.T}$ | 0.990 | 0.960 | 0.917 | 0.897 | 0.866 | 0.780 | 0.735 | 0.742 | 0.754 | 0.748 | 0.732 | 0.674 |
| | $P_{uT}/P_{nDFT.T}$ | 1.312 | 1.357 | 1.434 | 1.522 | 1.545 | 1.519 | 1.499 | 1.574 | 1.655 | 1.693 | 1.701 | 1.609 |
| | $P_{uT}/P_{nFTD.T}$ | 1.300 | 1.314 | 1.339 | 1.417 | 1.468 | 1.414 | 1.418 | 1.521 | 1.639 | 1.720 | 1.776 | 1.727 |
| 500 | $\lambda_{FT.T}$ | 0.289 | 0.530 | 0.771 | 1.011 | 1.252 | 1.493 | 1.734 | 1.974 | 2.215 | 2.456 | 2.697 | 2.938 |
| | $\lambda_{D.T}$ | 0.282 | 0.517 | 0.752 | 0.987 | 1.222 | 1.457 | 1.692 | 1.927 | 2.162 | 2.397 | 2.632 | 2.867 |
| | $P_{uT}/P_{yT}$ | 0.667 | 0.649 | 0.621 | 0.573 | 0.489 | 0.385 | 0.316 | 0.281 | 0.256 | 0.230 | 0.204 | 0.172 |
| | $P_{uT}/P_{nFT.T}$ | 0.910 | 0.938 | 0.985 | 1.033 | 1.037 | 0.993 | 0.934 | 0.945 | 0.961 | 0.956 | 0.931 | 0.854 |
| | $P_{uT}/P_{nD.T}$ | 0.983 | 0.955 | 0.914 | 0.901 | 0.876 | 0.790 | 0.738 | 0.742 | 0.755 | 0.752 | 0.736 | 0.679 |
| | $P_{uT}/P_{nDFT.T}$ | 1.340 | 1.381 | 1.450 | 1.521 | 1.540 | 1.507 | 1.466 | 1.536 | 1.618 | 1.665 | 1.676 | 1.587 |
| | $P_{uT}/P_{nFTD.T}$ | 1.329 | 1.344 | 1.370 | 1.455 | 1.512 | 1.450 | 1.439 | 1.532 | 1.645 | 1.729 | 1.783 | 1.729 |
| 600 | $\lambda_{FT.T}$ | 0.302 | 0.554 | 0.806 | 1.059 | 1.311 | 1.563 | 1.815 | 2.067 | 2.319 | 2.571 | 2.823 | 3.075 |
| | $\lambda_{D.T}$ | 0.295 | 0.541 | 0.787 | 1.033 | 1.279 | 1.525 | 1.771 | 2.017 | 2.263 | 2.509 | 2.754 | 3.000 |
| | $P_{uT}/P_{yT}$ | 0.603 | 0.583 | 0.555 | 0.514 | 0.442 | 0.351 | 0.291 | 0.262 | 0.239 | 0.213 | 0.190 | 0.160 |
| | $P_{uT}/P_{nFT.T}$ | 0.821 | 0.846 | 0.892 | 0.951 | 0.979 | 0.936 | 0.901 | 0.922 | 0.938 | 0.927 | 0.905 | 0.830 |
| | $P_{uT}/P_{nD.T}$ | 1.005 | 0.972 | 0.925 | 0.892 | 0.862 | 0.777 | 0.732 | 0.742 | 0.753 | 0.745 | 0.730 | 0.672 |
| | $P_{uT}/P_{nDFT.T}$ | 1.368 | 1.411 | 1.487 | 1.585 | 1.631 | 1.560 | 1.548 | 1.627 | 1.706 | 1.736 | 1.747 | 1.648 |
| | $P_{uT}/P_{nFTD.T}$ | 1.353 | 1.360 | 1.376 | 1.432 | 1.485 | 1.430 | 1.434 | 1.543 | 1.659 | 1.734 | 1.795 | 1.743 |
| 700 | $\lambda_{FT.T}$ | 0.307 | 0.564 | 0.820 | 1.076 | 1.332 | 1.588 | 1.845 | 2.101 | 2.357 | 2.613 | 2.869 | 3.126 |
| | $\lambda_{D.T}$ | 0.300 | 0.550 | 0.800 | 1.050 | 1.300 | 1.550 | 1.800 | 2.050 | 2.300 | 2.550 | 2.800 | 3.050 |
| | $P_{uT}/P_{yT}$ | 0.585 | 0.565 | 0.536 | 0.496 | 0.428 | 0.340 | 0.284 | 0.257 | 0.233 | 0.207 | 0.183 | 0.154 |
| | $P_{uT}/P_{nFT.T}$ | 0.769 | 0.795 | 0.844 | 0.909 | 0.950 | 0.921 | 0.892 | 0.916 | 0.932 | 0.916 | 0.889 | 0.815 |
| | $P_{uT}/P_{nD.T}$ | 1.014 | 0.979 | 0.929 | 0.890 | 0.857 | 0.772 | 0.731 | 0.744 | 0.753 | 0.741 | 0.721 | 0.664 |
| | $P_{uT}/P_{nDFT.T}$ | 1.333 | 1.378 | 1.462 | 1.575 | 1.647 | 1.596 | 1.581 | 1.665 | 1.739 | 1.759 | 1.756 | 1.655 |
| | $P_{uT}/P_{nFTD.T}$ | 1.316 | 1.322 | 1.338 | 1.388 | 1.442 | 1.393 | 1.409 | 1.527 | 1.644 | 1.716 | 1.769 | 1.723 |
| 800 | $\lambda_{FT.T}$ | 0.271 | 0.497 | 0.723 | 0.949 | 1.175 | 1.401 | 1.627 | 1.853 | 2.079 | 2.305 | 2.531 | 2.756 |
| | $\lambda_{D.T}$ | 0.265 | 0.485 | 0.706 | 0.926 | 1.146 | 1.367 | 1.587 | 1.808 | 2.028 | 2.249 | 2.469 | 2.690 |
| | $P_{uT}/P_{yT}$ | 0.700 | 0.682 | 0.655 | 0.612 | 0.533 | 0.428 | 0.343 | 0.302 | 0.273 | 0.249 | 0.224 | 0.189 |
| | $P_{uT}/P_{nFT.T}$ | 0.855 | 0.883 | 0.932 | 0.989 | 1.015 | 0.993 | 0.952 | 0.953 | 0.966 | 0.973 | 0.960 | 0.880 |
| | $P_{uT}/P_{nD.T}$ | 0.980 | 0.954 | 0.917 | 0.905 | 0.894 | 0.821 | 0.747 | 0.742 | 0.751 | 0.759 | 0.751 | 0.692 |
| | $P_{uT}/P_{nDFT.T}$ | 1.197 | 1.237 | 1.305 | 1.385 | 1.444 | 1.450 | 1.428 | 1.480 | 1.555 | 1.622 | 1.654 | 1.566 |
| | $P_{uT}/P_{nFTD.T}$ | 1.189 | 1.207 | 1.241 | 1.326 | 1.409 | 1.384 | 1.344 | 1.420 | 1.526 | 1.633 | 1.710 | 1.665 |

**Table I.8**: Numerical failure loads and their DSM estimates concerning the **LC8** column geometry with 12 room temperature stresses (corresponding to equally spaced slenderness values) and 8 temperatures varying from $T$=20/100 to $T$=800 ºC.

| $T$ (ºC) | $\lambda_{cr.20}$ | 0.20 | 0.45 | 0.70 | 0.95 | 1.20 | 1.45 | 1.70 | 1.95 | 2.20 | 2.45 | 2.70 | 2.95 |
|---|---|---|---|---|---|---|---|---|---|---|---|---|---|
| 20/100 | $\lambda_{FT.T}$ | 0.204 | 0.458 | 0.712 | 0.967 | 1.221 | 1.475 | 1.730 | 1.984 | 2.239 | 2.493 | 2.747 | 3.002 |
| | $\lambda_{D.T}$ | 0.200 | 0.450 | 0.700 | 0.950 | 1.200 | 1.450 | 1.700 | 1.950 | 2.200 | 2.450 | 2.700 | 2.950 |
| | $P_{uT}/P_{yT}$ | 0.986 | 0.968 | 0.932 | 0.789 | 0.567 | 0.427 | 0.358 | 0.304 | 0.257 | 0.215 | 0.178 | 0.149 |
| | $P_{uT}/P_{nFT.T}$ | 1.003 | 1.057 | 1.153 | 1.167 | 1.058 | 1.061 | 1.048 | 1.009 | 0.954 | 0.881 | 0.801 | 0.728 |
| | $P_{uT}/P_{nD.T}$ | 0.986 | 0.968 | 0.986 | 1.011 | 0.883 | 0.793 | 0.780 | 0.763 | 0.732 | 0.688 | 0.636 | 0.587 |
| | $P_{uT}/P_{nDFT.T}$ | 1.003 | 1.057 | 1.172 | 1.307 | 1.279 | 1.326 | 1.390 | 1.423 | 1.421 | 1.382 | 1.318 | 1.252 |
| | $P_{uT}/P_{nFTD.T}$ | 1.003 | 1.057 | 1.205 | 1.372 | 1.318 | 1.295 | 1.386 | 1.471 | 1.528 | 1.550 | 1.543 | 1.533 |
| 200 | $\lambda_{FT.T}$ | 0.202 | 0.455 | 0.708 | 0.961 | 1.214 | 1.467 | 1.720 | 1.973 | 2.226 | 2.479 | 2.732 | 2.985 |
| | $\lambda_{D.T}$ | 0.199 | 0.447 | 0.696 | 0.945 | 1.193 | 1.442 | 1.691 | 1.939 | 2.188 | 2.436 | 2.685 | 2.934 |
| | $P_{uT}/P_{yT}$ | 0.966 | 0.948 | 0.916 | 0.789 | 0.571 | 0.427 | 0.360 | 0.306 | 0.259 | 0.217 | 0.180 | 0.151 |
| | $P_{uT}/P_{nFT.T}$ | 1.091 | 1.138 | 1.225 | 1.233 | 1.094 | 1.051 | 1.047 | 1.011 | 0.957 | 0.885 | 0.806 | 0.733 |
| | $P_{uT}/P_{nD.T}$ | 0.988 | 0.970 | 0.980 | 1.015 | 0.890 | 0.794 | 0.782 | 0.766 | 0.736 | 0.692 | 0.640 | 0.591 |
| | $P_{uT}/P_{nDFT.T}$ | 1.116 | 1.165 | 1.258 | 1.372 | 1.318 | 1.325 | 1.396 | 1.432 | 1.431 | 1.393 | 1.329 | 1.263 |
| | $P_{uT}/P_{nFTD.T}$ | 1.115 | 1.163 | 1.296 | 1.470 | 1.403 | 1.354 | 1.435 | 1.511 | 1.556 | 1.565 | 1.545 | 1.522 |
| 300 | $\lambda_{FT.T}$ | 0.201 | 0.452 | 0.703 | 0.955 | 1.206 | 1.457 | 1.708 | 1.959 | 2.211 | 2.462 | 2.713 | 2.964 |
| | $\lambda_{D.T}$ | 0.197 | 0.444 | 0.691 | 0.938 | 1.185 | 1.432 | 1.679 | 1.925 | 2.172 | 2.419 | 2.666 | 2.913 |
| | $P_{uT}/P_{yT}$ | 0.815 | 0.795 | 0.769 | 0.714 | 0.563 | 0.416 | 0.356 | 0.309 | 0.262 | 0.220 | 0.183 | 0.153 |
| | $P_{uT}/P_{nFT.T}$ | 1.002 | 1.033 | 1.100 | 1.173 | 1.106 | 1.020 | 1.029 | 1.014 | 0.961 | 0.891 | 0.812 | 0.738 |
| | $P_{uT}/P_{nD.T}$ | 1.037 | 1.012 | 0.979 | 1.008 | 0.931 | 0.806 | 0.799 | 0.793 | 0.759 | 0.713 | 0.658 | 0.606 |
| | $P_{uT}/P_{nDFT.T}$ | 1.275 | 1.314 | 1.400 | 1.501 | 1.480 | 1.418 | 1.497 | 1.549 | 1.538 | 1.491 | 1.417 | 1.340 |
| | $P_{uT}/P_{nFTD.T}$ | 1.272 | 1.295 | 1.352 | 1.515 | 1.513 | 1.406 | 1.493 | 1.580 | 1.611 | 1.607 | 1.574 | 1.538 |
| 400 | $\lambda_{FT.T}$ | 0.196 | 0.441 | 0.686 | 0.932 | 1.177 | 1.422 | 1.667 | 1.912 | 2.157 | 2.402 | 2.648 | 2.893 |
| | $\lambda_{D.T}$ | 0.193 | 0.434 | 0.675 | 0.915 | 1.156 | 1.397 | 1.638 | 1.879 | 2.120 | 2.361 | 2.602 | 2.843 |
| | $P_{uT}/P_{yT}$ | 0.735 | 0.710 | 0.680 | 0.640 | 0.557 | 0.422 | 0.360 | 0.318 | 0.271 | 0.229 | 0.192 | 0.161 |
| | $P_{uT}/P_{nFT.T}$ | 0.960 | 0.973 | 1.015 | 1.079 | 1.101 | 1.015 | 1.017 | 1.022 | 0.974 | 0.909 | 0.832 | 0.758 |
| | $P_{uT}/P_{nD.T}$ | 1.138 | 1.099 | 1.053 | 1.011 | 0.982 | 0.850 | 0.827 | 0.829 | 0.793 | 0.745 | 0.689 | 0.634 |
| | $P_{uT}/P_{nDFT.T}$ | 1.486 | 1.505 | 1.571 | 1.671 | 1.704 | 1.595 | 1.640 | 1.705 | 1.683 | 1.628 | 1.545 | 1.455 |
| | $P_{uT}/P_{nFTD.T}$ | 1.480 | 1.474 | 1.493 | 1.545 | 1.615 | 1.494 | 1.549 | 1.649 | 1.671 | 1.662 | 1.623 | 1.574 |
| 500 | $\lambda_{FT.T}$ | 0.191 | 0.430 | 0.669 | 0.909 | 1.148 | 1.387 | 1.626 | 1.865 | 2.104 | 2.343 | 2.582 | 2.821 |
| | $\lambda_{D.T}$ | 0.188 | 0.423 | 0.658 | 0.893 | 1.128 | 1.363 | 1.598 | 1.833 | 2.068 | 2.303 | 2.538 | 2.773 |
| | $P_{uT}/P_{yT}$ | 0.753 | 0.730 | 0.702 | 0.664 | 0.581 | 0.441 | 0.369 | 0.328 | 0.281 | 0.239 | 0.201 | 0.169 |
| | $P_{uT}/P_{nFT.T}$ | 1.012 | 1.025 | 1.067 | 1.129 | 1.143 | 1.040 | 1.019 | 1.029 | 0.985 | 0.926 | 0.853 | 0.778 |
| | $P_{uT}/P_{nD.T}$ | 1.108 | 1.074 | 1.034 | 1.003 | 0.985 | 0.858 | 0.819 | 0.826 | 0.794 | 0.752 | 0.699 | 0.645 |
| | $P_{uT}/P_{nDFT.T}$ | 1.489 | 1.509 | 1.571 | 1.663 | 1.683 | 1.567 | 1.583 | 1.658 | 1.649 | 1.607 | 1.536 | 1.452 |
| | $P_{uT}/P_{nFTD.T}$ | 1.484 | 1.483 | 1.505 | 1.569 | 1.651 | 1.531 | 1.552 | 1.656 | 1.682 | 1.679 | 1.645 | 1.596 |
| 600 | $\lambda_{FT.T}$ | 0.200 | 0.450 | 0.701 | 0.951 | 1.201 | 1.452 | 1.702 | 1.952 | 2.202 | 2.453 | 2.703 | 2.953 |
| | $\lambda_{D.T}$ | 0.197 | 0.443 | 0.689 | 0.935 | 1.180 | 1.426 | 1.672 | 1.918 | 2.164 | 2.410 | 2.656 | 2.902 |
| | $P_{uT}/P_{yT}$ | 0.714 | 0.685 | 0.653 | 0.611 | 0.532 | 0.405 | 0.352 | 0.310 | 0.263 | 0.221 | 0.184 | 0.154 |
| | $P_{uT}/P_{nFT.T}$ | 0.957 | 0.964 | 1.002 | 1.060 | 1.085 | 1.007 | 1.013 | 1.015 | 0.963 | 0.894 | 0.815 | 0.741 |
| | $P_{uT}/P_{nD.T}$ | 1.190 | 1.142 | 1.089 | 1.018 | 0.986 | 0.852 | 0.841 | 0.838 | 0.796 | 0.743 | 0.683 | 0.627 |
| | $P_{uT}/P_{nDFT.T}$ | 1.595 | 1.607 | 1.670 | 1.766 | 1.808 | 1.678 | 1.729 | 1.781 | 1.743 | 1.671 | 1.574 | 1.478 |
| | $P_{uT}/P_{nFTD.T}$ | 1.588 | 1.569 | 1.575 | 1.585 | 1.649 | 1.523 | 1.599 | 1.691 | 1.702 | 1.680 | 1.630 | 1.578 |
| 700 | $\lambda_{FT.T}$ | 0.204 | 0.458 | 0.712 | 0.967 | 1.221 | 1.475 | 1.730 | 1.984 | 2.239 | 2.493 | 2.747 | 3.002 |
| | $\lambda_{D.T}$ | 0.200 | 0.450 | 0.700 | 0.950 | 1.200 | 1.450 | 1.700 | 1.950 | 2.200 | 2.450 | 2.700 | 2.950 |
| | $P_{uT}/P_{yT}$ | 0.704 | 0.673 | 0.639 | 0.595 | 0.517 | 0.395 | 0.346 | 0.304 | 0.257 | 0.215 | 0.178 | 0.149 |
| | $P_{uT}/P_{nFT.T}$ | 0.910 | 0.917 | 0.956 | 1.017 | 1.050 | 0.994 | 1.012 | 1.009 | 0.953 | 0.881 | 0.801 | 0.728 |
| | $P_{uT}/P_{nD.T}$ | 1.221 | 1.167 | 1.108 | 1.032 | 0.987 | 0.853 | 0.849 | 0.840 | 0.795 | 0.738 | 0.677 | 0.621 |
| | $P_{uT}/P_{nDFT.T}$ | 1.577 | 1.589 | 1.656 | 1.762 | 1.821 | 1.724 | 1.784 | 1.823 | 1.772 | 1.690 | 1.585 | 1.486 |
| | $P_{uT}/P_{nFTD.T}$ | 1.568 | 1.546 | 1.549 | 1.557 | 1.606 | 1.491 | 1.585 | 1.672 | 1.681 | 1.657 | 1.608 | 1.560 |
| 800 | $\lambda_{FT.T}$ | 0.179 | 0.404 | 0.628 | 0.853 | 1.077 | 1.301 | 1.526 | 1.750 | 1.974 | 2.199 | 2.423 | 2.647 |
| | $\lambda_{D.T}$ | 0.176 | 0.397 | 0.617 | 0.838 | 1.058 | 1.279 | 1.499 | 1.720 | 1.940 | 2.161 | 2.381 | 2.602 |
| | $P_{uT}/P_{yT}$ | 0.773 | 0.753 | 0.729 | 0.697 | 0.628 | 0.491 | 0.392 | 0.353 | 0.305 | 0.264 | 0.226 | 0.192 |
| | $P_{uT}/P_{nFT.T}$ | 0.931 | 0.948 | 0.993 | 1.063 | 1.108 | 1.039 | 1.022 | 1.044 | 1.008 | 0.963 | 0.902 | 0.832 |
| | $P_{uT}/P_{nD.T}$ | 1.082 | 1.054 | 1.020 | 0.993 | 0.998 | 0.892 | 0.813 | 0.828 | 0.802 | 0.772 | 0.730 | 0.680 |
| | $P_{uT}/P_{nDFT.T}$ | 1.303 | 1.328 | 1.390 | 1.488 | 1.562 | 1.504 | 1.514 | 1.606 | 1.611 | 1.599 | 1.554 | 1.485 |
| | $P_{uT}/P_{nFTD.T}$ | 1.299 | 1.307 | 1.338 | 1.408 | 1.523 | 1.458 | 1.418 | 1.536 | 1.580 | 1.610 | 1.610 | 1.585 |

**Table I.9**: Numerical failure loads and their DSM estimates concerning the **LC9** column geometry with 12 room temperature stresses (corresponding to equally spaced slenderness values) and 8 temperatures varying from $T$=20/100 to $T$=800 ºC.

| $T$ (ºC) | $\lambda_{cr.20}$ | 0.30 | 0.55 | 0.80 | 1.05 | 1.30 | 1.55 | 1.80 | 2.05 | 2.30 | 2.55 | 2.80 | 3.05 |
|---|---|---|---|---|---|---|---|---|---|---|---|---|---|
| 20/100 | $\lambda_{FT.T}$ | 0.303 | 0.556 | 0.809 | 1.062 | 1.314 | 1.567 | 1.820 | 2.073 | 2.325 | 2.578 | 2.831 | 3.084 |
| | $\lambda_{D.T}$ | 0.300 | 0.550 | 0.800 | 1.050 | 1.300 | 1.550 | 1.800 | 2.050 | 2.300 | 2.550 | 2.800 | 3.050 |
| | $P_{uT}/P_{yT}$ | 0.961 | 0.929 | 0.855 | 0.671 | 0.485 | 0.399 | 0.349 | 0.311 | 0.277 | 0.244 | 0.210 | 0.183 |
| | $P_{uT}/P_{nFT.T}$ | 0.999 | 1.057 | 1.124 | 1.076 | 0.999 | 1.066 | 1.068 | 1.071 | 1.060 | 1.028 | 0.960 | 0.905 |
| | $P_{uT}/P_{nD.T}$ | 0.961 | 0.929 | 0.971 | 0.932 | 0.813 | 0.793 | 0.807 | 0.822 | 0.829 | 0.818 | 0.778 | 0.746 |
| | $P_{uT}/P_{nDFT.T}$ | 0.999 | 1.057 | 1.187 | 1.251 | 1.235 | 1.364 | 1.458 | 1.550 | 1.621 | 1.653 | 1.619 | 1.595 |
| | $P_{uT}/P_{nFTD.T}$ | 0.999 | 1.057 | 1.236 | 1.309 | 1.251 | 1.331 | 1.470 | 1.622 | 1.766 | 1.878 | 1.921 | 1.978 |
| 200 | $\lambda_{FT.T}$ | 0.302 | 0.553 | 0.804 | 1.056 | 1.307 | 1.558 | 1.810 | 2.061 | 2.312 | 2.564 | 2.815 | 3.067 |
| | $\lambda_{D.T}$ | 0.298 | 0.547 | 0.796 | 1.044 | 1.293 | 1.541 | 1.790 | 2.039 | 2.287 | 2.536 | 2.784 | 3.033 |
| | $P_{uT}/P_{yT}$ | 0.941 | 0.910 | 0.843 | 0.672 | 0.488 | 0.398 | 0.348 | 0.310 | 0.247 | 0.245 | 0.213 | 0.184 |
| | $P_{uT}/P_{nFT.T}$ | 1.082 | 1.133 | 1.190 | 1.127 | 1.019 | 1.057 | 1.060 | 1.064 | 0.939 | 1.026 | 0.970 | 0.908 |
| | $P_{uT}/P_{nD.T}$ | 0.962 | 0.931 | 0.965 | 0.935 | 0.818 | 0.789 | 0.802 | 0.819 | 0.735 | 0.818 | 0.786 | 0.748 |
| | $P_{uT}/P_{nDFT.T}$ | 1.107 | 1.159 | 1.254 | 1.301 | 1.260 | 1.361 | 1.454 | 1.547 | 1.441 | 1.655 | 1.639 | 1.602 |
| | $P_{uT}/P_{nFTD.T}$ | 1.106 | 1.156 | 1.322 | 1.397 | 1.325 | 1.379 | 1.507 | 1.648 | 1.583 | 1.880 | 1.927 | 1.953 |
| 300 | $\lambda_{FT.T}$ | 0.299 | 0.549 | 0.799 | 1.048 | 1.298 | 1.547 | 1.797 | 2.047 | 2.296 | 2.546 | 2.795 | 3.045 |
| | $\lambda_{D.T}$ | 0.296 | 0.543 | 0.790 | 1.037 | 1.284 | 1.531 | 1.777 | 2.024 | 2.271 | 2.518 | 2.765 | 3.012 |
| | $P_{uT}/P_{yT}$ | 0.768 | 0.745 | 0.709 | 0.625 | 0.478 | 0.372 | 0.327 | 0.295 | 0.235 | 0.239 | 0.211 | 0.182 |
| | $P_{uT}/P_{nFT.T}$ | 0.960 | 0.999 | 1.063 | 1.092 | 1.014 | 0.981 | 0.989 | 1.006 | 0.888 | 0.993 | 0.954 | 0.892 |
| | $P_{uT}/P_{nD.T}$ | 0.977 | 0.948 | 0.925 | 0.938 | 0.844 | 0.766 | 0.776 | 0.797 | 0.712 | 0.808 | 0.788 | 0.748 |
| | $P_{uT}/P_{nDFT.T}$ | 1.222 | 1.272 | 1.353 | 1.420 | 1.384 | 1.388 | 1.472 | 1.571 | 1.453 | 1.698 | 1.701 | 1.655 |
| | $P_{uT}/P_{nFTD.T}$ | 1.214 | 1.245 | 1.320 | 1.451 | 1.406 | 1.367 | 1.480 | 1.619 | 1.538 | 1.851 | 1.912 | 1.921 |
| 400 | $\lambda_{FT.T}$ | 0.292 | 0.536 | 0.779 | 1.023 | 1.267 | 1.510 | 1.754 | 1.997 | 2.241 | 2.484 | 2.728 | 2.972 |
| | $\lambda_{D.T}$ | 0.289 | 0.530 | 0.771 | 1.012 | 1.253 | 1.494 | 1.735 | 1.975 | 2.216 | 2.457 | 2.698 | 2.939 |
| | $P_{uT}/P_{yT}$ | 0.654 | 0.634 | 0.606 | 0.562 | 0.474 | 0.364 | 0.315 | 0.288 | 0.228 | 0.239 | 0.213 | 0.188 |
| | $P_{uT}/P_{nFT.T}$ | 0.866 | 0.893 | 0.942 | 1.001 | 1.003 | 0.938 | 0.931 | 0.958 | 0.845 | 0.972 | 0.944 | 0.902 |
| | $P_{uT}/P_{nD.T}$ | 1.012 | 0.981 | 0.937 | 0.921 | 0.881 | 0.773 | 0.762 | 0.785 | 0.698 | 0.810 | 0.795 | 0.768 |
| | $P_{uT}/P_{nDFT.T}$ | 1.340 | 1.383 | 1.458 | 1.548 | 1.552 | 1.488 | 1.525 | 1.625 | 1.488 | 1.773 | 1.785 | 1.764 |
| | $P_{uT}/P_{nFTD.T}$ | 1.328 | 1.340 | 1.365 | 1.447 | 1.484 | 1.389 | 1.455 | 1.590 | 1.495 | 1.832 | 1.898 | 1.932 |
| 500 | $\lambda_{FT.T}$ | 0.285 | 0.523 | 0.760 | 0.998 | 1.235 | 1.473 | 1.710 | 1.948 | 2.186 | 2.423 | 2.661 | 2.898 |
| | $\lambda_{D.T}$ | 0.282 | 0.517 | 0.752 | 0.987 | 1.222 | 1.457 | 1.692 | 1.927 | 2.162 | 2.397 | 2.632 | 2.867 |
| | $P_{uT}/P_{yT}$ | 0.680 | 0.661 | 0.633 | 0.588 | 0.497 | 0.381 | 0.326 | 0.296 | 0.235 | 0.247 | 0.221 | 0.197 |
| | $P_{uT}/P_{nFT.T}$ | 0.926 | 0.953 | 1.000 | 1.052 | 1.039 | 0.966 | 0.941 | 0.964 | 0.851 | 0.980 | 0.957 | 0.924 |
| | $P_{uT}/P_{nD.T}$ | 1.001 | 0.973 | 0.932 | 0.925 | 0.889 | 0.782 | 0.761 | 0.781 | 0.695 | 0.808 | 0.798 | 0.780 |
| | $P_{uT}/P_{nDFT.T}$ | 1.363 | 1.403 | 1.472 | 1.548 | 1.545 | 1.471 | 1.485 | 1.580 | 1.449 | 1.734 | 1.757 | 1.756 |
| | $P_{uT}/P_{nFTD.T}$ | 1.353 | 1.367 | 1.393 | 1.485 | 1.523 | 1.424 | 1.468 | 1.593 | 1.494 | 1.831 | 1.902 | 1.951 |
| 600 | $\lambda_{FT.T}$ | 0.298 | 0.547 | 0.796 | 1.044 | 1.293 | 1.542 | 1.790 | 2.039 | 2.288 | 2.536 | 2.785 | 3.034 |
| | $\lambda_{D.T}$ | 0.295 | 0.541 | 0.787 | 1.033 | 1.279 | 1.525 | 1.771 | 2.017 | 2.263 | 2.509 | 2.754 | 3.000 |
| | $P_{uT}/P_{yT}$ | 0.620 | 0.598 | 0.570 | 0.529 | 0.451 | 0.348 | 0.304 | 0.279 | 0.222 | 0.232 | 0.206 | 0.180 |
| | $P_{uT}/P_{nFT.T}$ | 0.843 | 0.867 | 0.913 | 0.970 | 0.985 | 0.916 | 0.917 | 0.948 | 0.837 | 0.959 | 0.929 | 0.881 |
| | $P_{uT}/P_{nD.T}$ | 1.033 | 0.997 | 0.951 | 0.917 | 0.879 | 0.772 | 0.765 | 0.790 | 0.701 | 0.810 | 0.792 | 0.759 |
| | $P_{uT}/P_{nDFT.T}$ | 1.405 | 1.445 | 1.521 | 1.617 | 1.641 | 1.543 | 1.583 | 1.687 | 1.539 | 1.825 | 1.826 | 1.787 |
| | $P_{uT}/P_{nFTD.T}$ | 1.390 | 1.394 | 1.411 | 1.466 | 1.504 | 1.409 | 1.482 | 1.623 | 1.523 | 1.859 | 1.916 | 1.933 |
| 700 | $\lambda_{FT.T}$ | 0.303 | 0.556 | 0.809 | 1.062 | 1.314 | 1.567 | 1.820 | 2.073 | 2.325 | 2.578 | 2.831 | 3.084 |
| | $\lambda_{D.T}$ | 0.300 | 0.550 | 0.800 | 1.050 | 1.300 | 1.550 | 1.800 | 2.050 | 2.300 | 2.550 | 2.800 | 3.050 |
| | $P_{uT}/P_{yT}$ | 0.603 | 0.581 | 0.553 | 0.511 | 0.437 | 0.338 | 0.298 | 0.274 | 0.218 | 0.226 | 0.201 | 0.178 |
| | $P_{uT}/P_{nFT.T}$ | 0.792 | 0.816 | 0.865 | 0.928 | 0.956 | 0.901 | 0.912 | 0.945 | 0.834 | 0.952 | 0.919 | 0.880 |
| | $P_{uT}/P_{nD.T}$ | 1.045 | 1.007 | 0.958 | 0.917 | 0.875 | 0.768 | 0.768 | 0.794 | 0.704 | 0.810 | 0.789 | 0.764 |
| | $P_{uT}/P_{nDFT.T}$ | 1.372 | 1.415 | 1.499 | 1.608 | 1.657 | 1.562 | 1.624 | 1.730 | 1.574 | 1.855 | 1.848 | 1.826 |
| | $P_{uT}/P_{nFTD.T}$ | 1.356 | 1.358 | 1.375 | 1.423 | 1.462 | 1.372 | 1.464 | 1.611 | 1.515 | 1.846 | 1.902 | 1.944 |
| 800 | $\lambda_{FT.T}$ | 0.267 | 0.490 | 0.713 | 0.936 | 1.159 | 1.382 | 1.605 | 1.828 | 2.051 | 2.274 | 2.497 | 2.720 |
| | $\lambda_{D.T}$ | 0.265 | 0.485 | 0.706 | 0.926 | 1.146 | 1.367 | 1.587 | 1.808 | 2.028 | 2.249 | 2.469 | 2.690 |
| | $P_{uT}/P_{yT}$ | 0.709 | 0.691 | 0.667 | 0.626 | 0.543 | 0.426 | 0.348 | 0.314 | 0.249 | 0.265 | 0.241 | 0.216 |
| | $P_{uT}/P_{nFT.T}$ | 0.865 | 0.894 | 0.944 | 1.004 | 1.021 | 0.970 | 0.950 | 0.965 | 0.851 | 0.995 | 0.985 | 0.956 |
| | $P_{uT}/P_{nD.T}$ | 0.992 | 0.968 | 0.933 | 0.927 | 0.910 | 0.816 | 0.759 | 0.772 | 0.686 | 0.809 | 0.810 | 0.794 |
| | $P_{uT}/P_{nDFT.T}$ | 1.211 | 1.252 | 1.322 | 1.406 | 1.455 | 1.421 | 1.432 | 1.511 | 1.386 | 1.683 | 1.729 | 1.737 |
| | $P_{uT}/P_{nFTD.T}$ | 1.203 | 1.223 | 1.258 | 1.350 | 1.424 | 1.363 | 1.351 | 1.459 | 1.373 | 1.714 | 1.811 | 1.875 |

**Table I.10**: Numerical failure loads and their DSM estimates concerning the **LC10** column geometry with 12 room temperature stresses (corresponding to equally spaced slenderness values) and 8 temperatures varying from $T$=20/100 to $T$=800 ºC.

| $T$ (ºC) | $\lambda_{cr.20}$ | 0.40 | 0.65 | 0.90 | 1.15 | 1.40 | 1.65 | 1.90 | 2.15 | 2.40 | 2.65 | 2.90 | 3.15 |
|---|---|---|---|---|---|---|---|---|---|---|---|---|---|
| 20/100 | $\lambda_{FT.T}$ | 0.402 | 0.654 | 0.905 | 1.156 | 1.407 | 1.659 | 1.910 | 2.162 | 2.412 | 2.664 | 2.915 | 3.166 |
| | $\lambda_{D.T}$ | 0.400 | 0.650 | 0.900 | 1.150 | 1.400 | 1.650 | 1.900 | 2.151 | 2.400 | 2.650 | 2.900 | 3.150 |
| | $P_{uT}/P_{yT}$ | 0.935 | 0.886 | 0.777 | 0.597 | 0.441 | 0.376 | 0.335 | 0.297 | 0.261 | 0.224 | 0.196 | 0.174 |
| | $P_{uT}/P_{nFT.T}$ | 1.000 | 1.060 | 1.094 | 1.044 | 1.011 | 1.062 | 1.081 | 1.079 | 1.050 | 0.990 | 0.945 | 0.910 |
| | $P_{uT}/P_{nD.T}$ | 0.935 | 0.910 | 0.955 | 0.895 | 0.793 | 0.795 | 0.818 | 0.828 | 0.817 | 0.781 | 0.756 | 0.738 |
| | $P_{uT}/P_{nDFT.T}$ | 1.000 | 1.065 | 1.205 | 1.254 | 1.269 | 1.396 | 1.509 | 1.592 | 1.630 | 1.612 | 1.607 | 1.613 |
| | $P_{uT}/P_{nFTD.T}$ | 1.000 | 1.083 | 1.262 | 1.300 | 1.258 | 1.371 | 1.529 | 1.671 | 1.777 | 1.829 | 1.901 | 1.990 |
| 200 | $\lambda_{FT.T}$ | 0.400 | 0.650 | 0.900 | 1.150 | 1.399 | 1.649 | 1.900 | 2.150 | 2.399 | 2.649 | 2.898 | 3.149 |
| | $\lambda_{D.T}$ | 0.398 | 0.647 | 0.895 | 1.144 | 1.392 | 1.641 | 1.890 | 2.139 | 2.386 | 2.635 | 2.884 | 3.132 |
| | $P_{uT}/P_{yT}$ | 0.915 | 0.869 | 0.769 | 0.592 | 0.440 | 0.375 | 0.332 | 0.297 | 0.265 | 0.233 | 0.204 | 0.175 |
| | $P_{uT}/P_{nFT.T}$ | 1.080 | 1.130 | 1.152 | 1.072 | 1.007 | 1.051 | 1.064 | 1.073 | 1.063 | 1.024 | 0.977 | 0.906 |
| | $P_{uT}/P_{nD.T}$ | 0.936 | 0.907 | 0.951 | 0.890 | 0.790 | 0.790 | 0.808 | 0.825 | 0.828 | 0.809 | 0.782 | 0.736 |
| | $P_{uT}/P_{nDFT.T}$ | 1.104 | 1.156 | 1.261 | 1.280 | 1.270 | 1.390 | 1.493 | 1.590 | 1.655 | 1.671 | 1.665 | 1.610 |
| | $P_{uT}/P_{nFTD.T}$ | 1.103 | 1.171 | 1.346 | 1.369 | 1.314 | 1.414 | 1.551 | 1.695 | 1.816 | 1.891 | 1.948 | 1.948 |
| 300 | $\lambda_{FT.T}$ | 0.397 | 0.646 | 0.893 | 1.141 | 1.390 | 1.638 | 1.886 | 2.135 | 2.382 | 2.630 | 2.878 | 3.126 |
| | $\lambda_{D.T}$ | 0.395 | 0.642 | 0.889 | 1.136 | 1.382 | 1.629 | 1.877 | 2.124 | 2.370 | 2.617 | 2.863 | 3.110 |
| | $P_{uT}/P_{yT}$ | 0.744 | 0.715 | 0.662 | 0.556 | 0.432 | 0.345 | 0.307 | 0.279 | 0.253 | 0.225 | 0.199 | 0.172 |
| | $P_{uT}/P_{nFT.T}$ | 0.951 | 0.996 | 1.046 | 1.041 | 0.995 | 0.962 | 0.979 | 1.001 | 1.006 | 0.983 | 0.948 | 0.888 |
| | $P_{uT}/P_{nD.T}$ | 0.946 | 0.909 | 0.906 | 0.892 | 0.812 | 0.753 | 0.768 | 0.792 | 0.803 | 0.793 | 0.773 | 0.733 |
| | $P_{uT}/P_{nDFT.T}$ | 1.210 | 1.267 | 1.331 | 1.382 | 1.380 | 1.389 | 1.484 | 1.590 | 1.669 | 1.700 | 1.706 | 1.658 |
| | $P_{uT}/P_{nFTD.T}$ | 1.196 | 1.230 | 1.335 | 1.417 | 1.386 | 1.374 | 1.495 | 1.638 | 1.763 | 1.845 | 1.905 | 1.907 |
| 400 | $\lambda_{FT.T}$ | 0.388 | 0.630 | 0.872 | 1.114 | 1.356 | 1.598 | 1.841 | 2.083 | 2.324 | 2.567 | 2.809 | 3.051 |
| | $\lambda_{D.T}$ | 0.386 | 0.627 | 0.867 | 1.108 | 1.349 | 1.590 | 1.831 | 2.073 | 2.313 | 2.553 | 2.794 | 3.035 |
| | $P_{uT}/P_{yT}$ | 0.619 | 0.598 | 0.568 | 0.513 | 0.423 | 0.332 | 0.293 | 0.270 | 0.249 | 0.225 | 0.201 | 0.182 |
| | $P_{uT}/P_{nFT.T}$ | 0.837 | 0.873 | 0.927 | 0.970 | 0.963 | 0.905 | 0.913 | 0.947 | 0.968 | 0.961 | 0.935 | 0.918 |
| | $P_{uT}/P_{nD.T}$ | 0.958 | 0.926 | 0.880 | 0.882 | 0.831 | 0.745 | 0.745 | 0.773 | 0.793 | 0.793 | 0.777 | 0.770 |
| | $P_{uT}/P_{nDFT.T}$ | 1.295 | 1.351 | 1.435 | 1.501 | 1.510 | 1.454 | 1.515 | 1.627 | 1.722 | 1.770 | 1.780 | 1.805 |
| | $P_{uT}/P_{nFTD.T}$ | 1.274 | 1.293 | 1.321 | 1.421 | 1.431 | 1.366 | 1.450 | 1.592 | 1.726 | 1.820 | 1.881 | 1.960 |
| 500 | $\lambda_{FT.T}$ | 0.378 | 0.614 | 0.850 | 1.086 | 1.323 | 1.559 | 1.795 | 2.032 | 2.267 | 2.503 | 2.739 | 2.976 |
| | $\lambda_{D.T}$ | 0.376 | 0.611 | 0.846 | 1.081 | 1.316 | 1.551 | 1.786 | 2.021 | 2.255 | 2.491 | 2.725 | 2.961 |
| | $P_{uT}/P_{yT}$ | 0.650 | 0.628 | 0.597 | 0.538 | 0.444 | 0.349 | 0.304 | 0.279 | 0.257 | 0.233 | 0.209 | 0.189 |
| | $P_{uT}/P_{nFT.T}$ | 0.902 | 0.935 | 0.984 | 1.016 | 0.992 | 0.929 | 0.923 | 0.953 | 0.976 | 0.974 | 0.950 | 0.928 |
| | $P_{uT}/P_{nD.T}$ | 0.957 | 0.925 | 0.888 | 0.889 | 0.839 | 0.755 | 0.746 | 0.770 | 0.792 | 0.796 | 0.783 | 0.772 |
| | $P_{uT}/P_{nDFT.T}$ | 1.327 | 1.376 | 1.449 | 1.496 | 1.490 | 1.436 | 1.479 | 1.584 | 1.683 | 1.740 | 1.758 | 1.774 |
| | $P_{uT}/P_{nFTD.T}$ | 1.309 | 1.327 | 1.364 | 1.461 | 1.468 | 1.403 | 1.465 | 1.596 | 1.730 | 1.828 | 1.890 | 1.954 |
| 600 | $\lambda_{FT.T}$ | 0.396 | 0.643 | 0.890 | 1.137 | 1.384 | 1.632 | 1.879 | 2.127 | 2.373 | 2.620 | 2.867 | 3.115 |
| | $\lambda_{D.T}$ | 0.394 | 0.640 | 0.885 | 1.131 | 1.377 | 1.623 | 1.870 | 2.116 | 2.361 | 2.607 | 2.853 | 3.099 |
| | $P_{uT}/P_{yT}$ | 0.577 | 0.558 | 0.531 | 0.482 | 0.403 | 0.317 | 0.282 | 0.262 | 0.241 | 0.218 | 0.194 | 0.164 |
| | $P_{uT}/P_{nFT.T}$ | 0.801 | 0.836 | 0.891 | 0.939 | 0.947 | 0.880 | 0.897 | 0.936 | 0.956 | 0.948 | 0.920 | 0.841 |
| | $P_{uT}/P_{nD.T}$ | 0.962 | 0.930 | 0.885 | 0.872 | 0.827 | 0.738 | 0.745 | 0.776 | 0.794 | 0.792 | 0.773 | 0.713 |
| | $P_{uT}/P_{nDFT.T}$ | 1.335 | 1.393 | 1.486 | 1.565 | 1.579 | 1.495 | 1.566 | 1.685 | 1.776 | 1.818 | 1.820 | 1.715 |
| | $P_{uT}/P_{nFTD.T}$ | 1.311 | 1.326 | 1.352 | 1.430 | 1.449 | 1.376 | 1.472 | 1.622 | 1.753 | 1.843 | 1.896 | 1.838 |
| 700 | $\lambda_{FT.T}$ | 0.402 | 0.654 | 0.905 | 1.156 | 1.407 | 1.659 | 1.910 | 2.162 | 2.412 | 2.664 | 2.915 | 3.166 |
| | $\lambda_{D.T}$ | 0.400 | 0.650 | 0.900 | 1.150 | 1.400 | 1.650 | 1.900 | 2.151 | 2.400 | 2.650 | 2.900 | 3.150 |
| | $P_{uT}/P_{yT}$ | 0.556 | 0.537 | 0.512 | 0.465 | 0.390 | 0.306 | 0.276 | 0.257 | 0.236 | 0.213 | 0.189 | 0.159 |
| | $P_{uT}/P_{nFT.T}$ | 0.746 | 0.783 | 0.843 | 0.901 | 0.924 | 0.864 | 0.892 | 0.933 | 0.950 | 0.940 | 0.910 | 0.829 |
| | $P_{uT}/P_{nD.T}$ | 0.964 | 0.931 | 0.887 | 0.868 | 0.822 | 0.733 | 0.747 | 0.779 | 0.795 | 0.791 | 0.771 | 0.707 |
| | $P_{uT}/P_{nDFT.T}$ | 1.293 | 1.357 | 1.462 | 1.562 | 1.601 | 1.518 | 1.603 | 1.726 | 1.811 | 1.847 | 1.844 | 1.728 |
| | $P_{uT}/P_{nFTD.T}$ | 1.266 | 1.283 | 1.312 | 1.385 | 1.406 | 1.339 | 1.453 | 1.609 | 1.740 | 1.831 | 1.885 | 1.824 |
| 800 | $\lambda_{FT.T}$ | 0.355 | 0.577 | 0.798 | 1.019 | 1.241 | 1.463 | 1.685 | 1.907 | 2.127 | 2.349 | 2.571 | 2.792 |
| | $\lambda_{D.T}$ | 0.353 | 0.574 | 0.794 | 1.014 | 1.235 | 1.455 | 1.676 | 1.897 | 2.116 | 2.337 | 2.557 | 2.778 |
| | $P_{uT}/P_{yT}$ | 0.683 | 0.662 | 0.632 | 0.579 | 0.489 | 0.389 | 0.326 | 0.296 | 0.274 | 0.253 | 0.229 | 0.206 |
| | $P_{uT}/P_{nFT.T}$ | 0.850 | 0.883 | 0.935 | 0.982 | 0.983 | 0.959 | 0.932 | 0.954 | 0.980 | 0.992 | 0.980 | 0.951 |
| | $P_{uT}/P_{nD.T}$ | 0.957 | 0.927 | 0.891 | 0.898 | 0.865 | 0.786 | 0.745 | 0.762 | 0.787 | 0.801 | 0.797 | 0.781 |
| | $P_{uT}/P_{nDFT.T}$ | 1.190 | 1.237 | 1.310 | 1.375 | 1.418 | 1.420 | 1.427 | 1.516 | 1.617 | 1.696 | 1.735 | 1.741 |
| | $P_{uT}/P_{nFTD.T}$ | 1.176 | 1.198 | 1.237 | 1.344 | 1.385 | 1.342 | 1.353 | 1.467 | 1.601 | 1.722 | 1.809 | 1.866 |

**Table I.11**: Numerical failure loads and their DSM estimates concerning the **LC11** column geometry with 12 room temperature stresses (corresponding to equally spaced slenderness values) and 8 temperatures varying from $T$=20/100 to $T$=800 ºC.

| $T$ (ºC) | $\lambda_{cr.20}$ | 0.30 | 0.55 | 0.80 | 1.05 | 1.30 | 1.55 | 1.80 | 2.05 | 2.30 | 2.55 | 2.80 | 3.05 |
|---|---|---|---|---|---|---|---|---|---|---|---|---|---|
| 20/100 | $\lambda_{FT.T}$ | 0.302 | 0.552 | 0.802 | 1.052 | 1.303 | 1.553 | 1.804 | 2.054 | 2.305 | 2.556 | 2.806 | 3.057 |
| | $\lambda_{D.T}$ | 0.301 | 0.550 | 0.800 | 1.050 | 1.300 | 1.550 | 1.800 | 2.050 | 2.300 | 2.550 | 2.800 | 3.050 |
| | $P_{uT}/P_{yT}$ | 0.956 | 0.921 | 0.850 | 0.688 | 0.505 | 0.401 | 0.347 | 0.306 | 0.269 | 0.231 | 0.200 | 0.177 |
| | $P_{uT}/P_{nFT.T}$ | 0.993 | 1.046 | 1.113 | 1.094 | 1.028 | 1.064 | 1.065 | 1.067 | 1.049 | 0.996 | 0.946 | 0.912 |
| | $P_{uT}/P_{nD.T}$ | 0.956 | 0.921 | 0.966 | 0.954 | 0.846 | 0.796 | 0.801 | 0.809 | 0.804 | 0.772 | 0.742 | 0.723 |
| | $P_{uT}/P_{nDFT.T}$ | 0.993 | 1.046 | 1.176 | 1.275 | 1.276 | 1.364 | 1.451 | 1.537 | 1.591 | 1.583 | 1.570 | 1.577 |
| | $P_{uT}/P_{nFTD.T}$ | 0.993 | 1.046 | 1.224 | 1.333 | 1.293 | 1.324 | 1.445 | 1.578 | 1.692 | 1.748 | 1.803 | 1.887 |
| 200 | $\lambda_{FT.T}$ | 0.300 | 0.549 | 0.797 | 1.047 | 1.296 | 1.545 | 1.794 | 2.043 | 2.292 | 2.541 | 2.790 | 3.040 |
| | $\lambda_{D.T}$ | 0.299 | 0.547 | 0.795 | 1.044 | 1.293 | 1.541 | 1.790 | 2.038 | 2.287 | 2.536 | 2.784 | 3.033 |
| | $P_{uT}/P_{yT}$ | 0.936 | 0.903 | 0.837 | 0.688 | 0.507 | 0.400 | 0.346 | 0.306 | 0.269 | 0.232 | 0.202 | 0.174 |
| | $P_{uT}/P_{nFT.T}$ | 1.076 | 1.122 | 1.177 | 1.146 | 1.047 | 1.055 | 1.057 | 1.060 | 1.046 | 0.998 | 0.950 | 0.890 |
| | $P_{uT}/P_{nD.T}$ | 0.958 | 0.923 | 0.959 | 0.957 | 0.850 | 0.793 | 0.797 | 0.806 | 0.803 | 0.775 | 0.746 | 0.707 |
| | $P_{uT}/P_{nDFT.T}$ | 1.101 | 1.147 | 1.241 | 1.326 | 1.299 | 1.362 | 1.447 | 1.533 | 1.591 | 1.591 | 1.581 | 1.543 |
| | $P_{uT}/P_{nFTD.T}$ | 1.100 | 1.145 | 1.308 | 1.423 | 1.367 | 1.374 | 1.483 | 1.606 | 1.710 | 1.759 | 1.803 | 1.817 |
| 300 | $\lambda_{FT.T}$ | 0.298 | 0.545 | 0.792 | 1.039 | 1.287 | 1.534 | 1.781 | 2.028 | 2.276 | 2.524 | 2.771 | 3.019 |
| | $\lambda_{D.T}$ | 0.297 | 0.543 | 0.790 | 1.037 | 1.284 | 1.530 | 1.777 | 2.024 | 2.271 | 2.518 | 2.764 | 3.012 |
| | $P_{uT}/P_{yT}$ | 0.761 | 0.736 | 0.700 | 0.636 | 0.491 | 0.372 | 0.323 | 0.289 | 0.258 | 0.227 | 0.199 | 0.177 |
| | $P_{uT}/P_{nFT.T}$ | 0.951 | 0.986 | 1.045 | 1.104 | 1.031 | 0.976 | 0.979 | 0.994 | 0.995 | 0.967 | 0.929 | 0.897 |
| | $P_{uT}/P_{nD.T}$ | 0.969 | 0.937 | 0.912 | 0.955 | 0.866 | 0.767 | 0.766 | 0.779 | 0.784 | 0.768 | 0.744 | 0.724 |
| | $P_{uT}/P_{nDFT.T}$ | 1.211 | 1.254 | 1.330 | 1.438 | 1.410 | 1.383 | 1.455 | 1.546 | 1.616 | 1.638 | 1.636 | 1.638 |
| | $P_{uT}/P_{nFTD.T}$ | 1.203 | 1.228 | 1.299 | 1.471 | 1.435 | 1.360 | 1.449 | 1.567 | 1.675 | 1.740 | 1.784 | 1.837 |
| 400 | $\lambda_{FT.T}$ | 0.291 | 0.532 | 0.772 | 1.014 | 1.256 | 1.497 | 1.738 | 1.980 | 2.221 | 2.463 | 2.704 | 2.946 |
| | $\lambda_{D.T}$ | 0.290 | 0.530 | 0.771 | 1.012 | 1.253 | 1.493 | 1.734 | 1.975 | 2.216 | 2.457 | 2.698 | 2.939 |
| | $P_{uT}/P_{yT}$ | 0.632 | 0.615 | 0.592 | 0.555 | 0.488 | 0.374 | 0.309 | 0.279 | 0.253 | 0.226 | 0.200 | 0.180 |
| | $P_{uT}/P_{nFT.T}$ | 0.837 | 0.866 | 0.918 | 0.984 | 1.024 | 0.963 | 0.915 | 0.937 | 0.953 | 0.943 | 0.911 | 0.891 |
| | $P_{uT}/P_{nD.T}$ | 0.978 | 0.952 | 0.916 | 0.911 | 0.908 | 0.796 | 0.748 | 0.761 | 0.773 | 0.767 | 0.745 | 0.733 |
| | $P_{uT}/P_{nDFT.T}$ | 1.296 | 1.340 | 1.421 | 1.523 | 1.585 | 1.528 | 1.498 | 1.585 | 1.668 | 1.706 | 1.704 | 1.720 |
| | $P_{uT}/P_{nFTD.T}$ | 1.284 | 1.300 | 1.332 | 1.426 | 1.521 | 1.421 | 1.418 | 1.528 | 1.642 | 1.718 | 1.759 | 1.822 |
| 500 | $\lambda_{FT.T}$ | 0.284 | 0.518 | 0.753 | 0.989 | 1.225 | 1.460 | 1.696 | 1.931 | 2.167 | 2.402 | 2.637 | 2.873 |
| | $\lambda_{D.T}$ | 0.283 | 0.517 | 0.752 | 0.987 | 1.222 | 1.456 | 1.692 | 1.926 | 2.162 | 2.396 | 2.631 | 2.867 |
| | $P_{uT}/P_{yT}$ | 0.663 | 0.645 | 0.621 | 0.582 | 0.513 | 0.393 | 0.321 | 0.288 | 0.262 | 0.235 | 0.209 | 0.187 |
| | $P_{uT}/P_{nFT.T}$ | 0.903 | 0.929 | 0.978 | 1.036 | 1.064 | 0.985 | 0.928 | 0.946 | 0.963 | 0.957 | 0.928 | 0.905 |
| | $P_{uT}/P_{nD.T}$ | 0.977 | 0.950 | 0.915 | 0.915 | 0.917 | 0.807 | 0.750 | 0.760 | 0.774 | 0.772 | 0.753 | 0.739 |
| | $P_{uT}/P_{nDFT.T}$ | 1.330 | 1.368 | 1.440 | 1.525 | 1.584 | 1.503 | 1.465 | 1.547 | 1.632 | 1.680 | 1.686 | 1.699 |
| | $P_{uT}/P_{nFTD.T}$ | 1.320 | 1.333 | 1.364 | 1.465 | 1.565 | 1.461 | 1.438 | 1.539 | 1.651 | 1.732 | 1.775 | 1.829 |
| 600 | $\lambda_{FT.T}$ | 0.297 | 0.543 | 0.789 | 1.035 | 1.282 | 1.528 | 1.775 | 2.021 | 2.268 | 2.514 | 2.760 | 3.007 |
| | $\lambda_{D.T}$ | 0.296 | 0.541 | 0.787 | 1.033 | 1.279 | 1.524 | 1.771 | 2.016 | 2.263 | 2.508 | 2.754 | 3.000 |
| | $P_{uT}/P_{yT}$ | 0.590 | 0.575 | 0.553 | 0.524 | 0.465 | 0.360 | 0.297 | 0.269 | 0.244 | 0.218 | 0.192 | 0.171 |
| | $P_{uT}/P_{nFT.T}$ | 0.802 | 0.831 | 0.882 | 0.956 | 1.005 | 0.940 | 0.897 | 0.923 | 0.939 | 0.927 | 0.893 | 0.864 |
| | $P_{uT}/P_{nD.T}$ | 0.983 | 0.958 | 0.921 | 0.910 | 0.905 | 0.798 | 0.745 | 0.760 | 0.772 | 0.763 | 0.739 | 0.718 |
| | $P_{uT}/P_{nDFT.T}$ | 1.336 | 1.385 | 1.469 | 1.594 | 1.676 | 1.585 | 1.547 | 1.638 | 1.717 | 1.748 | 1.738 | 1.731 |
| | $P_{uT}/P_{nFTD.T}$ | 1.322 | 1.337 | 1.364 | 1.449 | 1.542 | 1.447 | 1.436 | 1.551 | 1.663 | 1.734 | 1.768 | 1.808 |
| 700 | $\lambda_{FT.T}$ | 0.302 | 0.552 | 0.802 | 1.052 | 1.303 | 1.553 | 1.804 | 2.054 | 2.305 | 2.556 | 2.806 | 3.057 |
| | $\lambda_{D.T}$ | 0.301 | 0.550 | 0.800 | 1.050 | 1.300 | 1.550 | 1.800 | 2.050 | 2.300 | 2.550 | 2.800 | 3.050 |
| | $P_{uT}/P_{yT}$ | 0.569 | 0.554 | 0.533 | 0.507 | 0.449 | 0.349 | 0.289 | 0.263 | 0.239 | 0.212 | 0.186 | 0.166 |
| | $P_{uT}/P_{nFT.T}$ | 0.747 | 0.778 | 0.830 | 0.914 | 0.973 | 0.925 | 0.889 | 0.918 | 0.932 | 0.917 | 0.881 | 0.852 |
| | $P_{uT}/P_{nD.T}$ | 0.987 | 0.961 | 0.923 | 0.908 | 0.899 | 0.793 | 0.745 | 0.762 | 0.772 | 0.760 | 0.733 | 0.713 |
| | $P_{uT}/P_{nDFT.T}$ | 1.295 | 1.348 | 1.439 | 1.583 | 1.687 | 1.604 | 1.581 | 1.675 | 1.750 | 1.774 | 1.755 | 1.746 |
| | $P_{uT}/P_{nFTD.T}$ | 1.279 | 1.295 | 1.322 | 1.406 | 1.495 | 1.410 | 1.411 | 1.533 | 1.646 | 1.716 | 1.748 | 1.793 |
| 800 | $\lambda_{FT.T}$ | 0.266 | 0.486 | 0.707 | 0.928 | 1.149 | 1.370 | 1.591 | 1.812 | 2.033 | 2.254 | 2.475 | 2.696 |
| | $\lambda_{D.T}$ | 0.265 | 0.485 | 0.705 | 0.926 | 1.146 | 1.367 | 1.587 | 1.808 | 2.028 | 2.249 | 2.469 | 2.690 |
| | $P_{uT}/P_{yT}$ | 0.697 | 0.679 | 0.656 | 0.618 | 0.549 | 0.439 | 0.347 | 0.308 | 0.280 | 0.255 | 0.229 | 0.204 |
| | $P_{uT}/P_{nFT.T}$ | 0.851 | 0.876 | 0.926 | 0.986 | 1.024 | 0.988 | 0.943 | 0.951 | 0.968 | 0.974 | 0.958 | 0.930 |
| | $P_{uT}/P_{nD.T}$ | 0.976 | 0.950 | 0.919 | 0.914 | 0.921 | 0.840 | 0.756 | 0.758 | 0.771 | 0.777 | 0.769 | 0.750 |
| | $P_{uT}/P_{nDFT.T}$ | 1.191 | 1.227 | 1.297 | 1.380 | 1.461 | 1.451 | 1.422 | 1.487 | 1.570 | 1.637 | 1.666 | 1.671 |
| | $P_{uT}/P_{nFTD.T}$ | 1.183 | 1.199 | 1.236 | 1.327 | 1.433 | 1.396 | 1.336 | 1.420 | 1.530 | 1.631 | 1.701 | 1.751 |

**Table I.12**: Numerical failure loads and their DSM estimates concerning the **LC12** column geometry with 12 room temperature stresses (corresponding to equally spaced slenderness values) and 8 temperatures varying from $T$=20/100 to $T$=800 ºC.

| $T$ (ºC) | $\lambda_{cr.20}$ | 0.25 | 0.50 | 0.75 | 1.00 | 1.25 | 1.50 | 1.75 | 2.00 | 2.25 | 2.50 | 2.75 | 3.00 |
|---|---|---|---|---|---|---|---|---|---|---|---|---|---|
| 20/100 | $\lambda_{FT.T}$ | 0.250 | 0.501 | 0.752 | 1.002 | 1.252 | 1.502 | 1.753 | 2.003 | 2.253 | 2.503 | 2.754 | 3.005 |
| | $\lambda_{D.T}$ | 0.250 | 0.500 | 0.751 | 1.000 | 1.250 | 1.500 | 1.750 | 2.000 | 2.250 | 2.499 | 2.750 | 3.000 |
| | $P_{uT}/P_{yT}$ | 0.982 | 0.963 | 0.915 | 0.742 | 0.532 | 0.424 | 0.364 | 0.317 | 0.274 | 0.235 | 0.199 | 0.167 |
| | $P_{uT}/P_{nFT.T}$ | 1.008 | 1.070 | 1.160 | 1.129 | 1.026 | 1.089 | 1.075 | 1.053 | 1.013 | 0.956 | 0.881 | 0.801 |
| | $P_{uT}/P_{nD.T}$ | 0.982 | 0.963 | 1.002 | 0.989 | 0.860 | 0.815 | 0.818 | 0.816 | 0.801 | 0.771 | 0.724 | 0.671 |
| | $P_{uT}/P_{nDFT.T}$ | 1.008 | 1.070 | 1.202 | 1.294 | 1.262 | 1.379 | 1.455 | 1.515 | 1.544 | 1.534 | 1.484 | 1.413 |
| | $P_{uT}/P_{nFTD.T}$ | 1.008 | 1.070 | 1.244 | 1.355 | 1.291 | 1.333 | 1.451 | 1.566 | 1.658 | 1.717 | 1.733 | 1.723 |
| 200 | $\lambda_{FT.T}$ | 0.249 | 0.498 | 0.748 | 0.996 | 1.245 | 1.494 | 1.743 | 1.992 | 2.241 | 2.489 | 2.739 | 2.988 |
| | $\lambda_{D.T}$ | 0.248 | 0.498 | 0.746 | 0.994 | 1.243 | 1.492 | 1.741 | 1.989 | 2.237 | 2.485 | 2.734 | 2.983 |
| | $P_{uT}/P_{yT}$ | 0.962 | 0.944 | 0.901 | 0.742 | 0.536 | 0.424 | 0.365 | 0.318 | 0.276 | 0.238 | 0.201 | 0.169 |
| | $P_{uT}/P_{nFT.T}$ | 1.094 | 1.150 | 1.232 | 1.189 | 1.056 | 1.074 | 1.072 | 1.053 | 1.016 | 0.960 | 0.885 | 0.806 |
| | $P_{uT}/P_{nD.T}$ | 0.984 | 0.965 | 0.996 | 0.993 | 0.867 | 0.815 | 0.818 | 0.818 | 0.804 | 0.775 | 0.728 | 0.675 |
| | $P_{uT}/P_{nDFT.T}$ | 1.120 | 1.177 | 1.280 | 1.352 | 1.297 | 1.374 | 1.459 | 1.521 | 1.552 | 1.544 | 1.495 | 1.424 |
| | $P_{uT}/P_{nFTD.T}$ | 1.119 | 1.174 | 1.335 | 1.451 | 1.373 | 1.391 | 1.500 | 1.606 | 1.689 | 1.735 | 1.737 | 1.714 |
| 300 | $\lambda_{FT.T}$ | 0.247 | 0.495 | 0.742 | 0.989 | 1.236 | 1.483 | 1.731 | 1.978 | 2.225 | 2.472 | 2.719 | 2.967 |
| | $\lambda_{D.T}$ | 0.247 | 0.494 | 0.741 | 0.987 | 1.234 | 1.481 | 1.728 | 1.975 | 2.221 | 2.468 | 2.715 | 2.962 |
| | $P_{uT}/P_{yT}$ | 0.806 | 0.786 | 0.759 | 0.690 | 0.529 | 0.410 | 0.359 | 0.317 | 0.278 | 0.240 | 0.204 | 0.172 |
| | $P_{uT}/P_{nFT.T}$ | 0.998 | 1.035 | 1.106 | 1.159 | 1.066 | 1.031 | 1.046 | 1.043 | 1.015 | 0.964 | 0.891 | 0.813 |
| | $P_{uT}/P_{nD.T}$ | 1.025 | 1.001 | 0.973 | 1.004 | 0.904 | 0.819 | 0.828 | 0.836 | 0.824 | 0.796 | 0.747 | 0.692 |
| | $P_{uT}/P_{nDFT.T}$ | 1.270 | 1.317 | 1.407 | 1.496 | 1.445 | 1.451 | 1.546 | 1.622 | 1.655 | 1.646 | 1.588 | 1.509 |
| | $P_{uT}/P_{nFTD.T}$ | 1.264 | 1.295 | 1.362 | 1.524 | 1.476 | 1.432 | 1.546 | 1.660 | 1.740 | 1.780 | 1.770 | 1.734 |
| 400 | $\lambda_{FT.T}$ | 0.241 | 0.483 | 0.724 | 0.965 | 1.206 | 1.448 | 1.689 | 1.930 | 2.171 | 2.412 | 2.654 | 2.895 |
| | $\lambda_{D.T}$ | 0.241 | 0.482 | 0.723 | 0.964 | 1.205 | 1.445 | 1.687 | 1.927 | 2.168 | 2.408 | 2.650 | 2.891 |
| | $P_{uT}/P_{yT}$ | 0.714 | 0.696 | 0.667 | 0.624 | 0.530 | 0.405 | 0.360 | 0.323 | 0.283 | 0.249 | 0.213 | 0.180 |
| | $P_{uT}/P_{nFT.T}$ | 0.938 | 0.965 | 1.011 | 1.073 | 1.071 | 0.996 | 1.026 | 1.037 | 1.011 | 0.979 | 0.912 | 0.835 |
| | $P_{uT}/P_{nD.T}$ | 1.105 | 1.078 | 1.032 | 1.003 | 0.959 | 0.838 | 0.849 | 0.860 | 0.845 | 0.827 | 0.780 | 0.723 |
| | $P_{uT}/P_{nDFT.T}$ | 1.452 | 1.494 | 1.565 | 1.661 | 1.657 | 1.575 | 1.673 | 1.753 | 1.775 | 1.783 | 1.722 | 1.633 |
| | $P_{uT}/P_{nFTD.T}$ | 1.442 | 1.457 | 1.478 | 1.547 | 1.586 | 1.477 | 1.591 | 1.708 | 1.774 | 1.832 | 1.820 | 1.778 |
| 500 | $\lambda_{FT.T}$ | 0.235 | 0.471 | 0.707 | 0.941 | 1.177 | 1.412 | 1.648 | 1.883 | 2.118 | 2.353 | 2.588 | 2.824 |
| | $\lambda_{D.T}$ | 0.235 | 0.470 | 0.705 | 0.940 | 1.175 | 1.410 | 1.645 | 1.880 | 2.114 | 2.349 | 2.584 | 2.820 |
| | $P_{uT}/P_{yT}$ | 0.737 | 0.717 | 0.690 | 0.649 | 0.553 | 0.419 | 0.368 | 0.331 | 0.290 | 0.258 | 0.223 | 0.190 |
| | $P_{uT}/P_{nFT.T}$ | 0.997 | 1.019 | 1.064 | 1.123 | 1.111 | 1.008 | 1.027 | 1.039 | 1.013 | 0.992 | 0.932 | 0.858 |
| | $P_{uT}/P_{nD.T}$ | 1.086 | 1.056 | 1.016 | 0.999 | 0.964 | 0.836 | 0.839 | 0.852 | 0.837 | 0.830 | 0.788 | 0.736 |
| | $P_{uT}/P_{nDFT.T}$ | 1.467 | 1.500 | 1.567 | 1.654 | 1.645 | 1.530 | 1.614 | 1.697 | 1.720 | 1.752 | 1.708 | 1.631 |
| | $P_{uT}/P_{nFTD.T}$ | 1.460 | 1.469 | 1.494 | 1.576 | 1.623 | 1.497 | 1.591 | 1.705 | 1.766 | 1.842 | 1.840 | 1.802 |
| 600 | $\lambda_{FT.T}$ | 0.246 | 0.493 | 0.740 | 0.985 | 1.232 | 1.478 | 1.725 | 1.970 | 2.217 | 2.463 | 2.709 | 2.956 |
| | $\lambda_{D.T}$ | 0.246 | 0.492 | 0.738 | 0.984 | 1.230 | 1.476 | 1.722 | 1.967 | 2.213 | 2.459 | 2.705 | 2.951 |
| | $P_{uT}/P_{yT}$ | 0.693 | 0.669 | 0.638 | 0.594 | 0.507 | 0.394 | 0.352 | 0.302 | 0.277 | 0.242 | 0.205 | 0.173 |
| | $P_{uT}/P_{nFT.T}$ | 0.935 | 0.953 | 0.994 | 1.051 | 1.057 | 1.002 | 1.024 | 0.990 | 1.010 | 0.967 | 0.894 | 0.816 |
| | $P_{uT}/P_{nD.T}$ | 1.155 | 1.116 | 1.063 | 1.012 | 0.963 | 0.850 | 0.864 | 0.835 | 0.857 | 0.828 | 0.775 | 0.716 |
| | $P_{uT}/P_{nDFT.T}$ | 1.558 | 1.589 | 1.657 | 1.752 | 1.761 | 1.669 | 1.761 | 1.757 | 1.853 | 1.835 | 1.756 | 1.657 |
| | $P_{uT}/P_{nFTD.T}$ | 1.547 | 1.543 | 1.553 | 1.589 | 1.619 | 1.523 | 1.644 | 1.684 | 1.826 | 1.860 | 1.834 | 1.782 |
| 700 | $\lambda_{FT.T}$ | 0.250 | 0.501 | 0.752 | 1.002 | 1.252 | 1.502 | 1.753 | 2.003 | 2.253 | 2.503 | 2.754 | 3.005 |
| | $\lambda_{D.T}$ | 0.250 | 0.500 | 0.751 | 1.000 | 1.250 | 1.500 | 1.750 | 2.000 | 2.250 | 2.499 | 2.750 | 3.000 |
| | $P_{uT}/P_{yT}$ | 0.682 | 0.656 | 0.623 | 0.578 | 0.492 | 0.387 | 0.347 | 0.298 | 0.273 | 0.235 | 0.199 | 0.167 |
| | $P_{uT}/P_{nFT.T}$ | 0.887 | 0.905 | 0.948 | 1.008 | 1.025 | 0.994 | 1.024 | 0.990 | 1.011 | 0.956 | 0.881 | 0.801 |
| | $P_{uT}/P_{nD.T}$ | 1.182 | 1.137 | 1.080 | 1.019 | 0.963 | 0.858 | 0.873 | 0.843 | 0.865 | 0.826 | 0.769 | 0.708 |
| | $P_{uT}/P_{nDFT.T}$ | 1.537 | 1.569 | 1.644 | 1.747 | 1.776 | 1.723 | 1.817 | 1.807 | 1.904 | 1.861 | 1.771 | 1.665 |
| | $P_{uT}/P_{nFTD.T}$ | 1.524 | 1.518 | 1.525 | 1.553 | 1.577 | 1.505 | 1.631 | 1.675 | 1.823 | 1.841 | 1.812 | 1.761 |
| 800 | $\lambda_{FT.T}$ | 0.221 | 0.442 | 0.663 | 0.883 | 1.104 | 1.325 | 1.546 | 1.766 | 1.987 | 2.208 | 2.429 | 2.650 |
| | $\lambda_{D.T}$ | 0.220 | 0.441 | 0.662 | 0.882 | 1.102 | 1.323 | 1.544 | 1.764 | 1.984 | 2.204 | 2.425 | 2.646 |
| | $P_{uT}/P_{yT}$ | 0.759 | 0.742 | 0.718 | 0.684 | 0.603 | 0.466 | 0.389 | 0.350 | 0.306 | 0.282 | 0.246 | 0.214 |
| | $P_{uT}/P_{nFT.T}$ | 0.920 | 0.945 | 0.994 | 1.062 | 1.087 | 1.006 | 1.025 | 1.039 | 1.011 | 1.022 | 0.971 | 0.913 |
| | $P_{uT}/P_{nD.T}$ | 1.063 | 1.039 | 1.006 | 0.992 | 0.985 | 0.869 | 0.827 | 0.840 | 0.823 | 0.841 | 0.809 | 0.770 |
| | $P_{uT}/P_{nDFT.T}$ | 1.288 | 1.323 | 1.391 | 1.487 | 1.541 | 1.471 | 1.537 | 1.620 | 1.639 | 1.724 | 1.701 | 1.659 |
| | $P_{uT}/P_{nFTD.T}$ | 1.282 | 1.298 | 1.333 | 1.419 | 1.512 | 1.425 | 1.444 | 1.556 | 1.614 | 1.744 | 1.769 | 1.777 |

**Table I.13**: Numerical failure loads and their DSM estimates concerning the **LC13** column geometry with 12 room temperature stresses (corresponding to equally spaced slenderness values) and 8 temperatures varying from $T$=20/100 to $T$=800 ºC.

| $T$ (ºC) | $\lambda_{cr.20}$ | 0.35 | 0.60 | 0.85 | 1.10 | 1.35 | 1.60 | 1.85 | 2.10 | 2.35 | 2.60 | 2.85 | 3.10 |
|---|---|---|---|---|---|---|---|---|---|---|---|---|---|
| 20/100 | $\lambda_{FT.T}$ | 0.350 | 0.601 | 0.851 | 1.102 | 1.352 | 1.602 | 1.853 | 2.103 | 2.354 | 2.604 | 2.854 | 3.105 |
| | $\lambda_{D.T}$ | 0.350 | 0.600 | 0.850 | 1.100 | 1.350 | 1.600 | 1.850 | 2.100 | 2.350 | 2.600 | 2.850 | 3.100 |
| | $P_{uT}/P_{yT}$ | 0.959 | 0.925 | 0.832 | 0.630 | 0.456 | 0.386 | 0.341 | 0.300 | 0.264 | 0.226 | 0.194 | 0.168 |
| | $P_{uT}/P_{nFT.T}$ | 1.009 | 1.076 | 1.127 | 1.047 | 0.980 | 1.052 | 1.067 | 1.059 | 1.035 | 0.975 | 0.912 | 0.852 |
| | $P_{uT}/P_{nD.T}$ | 0.959 | 0.930 | 0.983 | 0.909 | 0.792 | 0.790 | 0.811 | 0.815 | 0.809 | 0.774 | 0.734 | 0.696 |
| | $P_{uT}/P_{nDFT.T}$ | 1.009 | 1.076 | 1.216 | 1.241 | 1.226 | 1.368 | 1.476 | 1.550 | 1.597 | 1.579 | 1.544 | 1.505 |
| | $P_{uT}/P_{nFTD.T}$ | 1.009 | 1.081 | 1.271 | 1.293 | 1.230 | 1.335 | 1.484 | 1.613 | 1.725 | 1.775 | 1.808 | 1.838 |
| 200 | $\lambda_{FT.T}$ | 0.348 | 0.597 | 0.846 | 1.096 | 1.345 | 1.594 | 1.843 | 2.092 | 2.341 | 2.590 | 2.839 | 3.088 |
| | $\lambda_{D.T}$ | 0.348 | 0.596 | 0.845 | 1.094 | 1.342 | 1.591 | 1.840 | 2.088 | 2.337 | 2.585 | 2.834 | 3.083 |
| | $P_{uT}/P_{yT}$ | 0.939 | 0.906 | 0.822 | 0.644 | 0.455 | 0.385 | 0.341 | 0.301 | 0.267 | 0.230 | 0.196 | 0.169 |
| | $P_{uT}/P_{nFT.T}$ | 1.092 | 1.150 | 1.191 | 1.114 | 0.985 | 1.045 | 1.060 | 1.054 | 1.042 | 0.984 | 0.915 | 0.856 |
| | $P_{uT}/P_{nD.T}$ | 0.960 | 0.929 | 0.978 | 0.930 | 0.789 | 0.787 | 0.807 | 0.813 | 0.816 | 0.781 | 0.737 | 0.699 |
| | $P_{uT}/P_{nDFT.T}$ | 1.117 | 1.176 | 1.279 | 1.311 | 1.235 | 1.366 | 1.473 | 1.549 | 1.612 | 1.597 | 1.553 | 1.514 |
| | $P_{uT}/P_{nFTD.T}$ | 1.116 | 1.175 | 1.358 | 1.405 | 1.289 | 1.384 | 1.522 | 1.641 | 1.758 | 1.796 | 1.803 | 1.819 |
| 300 | $\lambda_{FT.T}$ | 0.346 | 0.593 | 0.841 | 1.088 | 1.335 | 1.582 | 1.830 | 2.077 | 2.324 | 2.571 | 2.819 | 3.066 |
| | $\lambda_{D.T}$ | 0.345 | 0.592 | 0.839 | 1.086 | 1.333 | 1.580 | 1.827 | 2.074 | 2.320 | 2.567 | 2.814 | 3.061 |
| | $P_{uT}/P_{yT}$ | 0.765 | 0.741 | 0.700 | 0.615 | 0.442 | 0.361 | 0.324 | 0.289 | 0.258 | 0.233 | 0.196 | 0.168 |
| | $P_{uT}/P_{nFT.T}$ | 0.966 | 1.011 | 1.074 | 1.105 | 0.969 | 0.973 | 1.000 | 1.007 | 1.000 | 0.991 | 0.908 | 0.846 |
| | $P_{uT}/P_{nD.T}$ | 0.973 | 0.943 | 0.934 | 0.954 | 0.806 | 0.766 | 0.788 | 0.800 | 0.802 | 0.804 | 0.746 | 0.703 |
| | $P_{uT}/P_{nDFT.T}$ | 1.229 | 1.287 | 1.367 | 1.454 | 1.337 | 1.394 | 1.504 | 1.589 | 1.650 | 1.705 | 1.627 | 1.575 |
| | $P_{uT}/P_{nFTD.T}$ | 1.219 | 1.255 | 1.351 | 1.491 | 1.352 | 1.375 | 1.509 | 1.629 | 1.734 | 1.841 | 1.807 | 1.802 |
| 400 | $\lambda_{FT.T}$ | 0.337 | 0.579 | 0.820 | 1.062 | 1.303 | 1.544 | 1.785 | 2.027 | 2.268 | 2.509 | 2.751 | 2.992 |
| | $\lambda_{D.T}$ | 0.337 | 0.578 | 0.819 | 1.060 | 1.301 | 1.542 | 1.783 | 2.024 | 2.264 | 2.505 | 2.746 | 2.987 |
| | $P_{uT}/P_{yT}$ | 0.644 | 0.623 | 0.597 | 0.551 | 0.442 | 0.348 | 0.315 | 0.286 | 0.259 | 0.230 | 0.201 | 0.172 |
| | $P_{uT}/P_{nFT.T}$ | 0.860 | 0.892 | 0.948 | 1.007 | 0.962 | 0.916 | 0.951 | 0.974 | 0.979 | 0.959 | 0.914 | 0.842 |
| | $P_{uT}/P_{nD.T}$ | 0.996 | 0.964 | 0.924 | 0.925 | 0.844 | 0.759 | 0.781 | 0.799 | 0.807 | 0.796 | 0.765 | 0.712 |
| | $P_{uT}/P_{nDFT.T}$ | 1.331 | 1.380 | 1.468 | 1.558 | 1.503 | 1.463 | 1.569 | 1.665 | 1.734 | 1.759 | 1.734 | 1.652 |
| | $P_{uT}/P_{nFTD.T}$ | 1.315 | 1.330 | 1.364 | 1.468 | 1.432 | 1.371 | 1.498 | 1.623 | 1.731 | 1.801 | 1.824 | 1.786 |
| 500 | $\lambda_{FT.T}$ | 0.329 | 0.565 | 0.800 | 1.035 | 1.271 | 1.506 | 1.741 | 1.977 | 2.212 | 2.447 | 2.683 | 2.918 |
| | $\lambda_{D.T}$ | 0.329 | 0.564 | 0.799 | 1.034 | 1.269 | 1.504 | 1.739 | 1.974 | 2.209 | 2.444 | 2.679 | 2.914 |
| | $P_{uT}/P_{yT}$ | 0.670 | 0.652 | 0.626 | 0.596 | 0.483 | 0.366 | 0.325 | 0.295 | 0.267 | 0.243 | 0.211 | 0.179 |
| | $P_{uT}/P_{nFT.T}$ | 0.920 | 0.953 | 1.008 | 1.090 | 1.039 | 0.943 | 0.960 | 0.981 | 0.988 | 0.989 | 0.933 | 0.860 |
| | $P_{uT}/P_{nD.T}$ | 0.987 | 0.960 | 0.922 | 0.960 | 0.889 | 0.772 | 0.780 | 0.797 | 0.807 | 0.813 | 0.774 | 0.720 |
| | $P_{uT}/P_{nDFT.T}$ | 1.355 | 1.403 | 1.483 | 1.605 | 1.553 | 1.449 | 1.529 | 1.621 | 1.696 | 1.760 | 1.720 | 1.640 |
| | $P_{uT}/P_{nFTD.T}$ | 1.341 | 1.361 | 1.396 | 1.556 | 1.535 | 1.413 | 1.511 | 1.629 | 1.737 | 1.843 | 1.842 | 1.799 |
| 600 | $\lambda_{FT.T}$ | 0.344 | 0.591 | 0.837 | 1.084 | 1.330 | 1.576 | 1.823 | 2.069 | 2.315 | 2.562 | 2.808 | 3.054 |
| | $\lambda_{D.T}$ | 0.344 | 0.590 | 0.836 | 1.082 | 1.328 | 1.574 | 1.820 | 2.066 | 2.312 | 2.558 | 2.804 | 3.050 |
| | $P_{uT}/P_{yT}$ | 0.611 | 0.586 | 0.559 | 0.536 | 0.425 | 0.335 | 0.305 | 0.278 | 0.251 | 0.223 | 0.205 | 0.166 |
| | $P_{uT}/P_{nFT.T}$ | 0.838 | 0.862 | 0.913 | 1.007 | 0.956 | 0.899 | 0.941 | 0.965 | 0.969 | 0.947 | 0.949 | 0.831 |
| | $P_{uT}/P_{nD.T}$ | 1.018 | 0.977 | 0.932 | 0.948 | 0.850 | 0.760 | 0.786 | 0.804 | 0.810 | 0.796 | 0.804 | 0.710 |
| | $P_{uT}/P_{nDFT.T}$ | 1.397 | 1.436 | 1.522 | 1.679 | 1.593 | 1.522 | 1.635 | 1.729 | 1.793 | 1.810 | 1.871 | 1.691 |
| | $P_{uT}/P_{nFTD.T}$ | 1.377 | 1.378 | 1.400 | 1.531 | 1.466 | 1.396 | 1.531 | 1.658 | 1.763 | 1.828 | 1.941 | 1.805 |
| 700 | $\lambda_{FT.T}$ | 0.350 | 0.601 | 0.851 | 1.102 | 1.352 | 1.602 | 1.853 | 2.103 | 2.354 | 2.604 | 2.854 | 3.105 |
| | $\lambda_{D.T}$ | 0.350 | 0.600 | 0.850 | 1.100 | 1.350 | 1.600 | 1.850 | 2.100 | 2.350 | 2.600 | 2.850 | 3.100 |
| | $P_{uT}/P_{yT}$ | 0.595 | 0.569 | 0.540 | 0.500 | 0.412 | 0.327 | 0.300 | 0.273 | 0.246 | 0.218 | 0.181 | 0.162 |
| | $P_{uT}/P_{nFT.T}$ | 0.789 | 0.812 | 0.864 | 0.933 | 0.931 | 0.892 | 0.937 | 0.962 | 0.964 | 0.938 | 0.850 | 0.824 |
| | $P_{uT}/P_{nD.T}$ | 1.031 | 0.986 | 0.936 | 0.915 | 0.847 | 0.763 | 0.791 | 0.809 | 0.812 | 0.795 | 0.725 | 0.709 |
| | $P_{uT}/P_{nDFT.T}$ | 1.367 | 1.408 | 1.497 | 1.617 | 1.613 | 1.547 | 1.678 | 1.772 | 1.830 | 1.837 | 1.716 | 1.715 |
| | $P_{uT}/P_{nFTD.T}$ | 1.345 | 1.343 | 1.360 | 1.436 | 1.426 | 1.373 | 1.514 | 1.646 | 1.750 | 1.812 | 1.746 | 1.801 |
| 800 | $\lambda_{FT.T}$ | 0.309 | 0.530 | 0.751 | 0.972 | 1.192 | 1.413 | 1.634 | 1.855 | 2.076 | 2.297 | 2.517 | 2.738 |
| | $\lambda_{D.T}$ | 0.308 | 0.529 | 0.750 | 0.970 | 1.191 | 1.411 | 1.632 | 1.852 | 2.072 | 2.293 | 2.513 | 2.734 |
| | $P_{uT}/P_{yT}$ | 0.702 | 0.685 | 0.662 | 0.620 | 0.516 | 0.397 | 0.346 | 0.313 | 0.285 | 0.259 | 0.232 | 0.204 |
| | $P_{uT}/P_{nFT.T}$ | 0.864 | 0.898 | 0.955 | 1.017 | 0.996 | 0.933 | 0.961 | 0.979 | 0.993 | 0.990 | 0.966 | 0.921 |
| | $P_{uT}/P_{nD.T}$ | 0.983 | 0.959 | 0.926 | 0.938 | 0.888 | 0.782 | 0.772 | 0.787 | 0.801 | 0.804 | 0.791 | 0.762 |
| | $P_{uT}/P_{nDFT.T}$ | 1.210 | 1.257 | 1.336 | 1.424 | 1.430 | 1.377 | 1.461 | 1.547 | 1.629 | 1.685 | 1.705 | 1.681 |
| | $P_{uT}/P_{nFTD.T}$ | 1.199 | 1.223 | 1.265 | 1.381 | 1.401 | 1.315 | 1.381 | 1.491 | 1.606 | 1.703 | 1.769 | 1.793 |

**Table I.14**: Numerical failure loads and their DSM estimates concerning the **LC14** column geometry with 12 room temperature stresses (corresponding to equally spaced slenderness values) and 8 temperatures varying from $T$=20/100 to $T$=800 ºC.

| $T$ (ºC) | $\lambda_{cr,20}$ | 0.30 | 0.55 | 0.80 | 1.05 | 1.30 | 1.55 | 1.80 | 2.05 | 2.30 | 2.55 | 2.80 | 3.05 |
|---|---|---|---|---|---|---|---|---|---|---|---|---|---|
| 20/100 | $\lambda_{FT,T}$ | 0.300 | 0.550 | 0.800 | 1.050 | 1.300 | 1.550 | 1.800 | 2.050 | 2.300 | 2.550 | 2.800 | 3.050 |
| | $\lambda_{D,T}$ | 0.305 | 0.559 | 0.813 | 1.067 | 1.321 | 1.575 | 1.829 | 2.083 | 2.337 | 2.591 | 2.845 | 3.099 |
| | $P_{uT}/P_{yT}$ | 0.970 | 0.941 | 0.880 | 0.707 | 0.508 | 0.406 | 0.349 | 0.305 | 0.269 | 0.234 | 0.199 | 0.170 |
| | $P_{uT}/P_{nFT,T}$ | 1.007 | 1.068 | 1.150 | 1.121 | 1.030 | 1.073 | 1.062 | 1.051 | 1.032 | 0.990 | 0.918 | 0.851 |
| | $P_{uT}/P_{nD,T}$ | 0.970 | 0.941 | 1.010 | 0.994 | 0.864 | 0.818 | 0.818 | 0.822 | 0.818 | 0.797 | 0.750 | 0.705 |
| | $P_{uT}/P_{nDFT,T}$ | 1.007 | 1.068 | 1.225 | 1.322 | 1.296 | 1.395 | 1.471 | 1.544 | 1.598 | 1.611 | 1.565 | 1.513 |
| | $P_{uT}/P_{nFTD,T}$ | 1.007 | 1.068 | 1.275 | 1.380 | 1.309 | 1.347 | 1.458 | 1.579 | 1.693 | 1.771 | 1.789 | 1.801 |
| 200 | $\lambda_{FT,T}$ | 0.298 | 0.547 | 0.796 | 1.044 | 1.293 | 1.541 | 1.790 | 2.039 | 2.287 | 2.536 | 2.784 | 3.033 |
| | $\lambda_{D,T}$ | 0.303 | 0.556 | 0.808 | 1.061 | 1.313 | 1.566 | 1.819 | 2.071 | 2.324 | 2.576 | 2.829 | 3.082 |
| | $P_{uT}/P_{yT}$ | 0.950 | 0.922 | 0.866 | 0.707 | 0.512 | 0.405 | 0.348 | 0.306 | 0.270 | 0.235 | 0.201 | 0.172 |
| | $P_{uT}/P_{nFT,T}$ | 1.092 | 1.145 | 1.216 | 1.176 | 1.054 | 1.066 | 1.056 | 1.047 | 1.030 | 0.991 | 0.923 | 0.855 |
| | $P_{uT}/P_{nD,T}$ | 0.972 | 0.943 | 1.002 | 0.997 | 0.871 | 0.816 | 0.816 | 0.820 | 0.818 | 0.799 | 0.754 | 0.709 |
| | $P_{uT}/P_{nDFT,T}$ | 1.117 | 1.172 | 1.291 | 1.375 | 1.324 | 1.394 | 1.469 | 1.544 | 1.600 | 1.617 | 1.576 | 1.524 |
| | $P_{uT}/P_{nFTD,T}$ | 1.116 | 1.169 | 1.363 | 1.475 | 1.391 | 1.402 | 1.503 | 1.614 | 1.717 | 1.786 | 1.794 | 1.791 |
| 300 | $\lambda_{FT,T}$ | 0.296 | 0.543 | 0.790 | 1.037 | 1.284 | 1.531 | 1.777 | 2.024 | 2.271 | 2.518 | 2.765 | 3.012 |
| | $\lambda_{D,T}$ | 0.301 | 0.552 | 0.803 | 1.053 | 1.304 | 1.555 | 1.806 | 2.057 | 2.307 | 2.558 | 2.809 | 3.060 |
| | $P_{uT}/P_{yT}$ | 0.780 | 0.759 | 0.725 | 0.651 | 0.503 | 0.384 | 0.333 | 0.296 | 0.264 | 0.233 | 0.202 | 0.174 |
| | $P_{uT}/P_{nFT,T}$ | 0.975 | 1.015 | 1.083 | 1.128 | 1.054 | 1.003 | 1.002 | 1.007 | 1.003 | 0.976 | 0.922 | 0.861 |
| | $P_{uT}/P_{nD,T}$ | 0.993 | 0.965 | 0.951 | 0.988 | 0.900 | 0.802 | 0.802 | 0.812 | 0.816 | 0.803 | 0.768 | 0.725 |
| | $P_{uT}/P_{nDFT,T}$ | 1.241 | 1.292 | 1.378 | 1.477 | 1.454 | 1.436 | 1.508 | 1.592 | 1.660 | 1.687 | 1.661 | 1.611 |
| | $P_{uT}/P_{nFTD,T}$ | 1.233 | 1.265 | 1.351 | 1.516 | 1.482 | 1.412 | 1.503 | 1.617 | 1.724 | 1.796 | 1.815 | 1.811 |
| 400 | $\lambda_{FT,T}$ | 0.289 | 0.530 | 0.771 | 1.012 | 1.253 | 1.494 | 1.735 | 1.975 | 2.216 | 2.457 | 2.698 | 2.939 |
| | $\lambda_{D,T}$ | 0.294 | 0.538 | 0.783 | 1.028 | 1.273 | 1.518 | 1.762 | 2.007 | 2.252 | 2.497 | 2.741 | 2.986 |
| | $P_{uT}/P_{yT}$ | 0.676 | 0.654 | 0.625 | 0.582 | 0.498 | 0.381 | 0.325 | 0.293 | 0.265 | 0.238 | 0.213 | 0.182 |
| | $P_{uT}/P_{nFT,T}$ | 0.895 | 0.920 | 0.969 | 1.030 | 1.042 | 0.977 | 0.957 | 0.974 | 0.983 | 0.971 | 0.949 | 0.879 |
| | $P_{uT}/P_{nD,T}$ | 1.046 | 1.012 | 0.968 | 0.962 | 0.936 | 0.821 | 0.799 | 0.812 | 0.823 | 0.818 | 0.806 | 0.754 |
| | $P_{uT}/P_{nDFT,T}$ | 1.385 | 1.424 | 1.500 | 1.594 | 1.627 | 1.560 | 1.581 | 1.669 | 1.747 | 1.788 | 1.810 | 1.734 |
| | $P_{uT}/P_{nFTD,T}$ | 1.373 | 1.382 | 1.406 | 1.503 | 1.562 | 1.457 | 1.504 | 1.618 | 1.730 | 1.812 | 1.880 | 1.848 |
| 500 | $\lambda_{FT,T}$ | 0.282 | 0.517 | 0.752 | 0.987 | 1.222 | 1.457 | 1.692 | 1.927 | 2.162 | 2.397 | 2.632 | 2.867 |
| | $\lambda_{D,T}$ | 0.286 | 0.525 | 0.764 | 1.003 | 1.241 | 1.480 | 1.719 | 1.958 | 2.196 | 2.435 | 2.674 | 2.913 |
| | $P_{uT}/P_{yT}$ | 0.700 | 0.679 | 0.651 | 0.608 | 0.521 | 0.400 | 0.336 | 0.302 | 0.273 | 0.246 | 0.217 | 0.190 |
| | $P_{uT}/P_{nFT,T}$ | 0.953 | 0.978 | 1.025 | 1.081 | 1.079 | 0.999 | 0.965 | 0.979 | 0.988 | 0.980 | 0.948 | 0.899 |
| | $P_{uT}/P_{nD,T}$ | 1.030 | 1.000 | 0.959 | 0.964 | 0.942 | 0.831 | 0.797 | 0.808 | 0.819 | 0.818 | 0.798 | 0.764 |
| | $P_{uT}/P_{nDFT,T}$ | 1.403 | 1.440 | 1.509 | 1.591 | 1.612 | 1.535 | 1.539 | 1.622 | 1.701 | 1.751 | 1.756 | 1.723 |
| | $P_{uT}/P_{nFTD,T}$ | 1.392 | 1.403 | 1.430 | 1.539 | 1.601 | 1.497 | 1.517 | 1.622 | 1.731 | 1.816 | 1.859 | 1.866 |
| 600 | $\lambda_{FT,T}$ | 0.295 | 0.541 | 0.787 | 1.033 | 1.279 | 1.525 | 1.771 | 2.017 | 2.263 | 2.509 | 2.754 | 3.000 |
| | $\lambda_{D,T}$ | 0.300 | 0.550 | 0.800 | 1.049 | 1.299 | 1.549 | 1.799 | 2.049 | 2.299 | 2.549 | 2.799 | 3.048 |
| | $P_{uT}/P_{yT}$ | 0.644 | 0.622 | 0.592 | 0.550 | 0.474 | 0.365 | 0.315 | 0.285 | 0.258 | 0.231 | 0.205 | 0.175 |
| | $P_{uT}/P_{nFT,T}$ | 0.876 | 0.899 | 0.943 | 1.003 | 1.023 | 0.951 | 0.946 | 0.967 | 0.976 | 0.961 | 0.932 | 0.864 |
| | $P_{uT}/P_{nD,T}$ | 1.074 | 1.036 | 0.987 | 0.961 | 0.932 | 0.819 | 0.804 | 0.819 | 0.828 | 0.820 | 0.801 | 0.749 |
| | $P_{uT}/P_{nDFT,T}$ | 1.460 | 1.498 | 1.572 | 1.671 | 1.704 | 1.609 | 1.645 | 1.735 | 1.811 | 1.843 | 1.847 | 1.766 |
| | $P_{uT}/P_{nFTD,T}$ | 1.445 | 1.446 | 1.460 | 1.528 | 1.583 | 1.478 | 1.537 | 1.656 | 1.767 | 1.843 | 1.894 | 1.859 |
| 700 | $\lambda_{FT,T}$ | 0.300 | 0.550 | 0.800 | 1.050 | 1.300 | 1.550 | 1.800 | 2.050 | 2.300 | 2.550 | 2.800 | 3.050 |
| | $\lambda_{D,T}$ | 0.305 | 0.559 | 0.813 | 1.067 | 1.321 | 1.575 | 1.829 | 2.083 | 2.337 | 2.591 | 2.845 | 3.099 |
| | $P_{uT}/P_{yT}$ | 0.629 | 0.605 | 0.575 | 0.534 | 0.459 | 0.352 | 0.309 | 0.280 | 0.253 | 0.225 | 0.199 | 0.170 |
| | $P_{uT}/P_{nFT,T}$ | 0.825 | 0.849 | 0.895 | 0.960 | 0.993 | 0.932 | 0.942 | 0.965 | 0.973 | 0.954 | 0.918 | 0.851 |
| | $P_{uT}/P_{nD,T}$ | 1.090 | 1.049 | 0.996 | 0.963 | 0.929 | 0.812 | 0.808 | 0.824 | 0.832 | 0.820 | 0.795 | 0.743 |
| | $P_{uT}/P_{nDFT,T}$ | 1.430 | 1.471 | 1.552 | 1.665 | 1.721 | 1.616 | 1.687 | 1.779 | 1.851 | 1.874 | 1.862 | 1.779 |
| | $P_{uT}/P_{nFTD,T}$ | 1.413 | 1.413 | 1.426 | 1.486 | 1.538 | 1.435 | 1.518 | 1.642 | 1.755 | 1.829 | 1.870 | 1.842 |
| 800 | $\lambda_{FT,T}$ | 0.265 | 0.485 | 0.706 | 0.926 | 1.146 | 1.367 | 1.587 | 1.808 | 2.028 | 2.249 | 2.469 | 2.690 |
| | $\lambda_{D,T}$ | 0.269 | 0.493 | 0.717 | 0.941 | 1.165 | 1.389 | 1.613 | 1.837 | 2.061 | 2.285 | 2.509 | 2.733 |
| | $P_{uT}/P_{yT}$ | 0.727 | 0.708 | 0.683 | 0.646 | 0.567 | 0.448 | 0.360 | 0.321 | 0.291 | 0.264 | 0.238 | 0.211 |
| | $P_{uT}/P_{nFT,T}$ | 0.887 | 0.914 | 0.964 | 1.029 | 1.055 | 1.006 | 0.975 | 0.982 | 0.992 | 0.993 | 0.976 | 0.938 |
| | $P_{uT}/P_{nD,T}$ | 1.017 | 0.992 | 0.957 | 0.963 | 0.961 | 0.870 | 0.797 | 0.801 | 0.812 | 0.819 | 0.811 | 0.786 |
| | $P_{uT}/P_{nDFT,T}$ | 1.242 | 1.280 | 1.350 | 1.441 | 1.513 | 1.490 | 1.484 | 1.555 | 1.633 | 1.698 | 1.730 | 1.721 |
| | $P_{uT}/P_{nFTD,T}$ | 1.233 | 1.251 | 1.286 | 1.394 | 1.489 | 1.437 | 1.398 | 1.489 | 1.596 | 1.697 | 1.772 | 1.808 |

**Table I.15**: Numerical failure loads and their DSM estimates concerning the **LC15** column geometry with 12 room temperature stresses (corresponding to equally spaced slenderness values) and 8 temperatures varying from $T$=20/100 to $T$=800 ºC.

| $T$ (ºC) | $\lambda_{cr.20}$ | 0.45 | 0.70 | 0.95 | 1.20 | 1.45 | 1.70 | 1.95 | 2.20 | 2.45 | 2.70 | 2.95 | 3.20 |
|---|---|---|---|---|---|---|---|---|---|---|---|---|---|
| 20/100 | $\lambda_{FT.T}$ | 0.450 | 0.701 | 0.950 | 1.200 | 1.450 | 1.700 | 1.950 | 2.200 | 2.450 | 2.700 | 2.950 | 3.200 |
| | $\lambda_{D.T}$ | 0.474 | 0.738 | 1.000 | 1.263 | 1.526 | 1.789 | 2.052 | 2.315 | 2.578 | 2.841 | 3.105 | 3.368 |
| | $P_{uT}/P_{yT}$ | 0.923 | 0.861 | 0.685 | 0.514 | 0.422 | 0.370 | 0.332 | 0.300 | 0.270 | 0.240 | 0.210 | 0.184 |
| | $P_{uT}/P_{nFT.T}$ | 1.005 | 1.058 | 1.000 | 0.938 | 1.018 | 1.065 | 1.083 | 1.093 | 1.087 | 1.053 | 1.000 | 0.943 |
| | $P_{uT}/P_{nD.T}$ | 0.923 | 0.934 | 0.914 | 0.838 | 0.826 | 0.850 | 0.880 | 0.905 | 0.916 | 0.904 | 0.873 | 0.838 |
| | $P_{uT}/P_{nDFT.T}$ | 1.005 | 1.095 | 1.161 | 1.187 | 1.339 | 1.483 | 1.608 | 1.720 | 1.803 | 1.836 | 1.825 | 1.797 |
| | $P_{uT}/P_{nFTD.T}$ | 1.005 | 1.129 | 1.213 | 1.212 | 1.295 | 1.440 | 1.605 | 1.772 | 1.923 | 2.031 | 2.096 | 2.145 |
| 200 | $\lambda_{FT.T}$ | 0.448 | 0.697 | 0.945 | 1.193 | 1.442 | 1.691 | 1.939 | 2.188 | 2.436 | 2.685 | 2.933 | 3.182 |
| | $\lambda_{D.T}$ | 0.471 | 0.733 | 0.995 | 1.256 | 1.518 | 1.779 | 2.041 | 2.303 | 2.564 | 2.825 | 3.087 | 3.349 |
| | $P_{uT}/P_{yT}$ | 0.904 | 0.846 | 0.687 | 0.517 | 0.420 | 0.368 | 0.331 | 0.299 | 0.270 | 0.241 | 0.213 | 0.185 |
| | $P_{uT}/P_{nFT.T}$ | 1.082 | 1.125 | 1.062 | 0.971 | 1.005 | 1.053 | 1.073 | 1.084 | 1.080 | 1.052 | 1.008 | 0.943 |
| | $P_{uT}/P_{nD.T}$ | 0.925 | 0.927 | 0.919 | 0.843 | 0.820 | 0.843 | 0.873 | 0.898 | 0.911 | 0.903 | 0.881 | 0.838 |
| | $P_{uT}/P_{nDFT.T}$ | 1.107 | 1.168 | 1.220 | 1.221 | 1.330 | 1.474 | 1.598 | 1.710 | 1.796 | 1.837 | 1.843 | 1.799 |
| | $P_{uT}/P_{nFTD.T}$ | 1.105 | 1.214 | 1.307 | 1.294 | 1.350 | 1.485 | 1.641 | 1.797 | 1.938 | 2.038 | 2.107 | 2.121 |
| 300 | $\lambda_{FT.T}$ | 0.444 | 0.692 | 0.938 | 1.185 | 1.432 | 1.679 | 1.925 | 2.172 | 2.419 | 2.666 | 2.913 | 3.160 |
| | $\lambda_{D.T}$ | 0.468 | 0.728 | 0.987 | 1.247 | 1.507 | 1.767 | 2.027 | 2.286 | 2.546 | 2.805 | 3.066 | 3.326 |
| | $P_{uT}/P_{yT}$ | 0.735 | 0.701 | 0.628 | 0.491 | 0.383 | 0.336 | 0.304 | 0.279 | 0.254 | 0.230 | 0.205 | 0.182 |
| | $P_{uT}/P_{nFT.T}$ | 0.952 | 0.997 | 1.021 | 0.949 | 0.918 | 0.954 | 0.980 | 1.002 | 1.010 | 0.998 | 0.966 | 0.924 |
| | $P_{uT}/P_{nD.T}$ | 0.935 | 0.896 | 0.914 | 0.846 | 0.778 | 0.791 | 0.822 | 0.852 | 0.871 | 0.873 | 0.858 | 0.833 |
| | $P_{uT}/P_{nDFT.T}$ | 1.211 | 1.269 | 1.324 | 1.307 | 1.324 | 1.443 | 1.564 | 1.682 | 1.777 | 1.834 | 1.852 | 1.842 |
| | $P_{uT}/P_{nFTD.T}$ | 1.195 | 1.232 | 1.356 | 1.346 | 1.320 | 1.428 | 1.572 | 1.725 | 1.863 | 1.971 | 2.041 | 2.086 |
| 400 | $\lambda_{FT.T}$ | 0.434 | 0.675 | 0.916 | 1.156 | 1.397 | 1.638 | 1.879 | 2.120 | 2.361 | 2.601 | 2.843 | 3.084 |
| | $\lambda_{D.T}$ | 0.456 | 0.711 | 0.964 | 1.217 | 1.471 | 1.724 | 1.978 | 2.231 | 2.485 | 2.738 | 2.992 | 3.245 |
| | $P_{uT}/P_{yT}$ | 0.612 | 0.589 | 0.552 | 0.485 | 0.374 | 0.314 | 0.286 | 0.266 | 0.246 | 0.225 | 0.204 | 0.184 |
| | $P_{uT}/P_{nFT.T}$ | 0.836 | 0.875 | 0.922 | 0.945 | 0.881 | 0.873 | 0.903 | 0.935 | 0.956 | 0.956 | 0.938 | 0.914 |
| | $P_{uT}/P_{nD.T}$ | 0.946 | 0.912 | 0.886 | 0.884 | 0.785 | 0.756 | 0.783 | 0.816 | 0.843 | 0.853 | 0.846 | 0.835 |
| | $P_{uT}/P_{nDFT.T}$ | 1.294 | 1.355 | 1.427 | 1.474 | 1.411 | 1.446 | 1.557 | 1.679 | 1.785 | 1.855 | 1.887 | 1.904 |
| | $P_{uT}/P_{nFTD.T}$ | 1.268 | 1.289 | 1.344 | 1.430 | 1.349 | 1.375 | 1.504 | 1.653 | 1.796 | 1.909 | 1.989 | 2.057 |
| 500 | $\lambda_{FT.T}$ | 0.423 | 0.659 | 0.893 | 1.128 | 1.363 | 1.598 | 1.833 | 2.068 | 2.302 | 2.537 | 2.773 | 3.008 |
| | $\lambda_{D.T}$ | 0.445 | 0.693 | 0.940 | 1.187 | 1.434 | 1.682 | 1.929 | 2.176 | 2.423 | 2.670 | 2.918 | 3.165 |
| | $P_{uT}/P_{yT}$ | 0.642 | 0.619 | 0.580 | 0.501 | 0.389 | 0.327 | 0.297 | 0.275 | 0.254 | 0.234 | 0.212 | 0.192 |
| | $P_{uT}/P_{nFT.T}$ | 0.900 | 0.936 | 0.977 | 0.972 | 0.899 | 0.888 | 0.914 | 0.944 | 0.966 | 0.970 | 0.955 | 0.929 |
| | $P_{uT}/P_{nD.T}$ | 0.945 | 0.911 | 0.892 | 0.878 | 0.788 | 0.760 | 0.784 | 0.816 | 0.843 | 0.857 | 0.854 | 0.842 |
| | $P_{uT}/P_{nDFT.T}$ | 1.326 | 1.379 | 1.439 | 1.447 | 1.385 | 1.420 | 1.525 | 1.643 | 1.751 | 1.829 | 1.870 | 1.885 |
| | $P_{uT}/P_{nFTD.T}$ | 1.303 | 1.323 | 1.384 | 1.449 | 1.377 | 1.401 | 1.521 | 1.664 | 1.805 | 1.920 | 2.004 | 2.065 |
| 600 | $\lambda_{FT.T}$ | 0.443 | 0.689 | 0.935 | 1.181 | 1.426 | 1.672 | 1.918 | 2.164 | 2.410 | 2.656 | 2.902 | 3.148 |
| | $\lambda_{D.T}$ | 0.466 | 0.726 | 0.984 | 1.243 | 1.501 | 1.760 | 2.019 | 2.278 | 2.536 | 2.795 | 3.054 | 3.313 |
| | $P_{uT}/P_{yT}$ | 0.570 | 0.550 | 0.516 | 0.470 | 0.365 | 0.300 | 0.275 | 0.256 | 0.237 | 0.217 | 0.196 | 0.176 |
| | $P_{uT}/P_{nFT.T}$ | 0.800 | 0.839 | 0.888 | 0.944 | 0.887 | 0.850 | 0.884 | 0.919 | 0.940 | 0.938 | 0.919 | 0.892 |
| | $P_{uT}/P_{nD.T}$ | 0.950 | 0.916 | 0.880 | 0.899 | 0.798 | 0.750 | 0.779 | 0.814 | 0.840 | 0.847 | 0.840 | 0.824 |
| | $P_{uT}/P_{nDFT.T}$ | 1.334 | 1.398 | 1.480 | 1.574 | 1.502 | 1.482 | 1.596 | 1.721 | 1.826 | 1.889 | 1.917 | 1.923 |
| | $P_{uT}/P_{nFTD.T}$ | 1.303 | 1.321 | 1.359 | 1.480 | 1.395 | 1.387 | 1.522 | 1.675 | 1.816 | 1.924 | 2.000 | 2.057 |
| 700 | $\lambda_{FT.T}$ | 0.450 | 0.701 | 0.950 | 1.200 | 1.450 | 1.700 | 1.950 | 2.200 | 2.450 | 2.700 | 2.950 | 3.200 |
| | $\lambda_{D.T}$ | 0.474 | 0.738 | 1.000 | 1.263 | 1.526 | 1.789 | 2.052 | 2.315 | 2.578 | 2.841 | 3.105 | 3.368 |
| | $P_{uT}/P_{yT}$ | 0.549 | 0.529 | 0.498 | 0.439 | 0.339 | 0.292 | 0.269 | 0.251 | 0.232 | 0.211 | 0.192 | 0.171 |
| | $P_{uT}/P_{nFT.T}$ | 0.746 | 0.787 | 0.842 | 0.879 | 0.835 | 0.840 | 0.877 | 0.913 | 0.932 | 0.928 | 0.913 | 0.879 |
| | $P_{uT}/P_{nD.T}$ | 0.952 | 0.917 | 0.878 | 0.865 | 0.762 | 0.748 | 0.780 | 0.815 | 0.839 | 0.844 | 0.840 | 0.818 |
| | $P_{uT}/P_{nDFT.T}$ | 1.293 | 1.364 | 1.459 | 1.524 | 1.463 | 1.508 | 1.627 | 1.753 | 1.854 | 1.913 | 1.947 | 1.936 |
| | $P_{uT}/P_{nFTD.T}$ | 1.259 | 1.278 | 1.314 | 1.386 | 1.303 | 1.358 | 1.499 | 1.656 | 1.797 | 1.905 | 1.994 | 2.039 |
| 800 | $\lambda_{FT.T}$ | 0.397 | 0.618 | 0.838 | 1.058 | 1.279 | 1.499 | 1.720 | 1.940 | 2.161 | 2.381 | 2.602 | 2.822 |
| | $\lambda_{D.T}$ | 0.418 | 0.650 | 0.882 | 1.114 | 1.346 | 1.578 | 1.810 | 2.042 | 2.274 | 2.506 | 2.738 | 2.970 |
| | $P_{uT}/P_{yT}$ | 0.676 | 0.653 | 0.617 | 0.548 | 0.431 | 0.352 | 0.316 | 0.291 | 0.271 | 0.251 | 0.231 | 0.211 |
| | $P_{uT}/P_{nFT.T}$ | 0.850 | 0.886 | 0.933 | 0.955 | 0.894 | 0.900 | 0.920 | 0.946 | 0.971 | 0.983 | 0.980 | 0.963 |
| | $P_{uT}/P_{nD.T}$ | 0.946 | 0.915 | 0.895 | 0.901 | 0.815 | 0.764 | 0.779 | 0.806 | 0.835 | 0.856 | 0.863 | 0.859 |
| | $P_{uT}/P_{nDFT.T}$ | 1.190 | 1.241 | 1.306 | 1.365 | 1.328 | 1.375 | 1.465 | 1.573 | 1.682 | 1.772 | 1.835 | 1.870 |
| | $P_{uT}/P_{nFTD.T}$ | 1.171 | 1.196 | 1.257 | 1.353 | 1.302 | 1.294 | 1.395 | 1.524 | 1.664 | 1.792 | 1.900 | 1.985 |

**Table I.16**: Numerical failure loads and their DSM estimates concerning the **LC16** column geometry with 12 room temperature stresses (corresponding to equally spaced slenderness values) and 8 temperatures varying from $T$=20/100 to $T$=800 ºC.

| $T$ (ºC) | $\lambda_{cr.20}$ | 0.35 | 0.60 | 0.85 | 1.10 | 1.35 | 1.60 | 1.85 | 2.10 | 2.35 | 2.60 | 2.85 | 3.10 |
|---|---|---|---|---|---|---|---|---|---|---|---|---|---|
| 20/100 | $\lambda_{FT.T}$ | 0.350 | 0.600 | 0.850 | 1.100 | 1.350 | 1.600 | 1.850 | 2.100 | 2.350 | 2.600 | 2.850 | 3.100 |
| | $\lambda_{D.T}$ | 0.383 | 0.657 | 0.930 | 1.204 | 1.478 | 1.751 | 2.025 | 2.298 | 2.572 | 2.846 | 3.119 | 3.393 |
| | $P_{uT}/P_{yT}$ | 0.948 | 0.906 | 0.797 | 0.586 | 0.459 | 0.397 | 0.353 | 0.317 | 0.284 | 0.251 | 0.219 | 0.188 |
| | $P_{uT}/P_{nFT.T}$ | 0.998 | 1.054 | 1.079 | 0.973 | 0.985 | 1.077 | 1.092 | 1.097 | 1.085 | 1.051 | 0.994 | 0.918 |
| | $P_{uT}/P_{nD.T}$ | 0.948 | 0.934 | 1.005 | 0.916 | 0.870 | 0.891 | 0.923 | 0.948 | 0.959 | 0.949 | 0.916 | 0.862 |
| | $P_{uT}/P_{nDFT.T}$ | 0.998 | 1.063 | 1.226 | 1.231 | 1.323 | 1.510 | 1.639 | 1.755 | 1.838 | 1.877 | 1.866 | 1.803 |
| | $P_{uT}/P_{nFTD.T}$ | 0.998 | 1.081 | 1.278 | 1.266 | 1.302 | 1.435 | 1.597 | 1.758 | 1.900 | 2.006 | 2.065 | 2.068 |
| 200 | $\lambda_{FT.T}$ | 0.348 | 0.597 | 0.845 | 1.094 | 1.342 | 1.591 | 1.840 | 2.088 | 2.337 | 2.586 | 2.834 | 3.083 |
| | $\lambda_{D.T}$ | 0.381 | 0.653 | 0.925 | 1.197 | 1.469 | 1.741 | 2.014 | 2.286 | 2.558 | 2.830 | 3.102 | 3.374 |
| | $P_{uT}/P_{yT}$ | 0.928 | 0.888 | 0.788 | 0.587 | 0.457 | 0.395 | 0.352 | 0.316 | 0.284 | 0.252 | 0.218 | 0.189 |
| | $P_{uT}/P_{nFT.T}$ | 1.080 | 1.126 | 1.141 | 1.015 | 0.988 | 1.066 | 1.082 | 1.089 | 1.079 | 1.048 | 0.987 | 0.919 |
| | $P_{uT}/P_{nD.T}$ | 0.950 | 0.928 | 0.999 | 0.918 | 0.865 | 0.884 | 0.916 | 0.942 | 0.954 | 0.946 | 0.909 | 0.864 |
| | $P_{uT}/P_{nDFT.T}$ | 1.104 | 1.152 | 1.282 | 1.270 | 1.328 | 1.501 | 1.630 | 1.746 | 1.832 | 1.875 | 1.854 | 1.808 |
| | $P_{uT}/P_{nFTD.T}$ | 1.103 | 1.170 | 1.367 | 1.353 | 1.367 | 1.491 | 1.644 | 1.797 | 1.930 | 2.026 | 2.059 | 2.065 |
| 300 | $\lambda_{FT.T}$ | 0.346 | 0.592 | 0.839 | 1.086 | 1.333 | 1.580 | 1.827 | 2.074 | 2.320 | 2.567 | 2.814 | 3.061 |
| | $\lambda_{D.T}$ | 0.378 | 0.648 | 0.919 | 1.189 | 1.459 | 1.729 | 1.999 | 2.270 | 2.540 | 2.810 | 3.080 | 3.350 |
| | $P_{uT}/P_{yT}$ | 0.755 | 0.730 | 0.683 | 0.553 | 0.422 | 0.363 | 0.326 | 0.297 | 0.269 | 0.242 | 0.215 | 0.187 |
| | $P_{uT}/P_{nFT.T}$ | 0.954 | 0.995 | 1.048 | 0.992 | 0.924 | 0.974 | 0.995 | 1.014 | 1.017 | 1.000 | 0.963 | 0.903 |
| | $P_{uT}/P_{nD.T}$ | 0.961 | 0.929 | 0.953 | 0.917 | 0.833 | 0.838 | 0.868 | 0.900 | 0.918 | 0.920 | 0.902 | 0.860 |
| | $P_{uT}/P_{nDFT.T}$ | 1.213 | 1.267 | 1.344 | 1.358 | 1.344 | 1.481 | 1.603 | 1.726 | 1.821 | 1.879 | 1.893 | 1.851 |
| | $P_{uT}/P_{nFTD.T}$ | 1.203 | 1.235 | 1.367 | 1.409 | 1.363 | 1.456 | 1.596 | 1.748 | 1.880 | 1.983 | 2.045 | 2.049 |
| 400 | $\lambda_{FT.T}$ | 0.337 | 0.578 | 0.819 | 1.060 | 1.301 | 1.542 | 1.783 | 2.024 | 2.265 | 2.505 | 2.746 | 2.987 |
| | $\lambda_{D.T}$ | 0.369 | 0.633 | 0.896 | 1.160 | 1.424 | 1.687 | 1.951 | 2.215 | 2.478 | 2.742 | 3.006 | 3.270 |
| | $P_{uT}/P_{yT}$ | 0.632 | 0.613 | 0.586 | 0.529 | 0.412 | 0.343 | 0.309 | 0.285 | 0.262 | 0.238 | 0.214 | 0.190 |
| | $P_{uT}/P_{nFT.T}$ | 0.845 | 0.877 | 0.929 | 0.965 | 0.895 | 0.900 | 0.923 | 0.952 | 0.968 | 0.964 | 0.942 | 0.901 |
| | $P_{uT}/P_{nD.T}$ | 0.978 | 0.949 | 0.919 | 0.934 | 0.842 | 0.809 | 0.833 | 0.868 | 0.894 | 0.903 | 0.896 | 0.870 |
| | $P_{uT}/P_{nDFT.T}$ | 1.307 | 1.358 | 1.438 | 1.493 | 1.439 | 1.496 | 1.603 | 1.730 | 1.837 | 1.906 | 1.938 | 1.926 |
| | $P_{uT}/P_{nFTD.T}$ | 1.291 | 1.309 | 1.353 | 1.467 | 1.403 | 1.424 | 1.545 | 1.694 | 1.833 | 1.941 | 2.017 | 2.049 |
| 500 | $\lambda_{FT.T}$ | 0.329 | 0.564 | 0.799 | 1.034 | 1.269 | 1.504 | 1.739 | 1.974 | 2.209 | 2.444 | 2.679 | 2.914 |
| | $\lambda_{D.T}$ | 0.360 | 0.617 | 0.874 | 1.132 | 1.389 | 1.646 | 1.903 | 2.160 | 2.417 | 2.675 | 2.932 | 3.189 |
| | $P_{uT}/P_{yT}$ | 0.661 | 0.642 | 0.614 | 0.553 | 0.431 | 0.357 | 0.319 | 0.294 | 0.271 | 0.247 | 0.223 | 0.199 |
| | $P_{uT}/P_{nFT.T}$ | 0.908 | 0.939 | 0.988 | 1.010 | 0.926 | 0.916 | 0.934 | 0.961 | 0.979 | 0.977 | 0.958 | 0.923 |
| | $P_{uT}/P_{nD.T}$ | 0.973 | 0.946 | 0.921 | 0.939 | 0.851 | 0.813 | 0.833 | 0.867 | 0.894 | 0.906 | 0.902 | 0.882 |
| | $P_{uT}/P_{nDFT.T}$ | 1.337 | 1.382 | 1.454 | 1.499 | 1.429 | 1.470 | 1.570 | 1.693 | 1.803 | 1.879 | 1.919 | 1.921 |
| | $P_{uT}/P_{nFTD.T}$ | 1.323 | 1.341 | 1.390 | 1.506 | 1.442 | 1.452 | 1.563 | 1.706 | 1.844 | 1.955 | 2.033 | 2.075 |
| 600 | $\lambda_{FT.T}$ | 0.344 | 0.590 | 0.836 | 1.082 | 1.328 | 1.574 | 1.820 | 2.066 | 2.312 | 2.558 | 2.804 | 3.050 |
| | $\lambda_{D.T}$ | 0.377 | 0.646 | 0.915 | 1.184 | 1.454 | 1.723 | 1.992 | 2.261 | 2.530 | 2.799 | 3.069 | 3.338 |
| | $P_{uT}/P_{yT}$ | 0.595 | 0.575 | 0.549 | 0.499 | 0.393 | 0.328 | 0.297 | 0.275 | 0.253 | 0.230 | 0.206 | 0.183 |
| | $P_{uT}/P_{nFT.T}$ | 0.817 | 0.845 | 0.896 | 0.939 | 0.883 | 0.877 | 0.905 | 0.937 | 0.953 | 0.947 | 0.923 | 0.883 |
| | $P_{uT}/P_{nD.T}$ | 0.992 | 0.959 | 0.914 | 0.927 | 0.840 | 0.804 | 0.831 | 0.868 | 0.892 | 0.899 | 0.889 | 0.863 |
| | $P_{uT}/P_{nDFT.T}$ | 1.361 | 1.409 | 1.493 | 1.564 | 1.499 | 1.534 | 1.645 | 1.776 | 1.880 | 1.942 | 1.967 | 1.952 |
| | $P_{uT}/P_{nFTD.T}$ | 1.342 | 1.351 | 1.373 | 1.483 | 1.424 | 1.439 | 1.567 | 1.721 | 1.858 | 1.961 | 2.030 | 2.061 |
| 700 | $\lambda_{FT.T}$ | 0.350 | 0.600 | 0.850 | 1.100 | 1.350 | 1.600 | 1.850 | 2.100 | 2.350 | 2.600 | 2.850 | 3.100 |
| | $\lambda_{D.T}$ | 0.383 | 0.657 | 0.930 | 1.204 | 1.478 | 1.751 | 2.025 | 2.298 | 2.572 | 2.846 | 3.119 | 3.393 |
| | $P_{uT}/P_{yT}$ | 0.577 | 0.557 | 0.529 | 0.481 | 0.381 | 0.319 | 0.291 | 0.269 | 0.247 | 0.224 | 0.201 | 0.178 |
| | $P_{uT}/P_{nFT.T}$ | 0.765 | 0.795 | 0.846 | 0.896 | 0.859 | 0.866 | 0.898 | 0.932 | 0.946 | 0.938 | 0.912 | 0.869 |
| | $P_{uT}/P_{nD.T}$ | 1.000 | 0.965 | 0.918 | 0.921 | 0.835 | 0.802 | 0.832 | 0.870 | 0.893 | 0.897 | 0.884 | 0.855 |
| | $P_{uT}/P_{nDFT.T}$ | 1.326 | 1.377 | 1.467 | 1.553 | 1.509 | 1.561 | 1.677 | 1.809 | 1.910 | 1.967 | 1.985 | 1.961 |
| | $P_{uT}/P_{nFTD.T}$ | 1.304 | 1.313 | 1.333 | 1.431 | 1.381 | 1.407 | 1.542 | 1.700 | 1.837 | 1.940 | 2.008 | 2.035 |
| 800 | $\lambda_{FT.T}$ | 0.309 | 0.529 | 0.750 | 0.970 | 1.191 | 1.411 | 1.632 | 1.852 | 2.073 | 2.293 | 2.513 | 2.734 |
| | $\lambda_{D.T}$ | 0.338 | 0.579 | 0.820 | 1.062 | 1.303 | 1.544 | 1.786 | 2.027 | 2.268 | 2.510 | 2.751 | 2.992 |
| | $P_{uT}/P_{yT}$ | 0.694 | 0.675 | 0.649 | 0.596 | 0.474 | 0.385 | 0.341 | 0.312 | 0.288 | 0.265 | 0.242 | 0.219 |
| | $P_{uT}/P_{nFT.T}$ | 0.854 | 0.885 | 0.936 | 0.978 | 0.913 | 0.902 | 0.942 | 0.964 | 0.985 | 0.992 | 0.984 | 0.960 |
| | $P_{uT}/P_{nD.T}$ | 0.971 | 0.946 | 0.921 | 0.950 | 0.873 | 0.819 | 0.828 | 0.856 | 0.886 | 0.905 | 0.911 | 0.902 |
| | $P_{uT}/P_{nDFT.T}$ | 1.196 | 1.239 | 1.311 | 1.390 | 1.360 | 1.394 | 1.512 | 1.621 | 1.734 | 1.823 | 1.883 | 1.911 |
| | $P_{uT}/P_{nFTD.T}$ | 1.185 | 1.206 | 1.255 | 1.384 | 1.351 | 1.341 | 1.430 | 1.557 | 1.696 | 1.819 | 1.920 | 1.992 |

**Table I.17**: Numerical failure loads and their DSM estimates concerning the **LC17** column geometry with 12 room temperature stresses (corresponding to equally spaced slenderness values) and 8 temperatures varying from $T$=20/100 to $T$=800 ºC.

| $T$ (ºC) | $\lambda_{cr.20}$ | 0.26 | 0.52 | 0.78 | 1.04 | 1.31 | 1.57 | 1.83 | 2.09 | 2.35 | 2.61 | 2.87 | 3.13 |
|---|---|---|---|---|---|---|---|---|---|---|---|---|---|
| 20/100 | $\lambda_{FT.T}$ | 0.261 | 0.522 | 0.783 | 1.044 | 1.306 | 1.567 | 1.828 | 2.089 | 2.350 | 2.611 | 2.872 | 3.133 |
| | $\lambda_{D.T}$ | 0.292 | 0.583 | 0.875 | 1.166 | 1.458 | 1.749 | 2.041 | 2.332 | 2.624 | 2.915 | 3.207 | 3.498 |
| | $P_{uT}/P_{yT}$ | 0.974 | 0.949 | 0.886 | 0.663 | 0.488 | 0.406 | 0.349 | 0.302 | 0.256 | 0.213 | 0.179 | 0.152 |
| | $P_{uT}/P_{nFT.T}$ | 1.003 | 1.063 | 1.145 | 1.046 | 0.996 | 1.085 | 1.078 | 1.057 | 1.003 | 0.922 | 0.847 | 0.779 |
| | $P_{uT}/P_{nD.T}$ | 0.974 | 0.951 | 1.067 | 1.006 | 0.912 | 0.911 | 0.919 | 0.916 | 0.884 | 0.827 | 0.771 | 0.721 |
| | $P_{uT}/P_{nDFT.T}$ | 1.003 | 1.063 | 1.271 | 1.317 | 1.350 | 1.530 | 1.630 | 1.704 | 1.712 | 1.659 | 1.599 | 1.540 |
| | $P_{uT}/P_{nFTD.T}$ | 1.003 | 1.065 | 1.321 | 1.359 | 1.336 | 1.440 | 1.563 | 1.672 | 1.727 | 1.725 | 1.717 | 1.711 |
| 200 | $\lambda_{FT.T}$ | 0.260 | 0.519 | 0.779 | 1.039 | 1.298 | 1.558 | 1.818 | 2.077 | 2.337 | 2.597 | 2.856 | 3.116 |
| | $\lambda_{D.T}$ | 0.290 | 0.580 | 0.870 | 1.160 | 1.450 | 1.739 | 2.029 | 2.319 | 2.609 | 2.899 | 3.189 | 3.479 |
| | $P_{uT}/P_{yT}$ | 0.955 | 0.929 | 0.871 | 0.664 | 0.489 | 0.406 | 0.349 | 0.303 | 0.258 | 0.215 | 0.180 | 0.153 |
| | $P_{uT}/P_{nFT.T}$ | 1.088 | 1.141 | 1.211 | 1.099 | 1.012 | 1.079 | 1.074 | 1.055 | 1.006 | 0.926 | 0.850 | 0.783 |
| | $P_{uT}/P_{nD.T}$ | 0.976 | 0.950 | 1.056 | 1.010 | 0.913 | 0.908 | 0.917 | 0.916 | 0.888 | 0.831 | 0.775 | 0.725 |
| | $P_{uT}/P_{nDFT.T}$ | 1.113 | 1.167 | 1.331 | 1.366 | 1.368 | 1.527 | 1.630 | 1.704 | 1.721 | 1.669 | 1.608 | 1.550 |
| | $P_{uT}/P_{nFTD.T}$ | 1.113 | 1.165 | 1.412 | 1.459 | 1.416 | 1.506 | 1.622 | 1.722 | 1.772 | 1.758 | 1.736 | 1.717 |
| 300 | $\lambda_{FT.T}$ | 0.258 | 0.516 | 0.773 | 1.031 | 1.289 | 1.547 | 1.805 | 2.063 | 2.320 | 2.578 | 2.836 | 3.094 |
| | $\lambda_{D.T}$ | 0.288 | 0.576 | 0.864 | 1.151 | 1.439 | 1.727 | 2.015 | 2.303 | 2.591 | 2.879 | 3.167 | 3.454 |
| | $P_{uT}/P_{yT}$ | 0.788 | 0.767 | 0.733 | 0.634 | 0.463 | 0.386 | 0.337 | 0.296 | 0.256 | 0.214 | 0.181 | 0.154 |
| | $P_{uT}/P_{nFT.T}$ | 0.978 | 1.016 | 1.084 | 1.095 | 0.976 | 1.019 | 1.030 | 1.026 | 0.993 | 0.915 | 0.847 | 0.784 |
| | $P_{uT}/P_{nD.T}$ | 1.003 | 0.976 | 0.990 | 1.027 | 0.903 | 0.890 | 0.906 | 0.913 | 0.894 | 0.835 | 0.785 | 0.736 |
| | $P_{uT}/P_{nDFT.T}$ | 1.244 | 1.293 | 1.380 | 1.490 | 1.424 | 1.556 | 1.670 | 1.759 | 1.791 | 1.730 | 1.676 | 1.617 |
| | $P_{uT}/P_{nFTD.T}$ | 1.238 | 1.269 | 1.391 | 1.549 | 1.454 | 1.524 | 1.644 | 1.752 | 1.812 | 1.783 | 1.763 | 1.738 |
| 400 | $\lambda_{FT.T}$ | 0.252 | 0.503 | 0.755 | 1.006 | 1.258 | 1.510 | 1.761 | 2.013 | 2.265 | 2.516 | 2.768 | 3.019 |
| | $\lambda_{D.T}$ | 0.281 | 0.562 | 0.843 | 1.124 | 1.405 | 1.686 | 1.967 | 2.247 | 2.528 | 2.809 | 3.090 | 3.371 |
| | $P_{uT}/P_{yT}$ | 0.689 | 0.666 | 0.636 | 0.587 | 0.467 | 0.375 | 0.333 | 0.297 | 0.262 | 0.217 | 0.187 | 0.160 |
| | $P_{uT}/P_{nFT.T}$ | 0.906 | 0.930 | 0.979 | 1.034 | 0.982 | 0.967 | 0.993 | 1.006 | 0.990 | 0.907 | 0.856 | 0.793 |
| | $P_{uT}/P_{nD.T}$ | 1.066 | 1.031 | 0.985 | 1.017 | 0.946 | 0.884 | 0.905 | 0.920 | 0.912 | 0.845 | 0.806 | 0.754 |
| | $P_{uT}/P_{nDFT.T}$ | 1.402 | 1.439 | 1.515 | 1.601 | 1.581 | 1.614 | 1.735 | 1.838 | 1.889 | 1.806 | 1.773 | 1.704 |
| | $P_{uT}/P_{nFTD.T}$ | 1.393 | 1.399 | 1.424 | 1.571 | 1.554 | 1.537 | 1.659 | 1.777 | 1.852 | 1.800 | 1.800 | 1.764 |
| 500 | $\lambda_{FT.T}$ | 0.245 | 0.491 | 0.736 | 0.982 | 1.227 | 1.472 | 1.718 | 1.963 | 2.209 | 2.454 | 2.700 | 2.945 |
| | $\lambda_{D.T}$ | 0.274 | 0.548 | 0.822 | 1.096 | 1.370 | 1.644 | 1.918 | 2.192 | 2.466 | 2.740 | 3.014 | 3.288 |
| | $P_{uT}/P_{yT}$ | 0.711 | 0.690 | 0.662 | 0.614 | 0.487 | 0.388 | 0.342 | 0.306 | 0.270 | 0.226 | 0.196 | 0.167 |
| | $P_{uT}/P_{nFT.T}$ | 0.963 | 0.986 | 1.034 | 1.087 | 1.014 | 0.983 | 0.998 | 1.011 | 0.999 | 0.923 | 0.877 | 0.811 |
| | $P_{uT}/P_{nD.T}$ | 1.047 | 1.016 | 0.974 | 1.022 | 0.951 | 0.883 | 0.900 | 0.916 | 0.913 | 0.851 | 0.818 | 0.765 |
| | $P_{uT}/P_{nDFT.T}$ | 1.418 | 1.451 | 1.522 | 1.600 | 1.567 | 1.581 | 1.688 | 1.793 | 1.853 | 1.787 | 1.768 | 1.698 |
| | $P_{uT}/P_{nFTD.T}$ | 1.409 | 1.418 | 1.445 | 1.614 | 1.591 | 1.559 | 1.671 | 1.786 | 1.865 | 1.822 | 1.830 | 1.788 |
| 600 | $\lambda_{FT.T}$ | 0.257 | 0.514 | 0.771 | 1.027 | 1.284 | 1.541 | 1.798 | 2.055 | 2.312 | 2.569 | 2.826 | 3.082 |
| | $\lambda_{D.T}$ | 0.287 | 0.574 | 0.860 | 1.147 | 1.434 | 1.721 | 2.008 | 2.294 | 2.581 | 2.868 | 3.155 | 3.442 |
| | $P_{uT}/P_{yT}$ | 0.659 | 0.636 | 0.604 | 0.557 | 0.449 | 0.363 | 0.324 | 0.289 | 0.254 | 0.210 | 0.180 | 0.153 |
| | $P_{uT}/P_{nFT.T}$ | 0.890 | 0.911 | 0.956 | 1.011 | 0.972 | 0.955 | 0.985 | 0.998 | 0.978 | 0.894 | 0.840 | 0.777 |
| | $P_{uT}/P_{nD.T}$ | 1.098 | 1.059 | 1.007 | 1.015 | 0.947 | 0.890 | 0.912 | 0.925 | 0.913 | 0.841 | 0.799 | 0.747 |
| | $P_{uT}/P_{nDFT.T}$ | 1.483 | 1.518 | 1.593 | 1.685 | 1.653 | 1.676 | 1.799 | 1.900 | 1.940 | 1.843 | 1.800 | 1.725 |
| | $P_{uT}/P_{nFTD.T}$ | 1.471 | 1.471 | 1.484 | 1.599 | 1.584 | 1.574 | 1.702 | 1.818 | 1.884 | 1.821 | 1.813 | 1.772 |
| 700 | $\lambda_{FT.T}$ | 0.261 | 0.522 | 0.783 | 1.044 | 1.306 | 1.567 | 1.828 | 2.089 | 2.350 | 2.611 | 2.872 | 3.133 |
| | $\lambda_{D.T}$ | 0.292 | 0.583 | 0.875 | 1.166 | 1.458 | 1.749 | 2.041 | 2.332 | 2.624 | 2.915 | 3.207 | 3.498 |
| | $P_{uT}/P_{yT}$ | 0.644 | 0.620 | 0.588 | 0.540 | 0.435 | 0.356 | 0.318 | 0.284 | 0.248 | 0.205 | 0.175 | 0.149 |
| | $P_{uT}/P_{nFT.T}$ | 0.839 | 0.862 | 0.908 | 0.968 | 0.946 | 0.950 | 0.982 | 0.994 | 0.971 | 0.885 | 0.828 | 0.765 |
| | $P_{uT}/P_{nD.T}$ | 1.117 | 1.075 | 1.019 | 1.015 | 0.944 | 0.894 | 0.917 | 0.929 | 0.913 | 0.839 | 0.793 | 0.740 |
| | $P_{uT}/P_{nDFT.T}$ | 1.455 | 1.493 | 1.575 | 1.679 | 1.664 | 1.717 | 1.843 | 1.939 | 1.970 | 1.867 | 1.811 | 1.734 |
| | $P_{uT}/P_{nFTD.T}$ | 1.442 | 1.440 | 1.452 | 1.552 | 1.540 | 1.547 | 1.680 | 1.797 | 1.860 | 1.800 | 1.785 | 1.750 |
| 800 | $\lambda_{FT.T}$ | 0.230 | 0.461 | 0.691 | 0.921 | 1.151 | 1.382 | 1.612 | 1.842 | 2.073 | 2.303 | 2.533 | 2.763 |
| | $\lambda_{D.T}$ | 0.257 | 0.514 | 0.771 | 1.028 | 1.286 | 1.543 | 1.800 | 2.057 | 2.314 | 2.571 | 2.828 | 3.085 |
| | $P_{uT}/P_{yT}$ | 0.737 | 0.718 | 0.692 | 0.651 | 0.541 | 0.418 | 0.364 | 0.326 | 0.292 | 0.257 | 0.219 | 0.188 |
| | $P_{uT}/P_{nFT.T}$ | 0.894 | 0.919 | 0.970 | 1.034 | 1.010 | 0.952 | 0.999 | 1.015 | 1.015 | 0.989 | 0.921 | 0.859 |
| | $P_{uT}/P_{nD.T}$ | 1.031 | 1.005 | 0.969 | 1.017 | 0.986 | 0.888 | 0.891 | 0.909 | 0.915 | 0.901 | 0.848 | 0.800 |
| | $P_{uT}/P_{nDFT.T}$ | 1.251 | 1.287 | 1.358 | 1.464 | 1.506 | 1.483 | 1.616 | 1.722 | 1.801 | 1.833 | 1.778 | 1.723 |
| | $P_{uT}/P_{nFTD.T}$ | 1.245 | 1.261 | 1.297 | 1.457 | 1.504 | 1.436 | 1.522 | 1.637 | 1.735 | 1.795 | 1.773 | 1.753 |

**Table I.18**: Numerical failure loads and their DSM estimates concerning the **LC18** column geometry with 12 room temperature stresses (corresponding to equally spaced slenderness values) and 8 temperatures varying from $T$=20/100 to $T$=800 ºC.

| $T$ (ºC) | $\lambda_{cr.20}$ | 0.37 | 0.64 | 0.92 | 1.19 | 1.45 | 1.72 | 1.99 | 2.26 | 2.53 | 2.80 | 3.07 | 3.34 |
|---|---|---|---|---|---|---|---|---|---|---|---|---|---|
| 20/100 | $\lambda_{FT.T}$ | 0.374 | 0.643 | 0.916 | 1.185 | 1.454 | 1.724 | 1.994 | 2.263 | 2.533 | 2.803 | 3.071 | 3.341 |
| | $\lambda_{D.T}$ | 0.426 | 0.733 | 1.043 | 1.350 | 1.656 | 1.963 | 2.270 | 2.577 | 2.885 | 3.192 | 3.498 | 3.805 |
| | $P_{uT}/P_{yT}$ | 0.955 | 0.911 | 0.741 | 0.522 | 0.429 | 0.372 | 0.313 | 0.261 | 0.216 | 0.181 | 0.156 | 0.136 |
| | $P_{uT}/P_{nFT.T}$ | 1.012 | 1.083 | 1.053 | 0.940 | 1.041 | 1.102 | 1.077 | 1.023 | 0.951 | 0.887 | 0.841 | 0.799 |
| | $P_{uT}/P_{nD.T}$ | 0.955 | 0.985 | 1.023 | 0.906 | 0.911 | 0.941 | 0.924 | 0.883 | 0.827 | 0.778 | 0.744 | 0.713 |
| | $P_{uT}/P_{nDFT.T}$ | 1.012 | 1.126 | 1.270 | 1.259 | 1.460 | 1.641 | 1.707 | 1.716 | 1.678 | 1.642 | 1.625 | 1.608 |
| | $P_{uT}/P_{nFTD.T}$ | 1.012 | 1.156 | 1.320 | 1.272 | 1.383 | 1.539 | 1.623 | 1.663 | 1.666 | 1.674 | 1.705 | 1.741 |
| 200 | $\lambda_{FT.T}$ | 0.372 | 0.640 | 0.911 | 1.178 | 1.446 | 1.714 | 1.982 | 2.251 | 2.519 | 2.787 | 3.054 | 3.323 |
| | $\lambda_{D.T}$ | 0.424 | 0.728 | 1.037 | 1.342 | 1.647 | 1.952 | 2.258 | 2.563 | 2.869 | 3.174 | 3.478 | 3.784 |
| | $P_{uT}/P_{yT}$ | 0.944 | 0.879 | 0.744 | 0.528 | 0.426 | 0.371 | 0.313 | 0.262 | 0.217 | 0.183 | 0.157 | 0.137 |
| | $P_{uT}/P_{nFT.T}$ | 1.105 | 1.137 | 1.123 | 0.980 | 1.024 | 1.092 | 1.072 | 1.022 | 0.951 | 0.889 | 0.841 | 0.801 |
| | $P_{uT}/P_{nD.T}$ | 0.966 | 0.960 | 1.029 | 0.916 | 0.902 | 0.935 | 0.921 | 0.884 | 0.828 | 0.780 | 0.745 | 0.715 |
| | $P_{uT}/P_{nDFT.T}$ | 1.130 | 1.182 | 1.335 | 1.301 | 1.444 | 1.633 | 1.705 | 1.719 | 1.682 | 1.648 | 1.628 | 1.614 |
| | $P_{uT}/P_{nFTD.T}$ | 1.129 | 1.226 | 1.428 | 1.369 | 1.444 | 1.599 | 1.677 | 1.710 | 1.699 | 1.696 | 1.711 | 1.737 |
| 300 | $\lambda_{FT.T}$ | 0.369 | 0.635 | 0.905 | 1.170 | 1.436 | 1.702 | 1.968 | 2.235 | 2.501 | 2.767 | 3.033 | 3.299 |
| | $\lambda_{D.T}$ | 0.421 | 0.723 | 1.030 | 1.333 | 1.635 | 1.939 | 2.242 | 2.545 | 2.848 | 3.152 | 3.454 | 3.757 |
| | $P_{uT}/P_{yT}$ | 0.764 | 0.724 | 0.654 | 0.524 | 0.394 | 0.342 | 0.296 | 0.253 | 0.213 | 0.181 | 0.155 | 0.135 |
| | $P_{uT}/P_{nFT.T}$ | 0.970 | 1.005 | 1.042 | 1.002 | 0.947 | 1.000 | 1.005 | 0.978 | 0.927 | 0.873 | 0.822 | 0.785 |
| | $P_{uT}/P_{nD.T}$ | 0.972 | 0.925 | 0.979 | 0.955 | 0.862 | 0.884 | 0.887 | 0.864 | 0.823 | 0.779 | 0.739 | 0.709 |
| | $P_{uT}/P_{nDFT.T}$ | 1.234 | 1.278 | 1.375 | 1.436 | 1.439 | 1.600 | 1.699 | 1.737 | 1.725 | 1.695 | 1.662 | 1.646 |
| | $P_{uT}/P_{nFTD.T}$ | 1.222 | 1.247 | 1.424 | 1.488 | 1.430 | 1.557 | 1.654 | 1.702 | 1.710 | 1.705 | 1.700 | 1.716 |
| 400 | $\lambda_{FT.T}$ | 0.360 | 0.620 | 0.883 | 1.142 | 1.401 | 1.661 | 1.921 | 2.181 | 2.441 | 2.701 | 2.960 | 3.220 |
| | $\lambda_{D.T}$ | 0.410 | 0.706 | 1.005 | 1.300 | 1.596 | 1.892 | 2.188 | 2.484 | 2.780 | 3.076 | 3.371 | 3.667 |
| | $P_{uT}/P_{yT}$ | 0.635 | 0.609 | 0.567 | 0.498 | 0.375 | 0.319 | 0.285 | 0.250 | 0.214 | 0.183 | 0.158 | 0.139 |
| | $P_{uT}/P_{nFT.T}$ | 0.852 | 0.884 | 0.930 | 0.960 | 0.886 | 0.910 | 0.945 | 0.944 | 0.907 | 0.863 | 0.819 | 0.786 |
| | $P_{uT}/P_{nD.T}$ | 0.982 | 0.942 | 0.927 | 0.951 | 0.842 | 0.837 | 0.860 | 0.856 | 0.823 | 0.785 | 0.747 | 0.721 |
| | $P_{uT}/P_{nDFT.T}$ | 1.319 | 1.368 | 1.439 | 1.526 | 1.470 | 1.574 | 1.708 | 1.780 | 1.781 | 1.760 | 1.730 | 1.718 |
| | $P_{uT}/P_{nFTD.T}$ | 1.301 | 1.312 | 1.385 | 1.514 | 1.423 | 1.494 | 1.618 | 1.694 | 1.711 | 1.712 | 1.708 | 1.724 |
| 500 | $\lambda_{FT.T}$ | 0.351 | 0.605 | 0.861 | 1.114 | 1.367 | 1.620 | 1.874 | 2.127 | 2.381 | 2.634 | 2.887 | 3.140 |
| | $\lambda_{D.T}$ | 0.400 | 0.688 | 0.980 | 1.268 | 1.557 | 1.845 | 2.134 | 2.422 | 2.711 | 3.000 | 3.288 | 3.576 |
| | $P_{uT}/P_{yT}$ | 0.665 | 0.639 | 0.599 | 0.516 | 0.393 | 0.334 | 0.297 | 0.261 | 0.224 | 0.192 | 0.166 | 0.144 |
| | $P_{uT}/P_{nFT.T}$ | 0.918 | 0.947 | 0.994 | 0.993 | 0.910 | 0.928 | 0.959 | 0.959 | 0.925 | 0.882 | 0.837 | 0.794 |
| | $P_{uT}/P_{nD.T}$ | 0.980 | 0.940 | 0.940 | 0.949 | 0.853 | 0.846 | 0.866 | 0.863 | 0.833 | 0.796 | 0.759 | 0.723 |
| | $P_{uT}/P_{nDFT.T}$ | 1.351 | 1.394 | 1.463 | 1.511 | 1.457 | 1.555 | 1.683 | 1.758 | 1.767 | 1.751 | 1.723 | 1.693 |
| | $P_{uT}/P_{nFTD.T}$ | 1.335 | 1.346 | 1.438 | 1.543 | 1.464 | 1.532 | 1.648 | 1.723 | 1.742 | 1.742 | 1.734 | 1.726 |
| 600 | $\lambda_{FT.T}$ | 0.368 | 0.633 | 0.901 | 1.166 | 1.431 | 1.696 | 1.961 | 2.226 | 2.492 | 2.757 | 3.022 | 3.287 |
| | $\lambda_{D.T}$ | 0.419 | 0.721 | 1.026 | 1.328 | 1.629 | 1.931 | 2.233 | 2.536 | 2.838 | 3.140 | 3.441 | 3.743 |
| | $P_{uT}/P_{yT}$ | 0.593 | 0.568 | 0.530 | 0.469 | 0.359 | 0.305 | 0.273 | 0.239 | 0.205 | 0.178 | 0.152 | 0.133 |
| | $P_{uT}/P_{nFT.T}$ | 0.817 | 0.849 | 0.895 | 0.933 | 0.877 | 0.889 | 0.924 | 0.922 | 0.888 | 0.855 | 0.803 | 0.765 |
| | $P_{uT}/P_{nD.T}$ | 0.988 | 0.947 | 0.917 | 0.938 | 0.840 | 0.830 | 0.852 | 0.845 | 0.813 | 0.785 | 0.739 | 0.707 |
| | $P_{uT}/P_{nDFT.T}$ | 1.362 | 1.414 | 1.492 | 1.572 | 1.527 | 1.609 | 1.741 | 1.806 | 1.807 | 1.804 | 1.753 | 1.725 |
| | $P_{uT}/P_{nFTD.T}$ | 1.340 | 1.348 | 1.398 | 1.522 | 1.445 | 1.507 | 1.631 | 1.701 | 1.719 | 1.738 | 1.714 | 1.715 |
| 700 | $\lambda_{FT.T}$ | 0.374 | 0.643 | 0.916 | 1.185 | 1.454 | 1.724 | 1.994 | 2.263 | 2.533 | 2.803 | 3.071 | 3.341 |
| | $\lambda_{D.T}$ | 0.426 | 0.733 | 1.043 | 1.350 | 1.656 | 1.963 | 2.270 | 2.577 | 2.885 | 3.192 | 3.498 | 3.805 |
| | $P_{uT}/P_{yT}$ | 0.572 | 0.548 | 0.511 | 0.454 | 0.348 | 0.296 | 0.266 | 0.232 | 0.199 | 0.170 | 0.147 | 0.130 |
| | $P_{uT}/P_{nFT.T}$ | 0.762 | 0.796 | 0.848 | 0.899 | 0.859 | 0.878 | 0.914 | 0.910 | 0.876 | 0.834 | 0.793 | 0.763 |
| | $P_{uT}/P_{nD.T}$ | 0.991 | 0.950 | 0.915 | 0.933 | 0.835 | 0.825 | 0.848 | 0.840 | 0.807 | 0.769 | 0.733 | 0.708 |
| | $P_{uT}/P_{nDFT.T}$ | 1.321 | 1.380 | 1.470 | 1.558 | 1.543 | 1.632 | 1.765 | 1.826 | 1.822 | 1.796 | 1.765 | 1.754 |
| | $P_{uT}/P_{nFTD.T}$ | 1.297 | 1.306 | 1.351 | 1.474 | 1.402 | 1.470 | 1.596 | 1.667 | 1.687 | 1.690 | 1.691 | 1.715 |
| 800 | $\lambda_{FT.T}$ | 0.330 | 0.567 | 0.808 | 1.045 | 1.283 | 1.520 | 1.758 | 1.996 | 2.234 | 2.472 | 2.709 | 2.947 |
| | $\lambda_{D.T}$ | 0.376 | 0.646 | 0.920 | 1.190 | 1.461 | 1.731 | 2.002 | 2.273 | 2.544 | 2.815 | 3.085 | 3.356 |
| | $P_{uT}/P_{yT}$ | 0.699 | 0.678 | 0.633 | 0.566 | 0.441 | 0.364 | 0.320 | 0.282 | 0.247 | 0.214 | 0.185 | 0.163 |
| | $P_{uT}/P_{nFT.T}$ | 0.865 | 0.902 | 0.941 | 0.976 | 0.919 | 0.947 | 0.967 | 0.973 | 0.955 | 0.922 | 0.874 | 0.838 |
| | $P_{uT}/P_{nD.T}$ | 0.979 | 0.949 | 0.934 | 0.974 | 0.894 | 0.860 | 0.869 | 0.870 | 0.855 | 0.826 | 0.786 | 0.757 |
| | $P_{uT}/P_{nDFT.T}$ | 1.211 | 1.262 | 1.317 | 1.431 | 1.423 | 1.520 | 1.626 | 1.710 | 1.751 | 1.756 | 1.727 | 1.714 |
| | $P_{uT}/P_{nFTD.T}$ | 1.198 | 1.223 | 1.293 | 1.439 | 1.403 | 1.428 | 1.523 | 1.608 | 1.660 | 1.686 | 1.682 | 1.698 |

**Table I.19**: Numerical failure loads and their DSM estimates concerning the **LC19** column geometry with 12 room temperature stresses (corresponding to equally spaced slenderness values) and 8 temperatures varying from $T$=20/100 to $T$=800 ºC.

| $T$ (ºC) | $\lambda_{cr.20}$ | 0.32 | 0.54 | 0.80 | 1.07 | 1.34 | 1.61 | 1.88 | 2.15 | 2.41 | 2.68 | 2.95 | 3.22 |
|---|---|---|---|---|---|---|---|---|---|---|---|---|---|
| 20/100 | $\lambda_{FT.T}$ | 0.322 | 0.536 | 0.805 | 1.073 | 1.341 | 1.609 | 1.878 | 2.146 | 2.414 | 2.682 | 2.951 | 3.219 |
| | $\lambda_{D.T}$ | 0.367 | 0.611 | 0.917 | 1.223 | 1.529 | 1.834 | 2.140 | 2.446 | 2.752 | 3.057 | 3.363 | 3.669 |
| | $P_{uT}/P_{yT}$ | 0.958 | 0.928 | 0.805 | 0.585 | 0.471 | 0.405 | 0.358 | 0.317 | 0.278 | 0.238 | 0.203 | 0.176 |
| | $P_{uT}/P_{nFT.T}$ | 1.000 | 1.047 | 1.056 | 0.947 | 1.001 | 1.106 | 1.119 | 1.114 | 1.086 | 1.022 | 0.948 | 0.887 |
| | $P_{uT}/P_{nD.T}$ | 0.958 | 0.937 | 1.004 | 0.927 | 0.923 | 0.954 | 0.991 | 1.013 | 1.013 | 0.976 | 0.926 | 0.885 |
| | $P_{uT}/P_{nDFT.T}$ | 1.000 | 1.048 | 1.200 | 1.224 | 1.387 | 1.608 | 1.756 | 1.873 | 1.943 | 1.934 | 1.892 | 1.857 |
| | $P_{uT}/P_{nFTD.T}$ | 1.000 | 1.056 | 1.248 | 1.256 | 1.356 | 1.512 | 1.689 | 1.851 | 1.980 | 2.037 | 2.062 | 2.098 |
| 200 | $\lambda_{FT.T}$ | 0.320 | 0.533 | 0.800 | 1.067 | 1.334 | 1.600 | 1.867 | 2.134 | 2.401 | 2.667 | 2.934 | 3.201 |
| | $\lambda_{D.T}$ | 0.365 | 0.608 | 0.912 | 1.216 | 1.520 | 1.824 | 2.128 | 2.432 | 2.736 | 3.040 | 3.344 | 3.648 |
| | $P_{uT}/P_{yT}$ | 0.937 | 0.910 | 0.800 | 0.584 | 0.469 | 0.403 | 0.357 | 0.316 | 0.279 | 0.240 | 0.205 | 0.177 |
| | $P_{uT}/P_{nFT.T}$ | 1.083 | 1.124 | 1.127 | 0.988 | 1.005 | 1.095 | 1.110 | 1.107 | 1.082 | 1.023 | 0.950 | 0.889 |
| | $P_{uT}/P_{nD.T}$ | 0.959 | 0.935 | 1.003 | 0.926 | 0.917 | 0.947 | 0.985 | 1.008 | 1.009 | 0.977 | 0.928 | 0.887 |
| | $P_{uT}/P_{nDFT.T}$ | 1.108 | 1.150 | 1.265 | 1.261 | 1.392 | 1.599 | 1.747 | 1.865 | 1.939 | 1.940 | 1.897 | 1.863 |
| | $P_{uT}/P_{nFTD.T}$ | 1.107 | 1.152 | 1.347 | 1.341 | 1.427 | 1.575 | 1.744 | 1.898 | 2.017 | 2.069 | 2.078 | 2.099 |
| 300 | $\lambda_{FT.T}$ | 0.318 | 0.530 | 0.795 | 1.059 | 1.324 | 1.589 | 1.854 | 2.119 | 2.384 | 2.649 | 2.913 | 3.178 |
| | $\lambda_{D.T}$ | 0.362 | 0.604 | 0.906 | 1.208 | 1.509 | 1.811 | 2.113 | 2.415 | 2.717 | 3.019 | 3.321 | 3.623 |
| | $P_{uT}/P_{yT}$ | 0.765 | 0.746 | 0.698 | 0.549 | 0.432 | 0.372 | 0.333 | 0.299 | 0.267 | 0.235 | 0.203 | 0.176 |
| | $P_{uT}/P_{nFT.T}$ | 0.959 | 0.993 | 1.045 | 0.968 | 0.938 | 1.003 | 1.028 | 1.041 | 1.030 | 0.994 | 0.934 | 0.877 |
| | $P_{uT}/P_{nD.T}$ | 0.973 | 0.949 | 0.966 | 0.923 | 0.878 | 0.898 | 0.938 | 0.969 | 0.979 | 0.965 | 0.925 | 0.886 |
| | $P_{uT}/P_{nDFT.T}$ | 1.221 | 1.264 | 1.340 | 1.342 | 1.397 | 1.572 | 1.721 | 1.851 | 1.937 | 1.969 | 1.942 | 1.908 |
| | $P_{uT}/P_{nFTD.T}$ | 1.212 | 1.239 | 1.364 | 1.398 | 1.419 | 1.542 | 1.705 | 1.862 | 1.986 | 2.062 | 2.080 | 2.094 |
| 400 | $\lambda_{FT.T}$ | 0.310 | 0.517 | 0.775 | 1.034 | 1.292 | 1.551 | 1.809 | 2.068 | 2.326 | 2.585 | 2.843 | 3.102 |
| | $\lambda_{D.T}$ | 0.354 | 0.589 | 0.884 | 1.178 | 1.473 | 1.768 | 2.062 | 2.357 | 2.651 | 2.946 | 3.241 | 3.535 |
| | $P_{uT}/P_{yT}$ | 0.647 | 0.630 | 0.600 | 0.528 | 0.411 | 0.351 | 0.317 | 0.290 | 0.262 | 0.234 | 0.206 | 0.180 |
| | $P_{uT}/P_{nFT.T}$ | 0.860 | 0.883 | 0.932 | 0.947 | 0.887 | 0.928 | 0.960 | 0.988 | 0.991 | 0.970 | 0.929 | 0.877 |
| | $P_{uT}/P_{nD.T}$ | 1.001 | 0.975 | 0.939 | 0.942 | 0.864 | 0.865 | 0.903 | 0.942 | 0.961 | 0.957 | 0.933 | 0.896 |
| | $P_{uT}/P_{nDFT.T}$ | 1.331 | 1.366 | 1.443 | 1.479 | 1.449 | 1.578 | 1.721 | 1.862 | 1.961 | 2.011 | 2.012 | 1.979 |
| | $P_{uT}/P_{nFTD.T}$ | 1.317 | 1.327 | 1.364 | 1.462 | 1.424 | 1.508 | 1.661 | 1.824 | 1.955 | 2.043 | 2.087 | 2.099 |
| 500 | $\lambda_{FT.T}$ | 0.303 | 0.504 | 0.756 | 1.008 | 1.261 | 1.513 | 1.765 | 2.017 | 2.269 | 2.521 | 2.773 | 3.025 |
| | $\lambda_{D.T}$ | 0.345 | 0.575 | 0.862 | 1.149 | 1.437 | 1.724 | 2.011 | 2.299 | 2.586 | 2.873 | 3.161 | 3.448 |
| | $P_{uT}/P_{yT}$ | 0.673 | 0.658 | 0.629 | 0.552 | 0.429 | 0.365 | 0.328 | 0.299 | 0.271 | 0.243 | 0.215 | 0.188 |
| | $P_{uT}/P_{nFT.T}$ | 0.919 | 0.943 | 0.991 | 0.993 | 0.916 | 0.942 | 0.970 | 0.997 | 1.003 | 0.987 | 0.949 | 0.896 |
| | $P_{uT}/P_{nD.T}$ | 0.991 | 0.968 | 0.939 | 0.947 | 0.871 | 0.867 | 0.901 | 0.941 | 0.962 | 0.963 | 0.943 | 0.906 |
| | $P_{uT}/P_{nDFT.T}$ | 1.354 | 1.389 | 1.459 | 1.481 | 1.437 | 1.549 | 1.684 | 1.825 | 1.930 | 1.990 | 2.001 | 1.970 |
| | $P_{uT}/P_{nFTD.T}$ | 1.342 | 1.355 | 1.399 | 1.503 | 1.461 | 1.535 | 1.678 | 1.838 | 1.971 | 2.064 | 2.113 | 2.120 |
| 600 | $\lambda_{FT.T}$ | 0.317 | 0.528 | 0.792 | 1.055 | 1.319 | 1.583 | 1.847 | 2.111 | 2.375 | 2.639 | 2.903 | 3.166 |
| | $\lambda_{D.T}$ | 0.361 | 0.602 | 0.902 | 1.203 | 1.504 | 1.805 | 2.105 | 2.406 | 2.707 | 3.008 | 3.308 | 3.609 |
| | $P_{uT}/P_{yT}$ | 0.611 | 0.594 | 0.563 | 0.501 | 0.392 | 0.337 | 0.307 | 0.281 | 0.253 | 0.226 | 0.198 | 0.174 |
| | $P_{uT}/P_{nFT.T}$ | 0.834 | 0.855 | 0.899 | 0.925 | 0.873 | 0.907 | 0.945 | 0.973 | 0.975 | 0.953 | 0.910 | 0.861 |
| | $P_{uT}/P_{nD.T}$ | 1.018 | 0.990 | 0.939 | 0.938 | 0.859 | 0.861 | 0.903 | 0.942 | 0.958 | 0.952 | 0.925 | 0.889 |
| | $P_{uT}/P_{nDFT.T}$ | 1.389 | 1.424 | 1.499 | 1.542 | 1.501 | 1.618 | 1.767 | 1.909 | 2.002 | 2.046 | 2.037 | 2.004 |
| | $P_{uT}/P_{nFTD.T}$ | 1.373 | 1.378 | 1.391 | 1.484 | 1.442 | 1.530 | 1.690 | 1.855 | 1.982 | 2.065 | 2.100 | 2.113 |
| 700 | $\lambda_{FT.T}$ | 0.322 | 0.536 | 0.805 | 1.073 | 1.341 | 1.609 | 1.878 | 2.146 | 2.414 | 2.682 | 2.951 | 3.219 |
| | $\lambda_{D.T}$ | 0.367 | 0.611 | 0.917 | 1.223 | 1.529 | 1.834 | 2.140 | 2.446 | 2.752 | 3.057 | 3.363 | 3.669 |
| | $P_{uT}/P_{yT}$ | 0.594 | 0.576 | 0.544 | 0.485 | 0.380 | 0.329 | 0.300 | 0.275 | 0.248 | 0.219 | 0.192 | 0.169 |
| | $P_{uT}/P_{nFT.T}$ | 0.782 | 0.804 | 0.850 | 0.886 | 0.851 | 0.898 | 0.938 | 0.966 | 0.966 | 0.939 | 0.897 | 0.850 |
| | $P_{uT}/P_{nD.T}$ | 1.029 | 0.998 | 0.944 | 0.935 | 0.855 | 0.862 | 0.905 | 0.943 | 0.957 | 0.945 | 0.918 | 0.884 |
| | $P_{uT}/P_{nDFT.T}$ | 1.356 | 1.393 | 1.474 | 1.535 | 1.511 | 1.648 | 1.800 | 1.939 | 2.029 | 2.058 | 2.049 | 2.018 |
| | $P_{uT}/P_{nFTD.T}$ | 1.337 | 1.341 | 1.353 | 1.437 | 1.400 | 1.498 | 1.664 | 1.829 | 1.956 | 2.031 | 2.072 | 2.093 |
| 800 | $\lambda_{FT.T}$ | 0.284 | 0.473 | 0.710 | 0.946 | 1.183 | 1.419 | 1.656 | 1.892 | 2.129 | 2.366 | 2.602 | 2.839 |
| | $\lambda_{D.T}$ | 0.324 | 0.539 | 0.809 | 1.079 | 1.348 | 1.618 | 1.887 | 2.157 | 2.427 | 2.696 | 2.966 | 3.236 |
| | $P_{uT}/P_{yT}$ | 0.703 | 0.690 | 0.663 | 0.597 | 0.469 | 0.391 | 0.348 | 0.318 | 0.290 | 0.263 | 0.236 | 0.209 |
| | $P_{uT}/P_{nFT.T}$ | 0.861 | 0.887 | 0.938 | 0.964 | 0.897 | 0.923 | 0.974 | 1.000 | 1.014 | 1.009 | 0.984 | 0.941 |
| | $P_{uT}/P_{nD.T}$ | 0.984 | 0.965 | 0.937 | 0.961 | 0.888 | 0.867 | 0.891 | 0.928 | 0.957 | 0.968 | 0.961 | 0.935 |
| | $P_{uT}/P_{nDFT.T}$ | 1.205 | 1.241 | 1.313 | 1.379 | 1.361 | 1.464 | 1.614 | 1.749 | 1.865 | 1.945 | 1.984 | 1.978 |
| | $P_{uT}/P_{nFTD.T}$ | 1.196 | 1.215 | 1.261 | 1.383 | 1.359 | 1.406 | 1.527 | 1.677 | 1.818 | 1.933 | 2.013 | 2.052 |

**Table I.20**: Numerical failure loads and their DSM estimates concerning the **LC20** column geometry with 12 room temperature stresses (corresponding to equally spaced slenderness values) and 8 temperatures varying from $T$=20/100 to $T$=800 ºC.

| $T$ (ºC) | $\lambda_{cr.20}$ | 0.31 | 0.56 | 0.82 | 1.08 | 1.33 | 1.59 | 1.85 | 2.10 | 2.36 | 2.62 | 2.87 | 3.13 |
|---|---|---|---|---|---|---|---|---|---|---|---|---|---|
| 20/100 | $\lambda_{FT.T}$ | 0.308 | 0.565 | 0.821 | 1.078 | 1.335 | 1.592 | 1.848 | 2.105 | 2.362 | 2.618 | 2.875 | 3.132 |
| | $\lambda_{D.T}$ | 0.355 | 0.650 | 0.946 | 1.241 | 1.537 | 1.832 | 2.128 | 2.424 | 2.719 | 3.015 | 3.310 | 3.606 |
| | $P_{uT}/P_{yT}$ | 0.955 | 0.920 | 0.818 | 0.603 | 0.478 | 0.399 | 0.333 | 0.274 | 0.224 | 0.190 | 0.163 | 0.140 |
| | $P_{uT}/P_{nFT.T}$ | 0.994 | 1.052 | 1.085 | 0.980 | 1.007 | 1.088 | 1.060 | 0.998 | 0.919 | 0.867 | 0.816 | 0.768 |
| | $P_{uT}/P_{nD.T}$ | 0.955 | 0.945 | 1.045 | 0.968 | 0.940 | 0.939 | 0.918 | 0.869 | 0.806 | 0.767 | 0.728 | 0.691 |
| | $P_{uT}/P_{nDFT.T}$ | 0.994 | 1.061 | 1.254 | 1.279 | 1.406 | 1.582 | 1.643 | 1.638 | 1.588 | 1.572 | 1.547 | 1.516 |
| | $P_{uT}/P_{nFTD.T}$ | 0.994 | 1.076 | 1.303 | 1.310 | 1.373 | 1.473 | 1.543 | 1.561 | 1.544 | 1.563 | 1.578 | 1.589 |
| 200 | $\lambda_{FT.T}$ | 0.306 | 0.562 | 0.817 | 1.072 | 1.327 | 1.583 | 1.838 | 2.093 | 2.348 | 2.604 | 2.859 | 3.114 |
| | $\lambda_{D.T}$ | 0.353 | 0.647 | 0.941 | 1.234 | 1.528 | 1.822 | 2.116 | 2.410 | 2.704 | 2.998 | 3.292 | 3.586 |
| | $P_{uT}/P_{yT}$ | 0.935 | 0.902 | 0.812 | 0.602 | 0.476 | 0.398 | 0.334 | 0.276 | 0.226 | 0.192 | 0.164 | 0.143 |
| | $P_{uT}/P_{nFT.T}$ | 1.077 | 1.127 | 1.155 | 1.023 | 1.013 | 1.079 | 1.057 | 0.998 | 0.921 | 0.868 | 0.817 | 0.779 |
| | $P_{uT}/P_{nD.T}$ | 0.956 | 0.940 | 1.041 | 0.967 | 0.936 | 0.934 | 0.917 | 0.870 | 0.809 | 0.768 | 0.729 | 0.701 |
| | $P_{uT}/P_{nDFT.T}$ | 1.101 | 1.153 | 1.316 | 1.318 | 1.413 | 1.575 | 1.643 | 1.642 | 1.596 | 1.577 | 1.551 | 1.540 |
| | $P_{uT}/P_{nFTD.T}$ | 1.100 | 1.169 | 1.403 | 1.400 | 1.448 | 1.539 | 1.605 | 1.615 | 1.589 | 1.594 | 1.596 | 1.617 |
| 300 | $\lambda_{FT.T}$ | 0.304 | 0.558 | 0.811 | 1.065 | 1.318 | 1.571 | 1.825 | 2.078 | 2.332 | 2.585 | 2.839 | 3.092 |
| | $\lambda_{D.T}$ | 0.350 | 0.642 | 0.934 | 1.226 | 1.518 | 1.809 | 2.101 | 2.393 | 2.685 | 2.977 | 3.269 | 3.561 |
| | $P_{uT}/P_{yT}$ | 0.764 | 0.738 | 0.697 | 0.568 | 0.442 | 0.370 | 0.318 | 0.267 | 0.224 | 0.190 | 0.163 | 0.142 |
| | $P_{uT}/P_{nFT.T}$ | 0.956 | 0.993 | 1.052 | 1.004 | 0.954 | 0.996 | 0.998 | 0.960 | 0.907 | 0.855 | 0.807 | 0.766 |
| | $P_{uT}/P_{nD.T}$ | 0.972 | 0.940 | 0.981 | 0.966 | 0.902 | 0.894 | 0.892 | 0.858 | 0.813 | 0.770 | 0.732 | 0.699 |
| | $P_{uT}/P_{nDFT.T}$ | 1.216 | 1.264 | 1.357 | 1.403 | 1.428 | 1.563 | 1.654 | 1.672 | 1.656 | 1.629 | 1.602 | 1.579 |
| | $P_{uT}/P_{nFTD.T}$ | 1.208 | 1.236 | 1.390 | 1.463 | 1.452 | 1.523 | 1.605 | 1.627 | 1.624 | 1.616 | 1.612 | 1.614 |
| 400 | $\lambda_{FT.T}$ | 0.297 | 0.544 | 0.792 | 1.039 | 1.286 | 1.534 | 1.781 | 2.028 | 2.276 | 2.523 | 2.770 | 3.018 |
| | $\lambda_{D.T}$ | 0.342 | 0.627 | 0.911 | 1.196 | 1.481 | 1.766 | 2.051 | 2.335 | 2.620 | 2.905 | 3.190 | 3.475 |
| | $P_{uT}/P_{yT}$ | 0.646 | 0.626 | 0.597 | 0.540 | 0.425 | 0.354 | 0.308 | 0.266 | 0.223 | 0.193 | 0.167 | 0.146 |
| | $P_{uT}/P_{nFT.T}$ | 0.857 | 0.884 | 0.934 | 0.972 | 0.913 | 0.928 | 0.944 | 0.931 | 0.880 | 0.846 | 0.806 | 0.769 |
| | $P_{uT}/P_{nD.T}$ | 1.000 | 0.968 | 0.941 | 0.974 | 0.897 | 0.870 | 0.873 | 0.856 | 0.808 | 0.778 | 0.743 | 0.712 |
| | $P_{uT}/P_{nDFT.T}$ | 1.326 | 1.369 | 1.445 | 1.524 | 1.495 | 1.581 | 1.679 | 1.728 | 1.700 | 1.697 | 1.674 | 1.653 |
| | $P_{uT}/P_{nFTD.T}$ | 1.313 | 1.325 | 1.372 | 1.511 | 1.474 | 1.508 | 1.590 | 1.638 | 1.621 | 1.633 | 1.631 | 1.632 |
| 500 | $\lambda_{FT.T}$ | 0.290 | 0.531 | 0.772 | 1.013 | 1.255 | 1.496 | 1.737 | 1.978 | 2.220 | 2.461 | 2.702 | 2.943 |
| | $\lambda_{D.T}$ | 0.333 | 0.611 | 0.889 | 1.167 | 1.444 | 1.722 | 2.000 | 2.278 | 2.556 | 2.833 | 3.111 | 3.389 |
| | $P_{uT}/P_{yT}$ | 0.672 | 0.653 | 0.625 | 0.566 | 0.444 | 0.369 | 0.321 | 0.278 | 0.237 | 0.202 | 0.174 | 0.152 |
| | $P_{uT}/P_{nFT.T}$ | 0.917 | 0.943 | 0.992 | 1.021 | 0.944 | 0.953 | 0.956 | 0.948 | 0.911 | 0.862 | 0.821 | 0.782 |
| | $P_{uT}/P_{nD.T}$ | 0.990 | 0.961 | 0.941 | 0.981 | 0.905 | 0.876 | 0.877 | 0.865 | 0.831 | 0.787 | 0.752 | 0.720 |
| | $P_{uT}/P_{nDFT.T}$ | 1.350 | 1.389 | 1.460 | 1.528 | 1.487 | 1.566 | 1.649 | 1.708 | 1.711 | 1.683 | 1.662 | 1.640 |
| | $P_{uT}/P_{nFTD.T}$ | 1.339 | 1.352 | 1.408 | 1.555 | 1.515 | 1.541 | 1.619 | 1.671 | 1.679 | 1.661 | 1.655 | 1.650 |
| 600 | $\lambda_{FT.T}$ | 0.303 | 0.556 | 0.808 | 1.061 | 1.313 | 1.566 | 1.818 | 2.071 | 2.323 | 2.576 | 2.828 | 3.081 |
| | $\lambda_{D.T}$ | 0.349 | 0.640 | 0.930 | 1.221 | 1.512 | 1.803 | 2.093 | 2.384 | 2.675 | 2.966 | 3.256 | 3.547 |
| | $P_{uT}/P_{yT}$ | 0.611 | 0.590 | 0.561 | 0.510 | 0.405 | 0.338 | 0.296 | 0.255 | 0.219 | 0.185 | 0.161 | 0.141 |
| | $P_{uT}/P_{nFT.T}$ | 0.832 | 0.857 | 0.902 | 0.946 | 0.898 | 0.907 | 0.925 | 0.912 | 0.880 | 0.830 | 0.792 | 0.757 |
| | $P_{uT}/P_{nD.T}$ | 1.018 | 0.983 | 0.934 | 0.965 | 0.892 | 0.864 | 0.867 | 0.848 | 0.816 | 0.770 | 0.737 | 0.707 |
| | $P_{uT}/P_{nDFT.T}$ | 1.386 | 1.428 | 1.504 | 1.577 | 1.548 | 1.619 | 1.717 | 1.760 | 1.762 | 1.723 | 1.702 | 1.680 |
| | $P_{uT}/P_{nFTD.T}$ | 1.371 | 1.376 | 1.391 | 1.527 | 1.492 | 1.524 | 1.609 | 1.651 | 1.665 | 1.644 | 1.644 | 1.645 |
| 700 | $\lambda_{FT.T}$ | 0.308 | 0.565 | 0.821 | 1.078 | 1.335 | 1.592 | 1.848 | 2.105 | 2.362 | 2.618 | 2.875 | 3.132 |
| | $\lambda_{D.T}$ | 0.355 | 0.650 | 0.946 | 1.241 | 1.537 | 1.832 | 2.128 | 2.424 | 2.719 | 3.015 | 3.310 | 3.606 |
| | $P_{uT}/P_{yT}$ | 0.594 | 0.572 | 0.543 | 0.493 | 0.393 | 0.329 | 0.288 | 0.248 | 0.212 | 0.180 | 0.156 | 0.137 |
| | $P_{uT}/P_{nFT.T}$ | 0.780 | 0.806 | 0.855 | 0.905 | 0.874 | 0.897 | 0.916 | 0.900 | 0.867 | 0.820 | 0.783 | 0.749 |
| | $P_{uT}/P_{nD.T}$ | 1.029 | 0.992 | 0.941 | 0.960 | 0.887 | 0.861 | 0.864 | 0.843 | 0.809 | 0.765 | 0.732 | 0.702 |
| | $P_{uT}/P_{nDFT.T}$ | 1.352 | 1.398 | 1.482 | 1.568 | 1.557 | 1.646 | 1.743 | 1.779 | 1.776 | 1.739 | 1.718 | 1.695 |
| | $P_{uT}/P_{nFTD.T}$ | 1.335 | 1.340 | 1.355 | 1.476 | 1.448 | 1.487 | 1.573 | 1.614 | 1.629 | 1.616 | 1.621 | 1.627 |
| 800 | $\lambda_{FT.T}$ | 0.272 | 0.498 | 0.724 | 0.951 | 1.177 | 1.404 | 1.630 | 1.856 | 2.083 | 2.309 | 2.536 | 2.762 |
| | $\lambda_{D.T}$ | 0.313 | 0.573 | 0.834 | 1.095 | 1.355 | 1.616 | 1.877 | 2.137 | 2.398 | 2.659 | 2.919 | 3.180 |
| | $P_{uT}/P_{yT}$ | 0.702 | 0.684 | 0.659 | 0.608 | 0.488 | 0.400 | 0.346 | 0.304 | 0.262 | 0.226 | 0.195 | 0.169 |
| | $P_{uT}/P_{nFT.T}$ | 0.858 | 0.887 | 0.938 | 0.985 | 0.930 | 0.929 | 0.966 | 0.970 | 0.941 | 0.902 | 0.858 | 0.814 |
| | $P_{uT}/P_{nD.T}$ | 0.983 | 0.957 | 0.938 | 0.988 | 0.928 | 0.885 | 0.881 | 0.879 | 0.851 | 0.818 | 0.780 | 0.743 |
| | $P_{uT}/P_{nDFT.T}$ | 1.201 | 1.241 | 1.313 | 1.416 | 1.417 | 1.479 | 1.597 | 1.675 | 1.694 | 1.690 | 1.667 | 1.638 |
| | $P_{uT}/P_{nFTD.T}$ | 1.193 | 1.212 | 1.267 | 1.422 | 1.416 | 1.426 | 1.496 | 1.569 | 1.594 | 1.605 | 1.601 | 1.595 |

**Table I.21**: Numerical failure loads and their DSM estimates concerning the **LC21** column geometry with 12 room temperature stresses (corresponding to equally spaced slenderness values) and 8 temperatures varying from $T$=20/100 to $T$=800 ºC.

| $T$ (ºC) | $\lambda_{cr.20}$ | 0.31 | 0.52 | 0.78 | 1.03 | 1.29 | 1.55 | 1.81 | 2.07 | 2.33 | 2.58 | 2.84 | 3.10 |
|---|---|---|---|---|---|---|---|---|---|---|---|---|---|
| 20/100 | $\lambda_{FT.T}$ | 0.310 | 0.517 | 0.775 | 1.034 | 1.292 | 1.551 | 1.809 | 2.068 | 2.326 | 2.585 | 2.843 | 3.101 |
| | $\lambda_{D.T}$ | 0.379 | 0.632 | 0.948 | 1.264 | 1.580 | 1.895 | 2.211 | 2.527 | 2.843 | 3.159 | 3.475 | 3.791 |
| | $P_{uT}/P_{yT}$ | 0.958 | 0.932 | 0.826 | 0.589 | 0.496 | 0.409 | 0.334 | 0.271 | 0.220 | 0.187 | 0.161 | 0.136 |
| | $P_{uT}/P_{nFT.T}$ | 0.997 | 1.043 | 1.063 | 0.921 | 0.997 | 1.086 | 1.039 | 0.969 | 0.886 | 0.841 | 0.802 | 0.740 |
| | $P_{uT}/P_{nD.T}$ | 0.958 | 0.949 | 1.057 | 0.961 | 1.003 | 0.997 | 0.957 | 0.899 | 0.828 | 0.793 | 0.763 | 0.710 |
| | $P_{uT}/P_{nDFT.T}$ | 0.997 | 1.048 | 1.242 | 1.238 | 1.454 | 1.645 | 1.683 | 1.667 | 1.609 | 1.606 | 1.602 | 1.541 |
| | $P_{uT}/P_{nFTD.T}$ | 0.997 | 1.059 | 1.286 | 1.264 | 1.417 | 1.507 | 1.544 | 1.542 | 1.509 | 1.533 | 1.561 | 1.536 |
| 200 | $\lambda_{FT.T}$ | 0.308 | 0.514 | 0.771 | 1.028 | 1.285 | 1.542 | 1.799 | 2.056 | 2.313 | 2.570 | 2.827 | 3.084 |
| | $\lambda_{D.T}$ | 0.377 | 0.628 | 0.942 | 1.257 | 1.571 | 1.885 | 2.199 | 2.513 | 2.827 | 3.142 | 3.456 | 3.770 |
| | $P_{uT}/P_{yT}$ | 0.938 | 0.913 | 0.822 | 0.587 | 0.494 | 0.408 | 0.335 | 0.273 | 0.233 | 0.189 | 0.163 | 0.137 |
| | $P_{uT}/P_{nFT.T}$ | 1.080 | 1.120 | 1.138 | 0.964 | 1.010 | 1.078 | 1.036 | 0.969 | 0.934 | 0.847 | 0.804 | 0.743 |
| | $P_{uT}/P_{nD.T}$ | 0.959 | 0.945 | 1.055 | 0.959 | 0.998 | 0.992 | 0.957 | 0.900 | 0.875 | 0.799 | 0.765 | 0.713 |
| | $P_{uT}/P_{nDFT.T}$ | 1.105 | 1.146 | 1.308 | 1.275 | 1.465 | 1.639 | 1.684 | 1.671 | 1.700 | 1.619 | 1.607 | 1.548 |
| | $P_{uT}/P_{nFTD.T}$ | 1.104 | 1.155 | 1.391 | 1.353 | 1.500 | 1.583 | 1.616 | 1.605 | 1.644 | 1.582 | 1.592 | 1.558 |
| 300 | $\lambda_{FT.T}$ | 0.306 | 0.510 | 0.766 | 1.021 | 1.276 | 1.531 | 1.786 | 2.042 | 2.297 | 2.552 | 2.807 | 3.062 |
| | $\lambda_{D.T}$ | 0.374 | 0.624 | 0.936 | 1.248 | 1.560 | 1.872 | 2.184 | 2.496 | 2.807 | 3.119 | 3.431 | 3.743 |
| | $P_{uT}/P_{yT}$ | 0.766 | 0.747 | 0.708 | 0.559 | 0.458 | 0.381 | 0.322 | 0.267 | 0.221 | 0.188 | 0.160 | 0.138 |
| | $P_{uT}/P_{nFT.T}$ | 0.958 | 0.989 | 1.044 | 0.958 | 0.954 | 0.998 | 0.989 | 0.941 | 0.879 | 0.837 | 0.783 | 0.740 |
| | $P_{uT}/P_{nD.T}$ | 0.974 | 0.951 | 0.998 | 0.964 | 0.960 | 0.951 | 0.939 | 0.894 | 0.839 | 0.803 | 0.756 | 0.719 |
| | $P_{uT}/P_{nDFT.T}$ | 1.219 | 1.258 | 1.352 | 1.364 | 1.475 | 1.622 | 1.704 | 1.711 | 1.678 | 1.673 | 1.632 | 1.603 |
| | $P_{uT}/P_{nFTD.T}$ | 1.211 | 1.235 | 1.390 | 1.430 | 1.508 | 1.577 | 1.638 | 1.640 | 1.613 | 1.619 | 1.594 | 1.585 |
| 400 | $\lambda_{FT.T}$ | 0.299 | 0.498 | 0.747 | 0.996 | 1.245 | 1.494 | 1.743 | 1.992 | 2.241 | 2.491 | 2.740 | 2.989 |
| | $\lambda_{D.T}$ | 0.365 | 0.609 | 0.913 | 1.218 | 1.522 | 1.827 | 2.131 | 2.435 | 2.740 | 3.044 | 3.349 | 3.653 |
| | $P_{uT}/P_{yT}$ | 0.651 | 0.634 | 0.606 | 0.544 | 0.418 | 0.364 | 0.315 | 0.266 | 0.224 | 0.192 | 0.165 | 0.142 |
| | $P_{uT}/P_{nFT.T}$ | 0.863 | 0.884 | 0.928 | 0.953 | 0.870 | 0.936 | 0.942 | 0.914 | 0.872 | 0.831 | 0.789 | 0.745 |
| | $P_{uT}/P_{nD.T}$ | 1.007 | 0.982 | 0.955 | 0.992 | 0.903 | 0.925 | 0.924 | 0.892 | 0.850 | 0.813 | 0.774 | 0.734 |
| | $P_{uT}/P_{nDFT.T}$ | 1.336 | 1.368 | 1.437 | 1.507 | 1.455 | 1.636 | 1.731 | 1.759 | 1.750 | 1.738 | 1.714 | 1.677 |
| | $P_{uT}/P_{nFTD.T}$ | 1.323 | 1.331 | 1.375 | 1.514 | 1.453 | 1.565 | 1.640 | 1.658 | 1.651 | 1.647 | 1.636 | 1.616 |
| 500 | $\lambda_{FT.T}$ | 0.291 | 0.486 | 0.729 | 0.972 | 1.215 | 1.457 | 1.700 | 1.943 | 2.186 | 2.429 | 2.672 | 2.915 |
| | $\lambda_{D.T}$ | 0.356 | 0.594 | 0.891 | 1.188 | 1.485 | 1.781 | 2.078 | 2.375 | 2.672 | 2.969 | 3.266 | 3.563 |
| | $P_{uT}/P_{yT}$ | 0.677 | 0.661 | 0.634 | 0.569 | 0.436 | 0.380 | 0.327 | 0.278 | 0.235 | 0.198 | 0.173 | 0.149 |
| | $P_{uT}/P_{nFT.T}$ | 0.923 | 0.943 | 0.987 | 1.001 | 0.898 | 0.950 | 0.956 | 0.931 | 0.889 | 0.838 | 0.804 | 0.758 |
| | $P_{uT}/P_{nD.T}$ | 0.996 | 0.973 | 0.956 | 0.998 | 0.908 | 0.931 | 0.930 | 0.902 | 0.861 | 0.814 | 0.784 | 0.743 |
| | $P_{uT}/P_{nDFT.T}$ | 1.358 | 1.389 | 1.453 | 1.513 | 1.446 | 1.609 | 1.706 | 1.742 | 1.738 | 1.707 | 1.703 | 1.666 |
| | $P_{uT}/P_{nFTD.T}$ | 1.347 | 1.358 | 1.411 | 1.557 | 1.490 | 1.602 | 1.674 | 1.695 | 1.688 | 1.660 | 1.664 | 1.638 |
| 600 | $\lambda_{FT.T}$ | 0.305 | 0.509 | 0.763 | 1.017 | 1.271 | 1.526 | 1.780 | 2.034 | 2.288 | 2.543 | 2.797 | 3.051 |
| | $\lambda_{D.T}$ | 0.373 | 0.622 | 0.932 | 1.243 | 1.554 | 1.865 | 2.175 | 2.486 | 2.797 | 3.108 | 3.419 | 3.729 |
| | $P_{uT}/P_{yT}$ | 0.617 | 0.599 | 0.570 | 0.516 | 0.399 | 0.349 | 0.302 | 0.255 | 0.217 | 0.185 | 0.159 | 0.137 |
| | $P_{uT}/P_{nFT.T}$ | 0.840 | 0.858 | 0.898 | 0.931 | 0.857 | 0.910 | 0.923 | 0.896 | 0.860 | 0.819 | 0.777 | 0.734 |
| | $P_{uT}/P_{nD.T}$ | 1.028 | 0.999 | 0.950 | 0.986 | 0.898 | 0.918 | 0.917 | 0.884 | 0.847 | 0.807 | 0.769 | 0.729 |
| | $P_{uT}/P_{nDFT.T}$ | 1.399 | 1.430 | 1.497 | 1.551 | 1.503 | 1.665 | 1.765 | 1.789 | 1.787 | 1.769 | 1.742 | 1.702 |
| | $P_{uT}/P_{nFTD.T}$ | 1.384 | 1.386 | 1.397 | 1.536 | 1.474 | 1.583 | 1.658 | 1.673 | 1.673 | 1.664 | 1.652 | 1.630 |
| 700 | $\lambda_{FT.T}$ | 0.310 | 0.517 | 0.775 | 1.034 | 1.292 | 1.551 | 1.809 | 2.068 | 2.326 | 2.585 | 2.843 | 3.101 |
| | $\lambda_{D.T}$ | 0.379 | 0.632 | 0.948 | 1.264 | 1.580 | 1.895 | 2.211 | 2.527 | 2.843 | 3.159 | 3.475 | 3.791 |
| | $P_{uT}/P_{yT}$ | 0.600 | 0.582 | 0.552 | 0.499 | 0.388 | 0.339 | 0.293 | 0.248 | 0.212 | 0.180 | 0.155 | 0.129 |
| | $P_{uT}/P_{nFT.T}$ | 0.788 | 0.807 | 0.850 | 0.889 | 0.834 | 0.900 | 0.913 | 0.886 | 0.858 | 0.809 | 0.769 | 0.701 |
| | $P_{uT}/P_{nD.T}$ | 1.040 | 1.009 | 0.957 | 0.982 | 0.895 | 0.915 | 0.912 | 0.879 | 0.849 | 0.802 | 0.764 | 0.699 |
| | $P_{uT}/P_{nDFT.T}$ | 1.367 | 1.399 | 1.473 | 1.541 | 1.510 | 1.690 | 1.787 | 1.808 | 1.821 | 1.783 | 1.757 | 1.657 |
| | $P_{uT}/P_{nFTD.T}$ | 1.349 | 1.351 | 1.361 | 1.485 | 1.432 | 1.542 | 1.617 | 1.634 | 1.654 | 1.633 | 1.626 | 1.553 |
| 800 | $\lambda_{FT.T}$ | 0.274 | 0.456 | 0.684 | 0.912 | 1.140 | 1.368 | 1.596 | 1.823 | 2.051 | 2.279 | 2.507 | 2.735 |
| | $\lambda_{D.T}$ | 0.334 | 0.557 | 0.836 | 1.114 | 1.393 | 1.672 | 1.950 | 2.229 | 2.507 | 2.786 | 3.065 | 3.343 |
| | $P_{uT}/P_{yT}$ | 0.706 | 0.692 | 0.667 | 0.614 | 0.475 | 0.412 | 0.354 | 0.306 | 0.260 | 0.226 | 0.192 | 0.166 |
| | $P_{uT}/P_{nFT.T}$ | 0.863 | 0.885 | 0.932 | 0.970 | 0.880 | 0.925 | 0.969 | 0.961 | 0.923 | 0.891 | 0.838 | 0.794 |
| | $P_{uT}/P_{nD.T}$ | 0.988 | 0.969 | 0.951 | 1.009 | 0.925 | 0.940 | 0.937 | 0.925 | 0.888 | 0.859 | 0.811 | 0.771 |
| | $P_{uT}/P_{nDFT.T}$ | 1.208 | 1.239 | 1.305 | 1.409 | 1.372 | 1.522 | 1.657 | 1.724 | 1.731 | 1.743 | 1.705 | 1.674 |
| | $P_{uT}/P_{nFTD.T}$ | 1.199 | 1.214 | 1.267 | 1.428 | 1.382 | 1.480 | 1.548 | 1.602 | 1.608 | 1.626 | 1.601 | 1.588 |